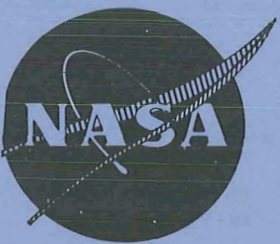


N 70 22842

NASA CR-72634

PWA FR-3481

# CASE FILE COPY



## SINGLE STAGE EXPERIMENTAL EVALUATION OF COMPRESSOR BLADING WITH SLOTS AND VORTEX GENERATORS

PART II - DATA AND PERFORMANCE FOR STAGE 5  
WITHOUT SLOTS OR VORTEX GENERATORS

By

J. A. Brent and B. A. Jones

Prepared For  
National Aeronautics and Space Administration  
Contract NAS3-10481

**Pratt & Whitney Aircraft**  
FLORIDA RESEARCH AND DEVELOPMENT CENTER  
BOX 2691, WEST PALM BEACH, FLORIDA 33402

DIVISION OF UNITED AIRCRAFT CORPORATION



## **NOTICE**

This report was prepared as an account of Government-sponsored work. Neither the United States, nor the National Aeronautics and Space Administration (NASA), nor any person acting on behalf of NASA:

- A.) Makes any warranty or representation, expressed or implied, with respect to the accuracy, completeness, or usefulness of the information contained in this report, or that the use of any information, apparatus, method, or process disclosed in this report may not infringe privately owned rights; or
- B.) Assumes any liabilities with respect to the use of, or for damages resulting from the use of, any information, apparatus, method, or process disclosed in this report.

As used above, "person acting on behalf of NASA" includes any employee or contractor of NASA, or employee of such contractor, to the extent that such employee or contractor of NASA or employee of such contractor prepares, disseminates, or provides access to any information pursuant to his employment or contract with NASA, or his employment with such contractor.

Requests for copies of this report should be referred to:

National Aeronautics and Space Administration  
Scientific and Technical Information Facility  
P.O. Box 33  
College Park, Md. 20740

SINGLE STAGE EXPERIMENTAL EVALUATION  
OF  
COMPRESSOR BLADING WITH SLOTS AND  
VORTEX GENERATORS

PART 11 - DATA AND PERFORMANCE FOR STAGE 5  
WITHOUT SLOTS OR VORTEX GENERATORS

By  
J. A. Brent and B. A. Jones

Prepared For  
National Aeronautics and Space Administration

20 March 1970

Contract NAS3-10481

Technical Management  
NASA Lewis Research Center  
Cleveland, Ohio

NASA Program Manager: L. Joseph Herrig  
Fluid System Components Division

Pratt & Whitney Aircraft  
FLORIDA RESEARCH AND DEVELOPMENT CENTER  
BOX 2691, WEST PALM BEACH, FLORIDA 33402

DIVISION OF UNITED AIRCRAFT CORPORATION





## ABSTRACT

Stage 5 of a series of highly-loaded slotted stages was tested without slots or vortex generators to establish a performance baseline for comparison with the results of subsequent tests planned with the addition of slots and vortex generators. Failure of the rotor due to bending flutter at high negative incidence angles precluded the latter series of tests. The rotor had an inlet hub/tip ratio of 0.8 and a design tip velocity of 757 feet per second. At design equivalent rotor speed, the rotor achieved a maximum efficiency of approximately 84% and a corresponding pressure ratio of 1.365. High stator losses resulted in substantially lower stage performance.

## CONTENTS

	PAGE
ILLUSTRATIONS . . . . .	vi
SUMMARY . . . . .	1
INTRODUCTION . . . . .	2
TEST EQUIPMENT . . . . .	3
Facility . . . . .	3
Compressor Test Rig . . . . .	3
Instrumentation . . . . .	4
Blading Design . . . . .	6
Design Predictions Without Slots and Vortex Generators . . . . .	7
PROCEDURES . . . . .	7
Test Procedures . . . . .	7
Data Reduction Procedures . . . . .	9
PRESENTATION OF DATA . . . . .	11
Overall Performance . . . . .	11
Rotor Blade Element Performance . . . . .	12
Stator Blade Element Performance . . . . .	14
CONCLUSION . . . . .	15
APPENDIX A - Definition of Symbols and Performance Variables . . . . .	63
- Definition of Overall Performance Variables . . .	65
- Definition of Blade Element Performance Variables . . . . .	66
APPENDIX B - Tabulated Performance . . . . .	67
REFERENCES . . . . .	97

## ILLUSTRATIONS

FIGURE		PAGE
1	Compressor Research Facility . . . . .	16
2	Single Stage Compressor Rig . . . . .	17
3	Flowpath Dimensions . . . . .	18
4	Boundary Layer Bleed System . . . . .	19
5	Instrumentation Layout . . . . .	20
6	Stator Static Pressure Instrumentation . . . . .	21
7	Total Pressure and Temperature Rakes . . . . .	22
8	Circumferential Total Pressure Rake . . . . .	23
9	Wedge Traverse Probes . . . . .	24
10	Typical Stall Transient Data . . . . .	25
11	Comparison of Stator Inlet and Exit Wall Static Pressures at Near Design Flow Conditions . . . . .	26
12	Station 0 Corrected Static Pressure vs Corrected Weight Flow. . . . .	27
13	Overall Performance - Rotor . . . . .	28
14	Overall Performance - Stage . . . . .	29
15	Rotor Inlet Relative Air Angle and Mach Number Distributions - Design Equivalent Rotor Speed. . . . .	30
16	Rotor Blade Element Performance - 5% Span From Tip . . . . .	31
17	Rotor Blade Element Performance - 10% Span From Tip . . . . .	32
18	Rotor Blade Element Performance - 15% Span From Tip . . . . .	33
19	Rotor Blade Element Performance - 30% Span From Tip . . . . .	34
20	Rotor Blade Element Performance - 50% Span From Tip . . . . .	35
21	Rotor Blade Element Performance - 70% Span From Tip . . . . .	36
22	Rotor Blade Element Performance - 85% Span From Tip . . . . .	37
23	Rotor Blade Element Performance - 90% Span From Tip . . . . .	38
24	Rotor Blade Element Performance - 95% Span From Tip . . . . .	39

## ILLUSTRATIONS (Continued)

FIGURE		PAGE
25	Variation of Rotor Tip Bleed Flow With Equivalent Rotor Speed and Corrected Flow . . . . .	40
26	Rotor Loss Parameter vs Diffuser Factor - 10% Span From Tip . . . . .	41
27	Rotor Loss Parameter vs Diffusion Factor - 30% Span From Tip . . . . .	42
28	Rotor Loss Parameter vs Diffusion Factor - 50% Span From Tip . . . . .	43
29	Rotor Loss Parameter vs Diffusion Factor - 70% Span From Tip . . . . .	44
30	Rotor Loss Parameter vs Diffusion Factor - 90% Span From Tip . . . . .	45
31	Stator Inlet Air Angle and Mach Number Distribution - Design Equivalent Rotor Speed . . . . .	46
32	Stator Blade Element Performance - 5% Span From Tip . . . . .	47
33	Stator Blade Element Performance - 10% Span From Tip . . . . .	48
34	Stator Blade Element Performance - 15% Span From Tip . . . . .	49
35	Stator Blade Element Performance - 30% Span From Tip . . . . .	50
36	Stator Blade Element Performance - 50% Span From Tip . . . . .	51
37	Stator Blade Element Performance - 70% Span From Tip . . . . .	52
38	Stator Blade Element Performance - 85% Span From Tip . . . . .	53
39	Stator Blade Element Performance - 90% Span From Tip . . . . .	54
40	Stator Blade Element Performance - 95% Span From Tip . . . . .	55
41	Stator Loss Parameter vs Diffusion Factor - 10% Span From Tip . . . . .	56
42	Stator Loss Parameter vs Diffusion Factor - 30% Span From Tip . . . . .	57
43	Stator Loss Parameter vs Diffusion Factor - 50% Span From Tip . . . . .	58
44	Stator Loss Parameter vs Diffusion Factor - 70% Span From Tip . . . . .	59

ILLUSTRATIONS (Continued)

FIGURE	PAGE
45      Stator Loss Parameter vs Diffusion Factor - 90% Span From Tip . . . . .	60
46      Stator Static Pressure Coefficients, 10% Span From Tip, 100% Design Equivalent Rotor Speed . . . . .	61
47      Stator Static Pressure Coefficients, 90% Span From Tip, 100% Design Equivalent Rotor Speed . . . . .	62

SINGLE STAGE EXPERIMENTAL EVALUATION  
OF  
COMPRESSOR BLADING WITH SLOTS AND  
VORTEX GENERATORS

PART II - DATA AND PERFORMANCE FOR STAGE 5  
WITHOUT SLOTS OR VORTEX GENERATORS

J. A. BRENT AND B. A. JONES

PRATT & WHITNEY AIRCRAFT  
FLORIDA RESEARCH AND DEVELOPMENT CENTER

SUMMARY

An 0.8 hub/tip ratio, single-stage, subsonic compressor was designed and tested to establish baseline performance data for comparison with the results of subsequent tests planned for this stage, with slots added to the rotor and stator blades, and vortex generators added to the walls. A rotor blade failure occurred near the end of the baseline test program. Because of the poor performance of the stage and the rotor blade failure, the test program with slots and vortex generators for this stage was canceled.

The stage was designed with zero rotor prewhirl, axial discharge flow, and constant exit total pressure across the span. It was assumed that the rotor and stator blade element losses would be reduced by the addition of slots and vortex generators, and the design velocity diagrams and predicted performance were based on this assumption. Accordingly, the rotor design pressure ratio was 1.414 and the predicted adiabatic efficiency was 89.3% at a rotor tip velocity of 757 feet per second. The stage design pressure ratio (with slots and vortex generators) was 1.375 and the stage predicted adiabatic efficiency was 81.7%. Without slots and vortex generators the rotor predicted pressure ratio was 1.404 and the adiabatic efficiency was 87.3%. The stage predicted pressure ratio and adiabatic efficiency were 1.353 and 78.1%, respectively. The rotor and stator blading were designed with 65-series airfoil sections. Blade aspect ratios, solidities, and maximum thickness distributions were generally consistent with design practice for a compressor middle stage. At design equivalent rotor speed, the rotor achieved a maximum adiabatic efficiency of approximately 84%, and a corresponding pressure ratio of 1.365. High stator losses resulted in a stage maximum efficiency of 70%

and corresponding pressure ratio of approximately 1.30. Rotor failure occurred during operation at 110% of design equivalent rotor speed and was attributed to high blade stresses caused by bending flutter at high negative incidence angles.

#### INTRODUCTION

Experience with highly loaded, axial flow compressors has shown that the region of the flow path most critical to achieving high performance is that area adjacent to the walls. In the wall region, the three-dimensional aspects of the flow are extremely significant, whereas at midstream the flow is more nearly two-dimensional. The three-dimensional effects present with a highly-loaded stage result in a marked reduction in adiabatic efficiency and associated low total pressure ratio and flow near the wall. Because these factors generally represent a conversion of kinetic energy into internal energy at an increase in entropy, the diffusion limits for a conventional blade row are reached near the wall and stall or compressor surge is induced. Further, the wall diffusion limits prevent the utilization of the full-loading capacity of the mid-stream portion of the blade, as the stalled regions near the walls cause an increase of the midspan velocity with a corresponding decrease in midspan loading. These factors indicated that advanced compressor design concepts for the increase of allowable stage loading and stable, low-loss operating range should be addressed to the problem of three-dimensional flow near the walls.

Previous attempts to increase allowable stage loading limits by means of slotted blading under NASA Contract NAS3-7603 (Reference 1) indicated good performance for the blade midspan regions, but poor performance near the walls. The relative effectiveness of the slots at midspan and their ineffectiveness near the wall was attributed to the chordal placement of the slots and their inability to sufficiently reduce the three-dimensional flows in the wall region. To attain the full potential of highly loaded blading, methods must be developed to reduce the three-dimensional flow losses in this region.

A single-stage experimental investigation was initiated with the following three approaches for the improvement of blade element performance in the wall region.

1. Addition of blade end slots and secondary flow fences to Stage 3 of Contract NAS3-7603
2. Design and test of two new stages, designated 4 and 5, with relatively high work input (blade camber) near the walls to compensate for the high losses
3. Evaluation of blade slots and wall vortex generators added to Stages 4 and 5 to reduce the wall losses.

Experimental results obtained with Stage 3, modified with blade end slots and secondary flow fences, and including discussion of the design modifications, are presented in Reference 2. Discussion of the aerodynamic and mechanical design of Stages 4 and 5 is presented in Reference 3. This report presents the data and performance obtained with Stage 5 without blade slots or wall vortex generators. Rotor 5 failed during test due to bending flutter at high negative incidence angles. Because of the poor performance of this stage, it was decided not to rebuild the blading, and tests with slots and vortex generators were canceled for this stage.

TEST EQUIPMENT  
Facility

A schematic of the compressor test facility is shown in figure 1. The compressor is driven by a single-stage turbine, powered by exhaust gases from a J75 slave engine, with compressor speed controlled by means of the engine throttle. The slave engine exhaust gas is also used to power an ejector for compressor wall boundary layer suction. Air enters the compressor test rig through a 103-ft combined inlet duct, plenum and bellmouth inlet, and is exhausted through an exit diffuser to the atmosphere. The inlet duct contains a flow measuring orifice designed and installed in accordance with ASME standards. An area contraction ratio from plenum to compressor inlet of approximately 10:1 provided stagnation conditions in the plenum. The inlet duct and plenum were mounted on a track and could be rolled away from the compressor rig inlet to facilitate configuration changes.

Compressor Test Rig

A schematic of the single stage compressor rig is shown in figure 2, and the flowpath dimensions are given in figure 3. The hub/tip ratio

at the rotor inlet is 0.798, the test section has a constant hub diameter of 32.85 inches, and the outer wall converges from a diameter of 41.14 inches at the rotor leading edge to 39.99 inches at the stator exit. Relatively high convergence was provided at the rotor and stator tip to control the diffusion factors. Rotor bearing loads are transmitted to the rig support through struts located in the inlet and exhaust case assemblies. The inlet struts are sufficiently far upstream so their wakes are dissipated ahead of the rotor. The stage design specifications of zero rotor prewhirl and axial discharge flow eliminated the need for inlet and exit guide vanes. Flowrate was varied with a set of motor-driven throttle vanes located in the exhaust case.

Porous walls were installed for boundary layer suction at the rotor tip and the stator hub and tip as shown in figure 4. The porous wall was 0.060-inch thick, and had 0.066-inch diameter holes on 0.187-inch centers, providing an 11% open area.

#### Instrumentation

Instrumentation was provided to obtain overall and blade element performance data for each blade row. The locations of axial instrumentation stations are indicated in figure 3. Axial and circumferential locations of the instrumentation are shown in figure 5.

Airflow was measured with the ASME standard thin plate orifice located in the inlet duct. Rotor speed was measured with an electromagnetic sensor mounted adjacent to a 60-tooth gear on the rotor shaft. Gear tooth passing frequency was displayed as rpm on a digital computer. Rotor rpm was also recorded on magnetic tape. Inlet total temperature was measured in the inlet plenum by means of six half-shielded total temperature probes; inlet total pressure was measured in the plenum by means of five Kiel-type total pressure probes. Six equally spaced static pressure taps were located on both the inner and outer walls, upstream of the rotor (station 0). From a rig calibration over a wide range of weight flows, a correlation between these static pressures and weight flow was derived and used to check subsequent weight flow measurements.

Stage exit total temperature was measured at nine radial positions at each of four circumferential locations, using shielded thermocouples installed in radial rakes at stations 2A and 3. The stage exit temperature distributions measured with these radial rakes were used for rotor performance calculations. Redundant total temperature measurements at stations 1, 2, and 2A were provided by means of thermocouples in the 20-degree wedge traverse probes located at each of these stations.

One 20-degree wedge traverse probe was provided at station 1 to measure rotor inlet total pressure and air angle. Two 20-degree wedge traverse probes were located at station 2 (rotor exit) for total pressure and air angle measurement; rotor exit total pressure was also measured at five radial positions at one circumferential location with a Kiel head rake. Three circumferential total pressure rakes were installed at station 2A (stator exit) for total pressure measurement. One probe had circumferential rakes located at 5, 30, and 85% span; the second probe had rakes at 15, 50, and 95% span; and the third probe had rakes at 10, 70, and 90% span. Two 20-degree wedge probes were located at station 2A for the measurement of stator exit air angle. Five rotor blades were each instrumented with three strain gages. These strain gage outputs were displayed on oscilloscopes and visually monitored during tests. Gage locations were determined with the aid of stresscoat and verified by a fatigue test.

Static pressures at stations 1, 2, and 2A were measured by means of 8-degree wedge traverse probes. Four inner wall and four outer wall static pressure taps, approximately equally spaced, were located at each of these axial stations. The pressure taps ahead of and behind the stator were located on extensions of the midchannel streamlines. Stations 2 and 2A also had four inner and four outer wall taps installed across a vane gap to measure the static pressure variation across the gap. Twenty static pressure taps were equally spaced between 20 and 83% chord at 10 and 90% span on two stator blades, as shown in figure 6.

Total pressure and temperature rakes are shown in figure 7. A typical circumferential total pressure rake is shown in figure 8. Twenty-degree and 8-degree wedge traverse probes are shown in figure 9. Steady-state pressure data were measured with a multichannel pressure transducer

scanning system that includes automatic data recording on computer cards. Steady-state temperature measurements were also automatically recorded on computer cards by a multichannel scanning system in conjunction with a temperature reference oven and a digital voltmeter. Traverse and transient pressure data were recorded on magnetic tape, at up to 600 samples per minute per channel. Two static pressure taps located in the plenum, two of the outer wall pressure taps at station 0, and the total pressure radial rake at station 2A (188 degrees in figure 5), were close-coupled to transducers for transient recording during operation into and out of stall. A high-response pressure transducer, mounted in a total pressure probe at 10% span from the tip behind the rotor was used to detect the initiation of rotating stall. The Kistler output was recorded on magnetic tape and correlated in time with the transient recording of bellmouth static and stage exit total pressures.

#### Blading Design

##### Design Approach

An important premise for the Stage 5 blading design was the assumption that slots and vortex generators would reduce the rotor and stator blade element losses below the levels of loss that were established as a function of loading from the data of Reference 4 through 9 (see Reference 3). Additionally, it was specified that the rotor inlet and stator exit velocities were to be axial, and that the stator exit total pressure was to be constant across the span. A design rotor tip velocity of 757 feet per second provided the desired tip inlet relative Mach number of approximately 0.8.

The design velocity diagrams were calculated by means of a computer program which solves the continuity, energy, and radial equilibrium equations for an axisymmetric flow. Radial gradients of enthalpy and entropy were included in the calculation, and the influence of wall and streamline curvature on the radial distribution of static pressure were taken into account.

Rotor and stator design velocity diagrams were selected in accordance with the foregoing assumption, design requirements and calculation procedure. NACA series 65 blade sections with  $A = 1.0$  meanlines were selected for the rotor and stator blading to be consistent with the blading

used under the Contract NAS3-7603 program (Reference 1). Other blade geometry variables such as chord length, aspect ratio, solidity, and maximum thickness were the same as, or very similar to, those for the NAS3-7603 blading (slight departures in aspect ratio and hub/tip ratio resulted from the wall convergence at the rotor and stator tip that was provided to limit the diffuser factors).

Design incidence (minimum loss) and deviation angles were calculated using the appropriate equations in Reference 10. For the rotor, two degrees were subtracted from the calculated incidence angles in accordance with the minimum loss incidence results obtained under the NAS3-7603 program.

Rotor and stator design velocity diagram data, blade element geometry data, and predicted performance for Stage 5, designed on the assumption that there would be reduced losses due to slots and vortex generators, are presented in Reference 3.

#### Design Predictions Without Slots And Vortex Generators

Velocity diagrams and overall performance were calculated for the Stage 5 blading without assuming reduced losses due to slots and vortex generators to provide comparative data for test results obtained with the baseline stage. The results of these calculations, together with the Reference 3 design geometry data, are presented in tables B1 and B2 of Appendix B. Symbols and performance variables are defined in Appendix A.

#### PROCEDURES Test Procedures

##### Wall Bleed Flow Selection

Provision was made for wall boundary layer bleed at the rotor tip and the stator hub and tip. Since the rotor and stator bleed flows were independently controlled, the rotor bleed flow was selected prior to determining the stator bleed flow. With the compressor operating at near design conditions, total pressures at 5% span from the tip downstream of the rotor, and 5 and 95% span downstream of the stator, were

monitored as the rotor and then the stator bleed flows were varied between zero and maximum. The maximum bleed flow (limited by the perforated shroud effective flow areas) provided the largest improvement in the observed total pressures and was therefore selected for both the rotor and stator.

#### Performance Tests

Overall and blade element performance data were obtained at 50, 70, 90 and 100% of design equivalent rotor speed. Four data points were recorded on each of the 50 and 70% speed lines, six on the 90% speed line, and ten on the 100% speed line to define stage performance between maximum attainable flow and near stall. The near stall point was determined on the basis of flow, stage exit pressure, and blade stresses monitored on oscilloscopes. At each test point, traverse surveys were followed by the recording of fixed pressure and temperature instrumentation data with the traverse probes withdrawn. Blade stresses were monitored during steady-state and stall transient operation at all rotor speeds.

The influence of wall boundary layer bleed flow on performance was evaluated at design equivalent rotor speed. Overall and blade element data were recorded for three bleed valve positions (fully open, half open, and closed) with the test rig throttle vanes positioned for stage operation at near design flow with maximum bleed flow. Overall and blade element data were also recorded for two bleed valve positions (fully open and half open) with the throttle vanes positioned for stage operation at near stall flow with maximum bleed. Stable operation of the stage at the latter throttle vane position could not be maintained with zero bleed.

Transient measurements of bellmouth static pressure, rotor speed, and stator exit total pressure were recorded ten times per second to define stall characteristics as the stage was operated into and out of stall. The output from a Kistler pressure transducer, mounted in a total pressure probe behind the rotor, was also recorded and correlated in time with the other transient measurements to detect the initiation of rotating stall. A typical plot of the transient data is compared with an oscillograph record of the Kistler transducer signal in figure 10.

## Data Reduction Procedures

### Steady-State Data

Data reduction was accomplished in two steps. The first step involved the use of two computer programs to: (1) convert millivolt readings to appropriate engineering units, and (2) provide a tabulated and plotted array of pressure, temperature and air angle data at each axial station. Conversion of data to absolute values, appropriate Mach number corrections, and correction of pressures and temperatures to NASA standard day conditions were performed in the second computer program.

The second step in the data reduction procedure involved the calculation of overall and blade element performance variables for the rotor and stator blades. The array of data provided in step one above was analyzed for the selection of radial distributions of pressure, temperature and air angle at each axial station for the overall and blade element performance computer program.

Pressure ratios were calculated for the rotor, and the rotor-stator stage. The rotor and stator exit total pressures were weighted according to local mass flow to obtain average values. The stator wake total pressures at each radial measuring station were mass averaged using the local total pressure in the wake and the 8-degree wedge probe static pressure to define local Mach number. Mass flux was then obtained from the relationship

$$\bar{m} = \frac{W\sqrt{T}}{PA} = \sqrt{\gamma g / R} M \left[ 1 + \frac{\gamma - 1}{2} M^2 \right]^{1/2} p/p$$

where T is the measured total temperature and A is the flow area associated with each total pressure tube. With the radial distribution of total pressure and mass flux calculated, the total pressures were mass-averaged in the radial direction. Behind the rotor, the total pressures obtained with the 20-degree wedge probes and the one Kiel probe were arithmetically averaged and the resulting radial distribution was mass-flow-averaged using the 8-degree wedge probe static pressure and stator exit radial temperature distribution to define weight flow.

Wall static pressure data at each station was used to check the 8-degree wedge probe data. In addition to the four equally-spaced static pressure taps in the outer wall at stations 2 and 2A, four taps were spaced across one stator gap to check the static pressure gradient associated with stator leading edges and/or wakes. These wall static pressures are compared with the 8-degree wedge probe data extrapolated to the wall in figure 11. The extrapolated pressures generally agree favorably with the local wall static pressure.

Stator exit total temperatures were used for the calculation of rotor blade element data and rotor efficiency.

Performance and velocity diagram calculations were performed for each blade row along design streamlines that pass through 5, 10, 15, 30, 50, 70, 85, 90, and 95% span at the rotor exit instrumentation station. The measured static pressures were used in conjunction with measured total pressures, total temperatures, and flow angles to define the velocity distributions at each axial station. The performance and velocity diagram data were calculated directly from the measurements obtained at the instrumentation stations. Translation of these measurements to the blade-row leading and trailing edges was not considered necessary because, with the small wall convergence, the data at the instrumentation stations very nearly approximates that at the leading and trailing edges.

#### Stall Transient Data

Bellmouth static pressure at incipient stall was determined from plots similar to the one shown in figure 10, and the corresponding weight flow was determined from the correlation of bellmouth static pressure and orifice flow shown in figure 12. Stage exit total pressure, also obtained from plots similar to the one shown in figure 10, were arithmetically averaged to obtain the general shape of the pressure ratio-flow characteristic up to the point of incipient stall. The steady-state data were extrapolated to the stall flow using the shape of the transient data curve as a guide line. Incipient stall points were determined in this manner for each rotor speed.

## PRESENTATION OF DATA

### Overall Performance

Overall performance data are presented in terms of pressure ratio and adiabatic efficiency as functions of corrected weight flow ( $W\sqrt{\theta}/\delta$ ) and equivalent rotor speed ( $N/\sqrt{\theta}$ ). Definition of the symbols and performance variables are presented in Appendix A. Overall performance for the rotor and stage are presented in figures 13 and 14. The solid symbol on the stall line is the stall point determined from the transient data. Also shown in these figures is the effect of boundary layer bleed flow on overall performance. Overall performance and bleed flow data for the steady-state data points are presented in table B-3 of Appendix B.

The rotor achieved an efficiency of 83.5% and a pressure ratio of 1.351 at design equivalent rotor speed and design corrected flow (110 lb/sec). Maximum rotor efficiency and corresponding pressure ratio were 84% and 1.365 respectively, compared with respective design values (without slots and vortex generators) of 87.3% and 1.404. The stage pressure ratio and efficiency at design equivalent rotor speed and flow conditions (see figure 14) were 1.277 and 66.8%, respectively, and maximum stage efficiency and pressure ratio were 70% and 1.30. Predicted pressure ratio is 1.353 and efficiency is 78.1% for Stage 5 without slots and vortex generators. The relatively poor rotor and stage performance is attributed to high total pressure loss at the rotor hub and tip, at the stator tip, and reduced midspan work due to the increased midspan axial velocity caused by the high losses near the wall. As indicated in figure 13, bleed flow had little effect on rotor pressure ratio. The improvement in efficiency between zero and maximum bleed is attributed to a decrease in mass average temperature, the result of bleeding high temperature air at the walls. The indicated improvement in efficiency includes the effect of both rotor and stator bleed flow, since stator exit temperature was used to calculate rotor efficiency. Both the pressure ratio and the efficiency of the stage were improved with bleed flow, as shown in figure 14. The improvement in stage pressure ratio was due to a reduction of the stator losses with increased bleed flow.

### Rotor Blade Element Performance

The rotor relative inlet air angle and Mach number distributions for design equivalent rotor speed are shown in figure 15. The design distributions (without slots and vortex generators) are included for comparison and, as indicated, the test data for near design corrected weight flow (110.97 lb/sec) agrees closely with the design values between 10 and 90% span. Within 5% span from the walls, the relative air angle increases rather sharply due to the low axial velocities in the wall boundary layer.

Rotor diffusion factor, deviation angle, and loss coefficient are shown as functions of incidence angle in figures 16 through 24. The losses in the hub and tip regions (15% of the span from either wall) are high, with loss coefficients of 0.25 to 0.35. Corresponding diffusion factors approximate values between 0.7 and 0.8. Between 30 and 70% span, the losses and diffusion factor are substantially lower. Deviation angles are 3 to 6 degrees greater than the indicated design values across the span.

An influence of rotor speed on loss coefficient is indicated for the data for the outer 50% of span. The higher loss coefficients at the higher rotor speed is probably due to the contribution of local shock-induced loss at inlet relative Mach numbers above the critical Mach number. For the blade section in the tip region, the estimated average critical Mach number is 0.68. At this Mach number, the loss coefficient is 40% larger than the loss coefficient at a Mach number of 0.40 (based on unpublished Pratt & Whitney Aircraft cascade data correlation). The inlet relative Mach number over the outer 50% span is equal to or greater than 0.68 for the data that corresponds to 90 and 100% of design equivalent rotor speed.

The variation of loss coefficient with the lower rotor speeds (50 and 70% of design equivalent rotor speed) in the outer 15% span region (figures 16, 17, and 18) may have been caused by the rotor tip bleed. At the lower corrected flows associated with the lower equivalent rotor speeds, the percentage of bleed flow was higher, as shown in figure 25. A second possible cause for the large variation of loss coefficient with

equivalent rotor speed in the outer 15% span region could be simply a Mach number dependency of secondary flow development in the wall adjacent flow at Mach numbers below the critical Mach number.

The effect of rotor tip bleed flow on blade element performance is indicated in figures 16, 17, and 18. Bleed flow resulted in a reduction of loss coefficient in the tip region, the amount of the reduction diminishing to zero at approximately 15% span. Examination of rotor inlet axial velocities and relative air angles in the tip region indicates that the higher bleed flows resulted in larger rotor incidence angles at a constant flow. However, it was observed at 5% span from the tip that the axial velocity ratio across the rotor,  $V_{z2}/V_{z1}$ , increased as the bleed flow was increased (Table I).

The corresponding loss coefficients at 5% span (see figure 16) vary from 0.43 at an incidence angle of -12.4 degrees for 0.12% bleed flow, to 0.265 at an incidence angle of -8.8 degrees for 1.24% bleed flow.

Table I. Rotor Axial Velocity Ratios at 5% Span From the Tip

<u>Orifice Flow</u>	Rotor Tip Bleed Flow (% Orifice Flow)	<u><math>V_{z2}/V_{z1}</math></u>
102.3	0.12*	0.793
101.5	0.66	0.837
101.8	1.24	1.055

\*Bleed valve leakage in closed position

Loss parameter versus diffusion factor is presented in figures 26 through 30. Correlation curves for the minimum loss data of References 4 through 9 and the Stage 5 design curves, are included in the figures for comparison with the data. The design curves are more optimistic than the data correlation curves because of the expected improvement from slots and wall vortex generators. For design equivalent rotor speed, the loss parameter values at 30 and 50% of span from the tip that correspond to minimum loss in figures 19 and 20 are approximately equal to the corresponding data correlation values. At the other span locations, the minimum loss parameter values are larger than the data correlation values.

### Stator Blade Element Performance

The stator inlet Mach number and air angle distributions for design equivalent rotor speed are shown in figure 31. The stator was operating with less than design incidence, at 25 to 75% span over the entire flow range. Design incidence at the tip section occurred at a flow of 116.37 pounds per second whereas design incidence at the hub section occurred at a flow of 110.97 pounds per second.

Stator diffusion factor, deviation angle, and loss coefficient are presented as functions of incidence angle in figures 32 through 40. The diffusion factors are lower than the indicated design values across the entire span, primarily because of the relatively large deviation angles seen in the figures and the associated high exit tangential velocities (see Table B-4 of Appendix B). The low diffusion factors in the hub region are also attributed to relatively high axial velocities compared to the tip region velocities and to the hub design axial velocity. Stator losses are high relative to the indicated predicted losses (without slots and vortex generators) across the entire span. There is an apparent Mach number effect on the minimum or choking incidence angle at all radial positions, and the effect on minimum loss appears to be minimal.

The effect of bleed flow on stator performance for design equivalent rotor speed is also indicated in figures 32 through 40. Increasing the bleed flow had little effect on the stator tip region performance, apparently because the high rotor tip loss precluded the effectiveness of the stator tip bleed. However, increasing the bleed flow produced a noticeable reduction of loss coefficient in the hub region.

Loss parameter is shown as a function of diffusion factor in figures 41 through 45. Correlation curves for the minimum loss data of References 4 through 9, and the Stage 5 design curves are included in the figures for comparison with the data. The design curves are more optimistic than the data correlation curves because of the expected improvement from slots and vortex generators. For design equivalent rotor speed, the loss parameter values corresponding to minimum loss are larger than the data correlation values except at midspan, where they are approximately equal.

Pressure coefficient distributions for the stator suction surface at 10 and 90% span from the tip are shown in figures 46 and 47. Data are shown for only one of the two sets of static pressure taps at 10% span because of the difference in level between the two sets. At near-design incidence, the static pressure rise at the hub was greater than the static pressure rise at the tip. This observation is consistent with the stator loss data. A slight effect of hub bleed flow on pressure rise is noticeable in figure 47. At approximately -5 degrees incidence the static pressure coefficient at 83% chord is slightly greater than the static pressure coefficient without bleed flow. The abrupt change in static pressure coefficient in the midchord region in figure 47 is thought to be associated with the stator vane spindle attachment. In this region the shroud bleed holes are blocked. It is noted that the abrupt change in static pressure coefficient does not occur for the near stall or zero bleed flow distributions.

#### CONCLUSION

Blade element and overall performance data were obtained over a range of rotor speeds from 50 to 100% of design equivalent rotor speed for a rotor and stator that were highly cambered near the walls to compensate for high wall losses. Poor performance of this stage, and failure of the rotor near the end of the baseline test program precluded testing this stage at 110% of design equivalent rotor speed or subsequent tests of the stage with slots and wall vortex generators added to reduce wall losses. The rotor failure was attributed to high rotor blade stresses caused by bending flutter at high negative incidence angles. The rotor produced a maximum efficiency and corresponding pressure ratio of 84% and 1.365, respectively, compared with respective design predictions (without slots and vortex generators) of 87.3% and 1.404. High stator losses resulted in a stage maximum efficiency of 70% and corresponding pressure ratio of 1.30 compared with respective design predictions (without slots and vortex generators) of 78.1% and 1.353. Therefore, the relatively high blade work near the walls for rotor 5 did not adequately compensate for the secondary flow and associated high losses that were generated in these regions. The resultant losses in the blade-end regions were larger than those indicated in the correlation of data from References 4 through 9.

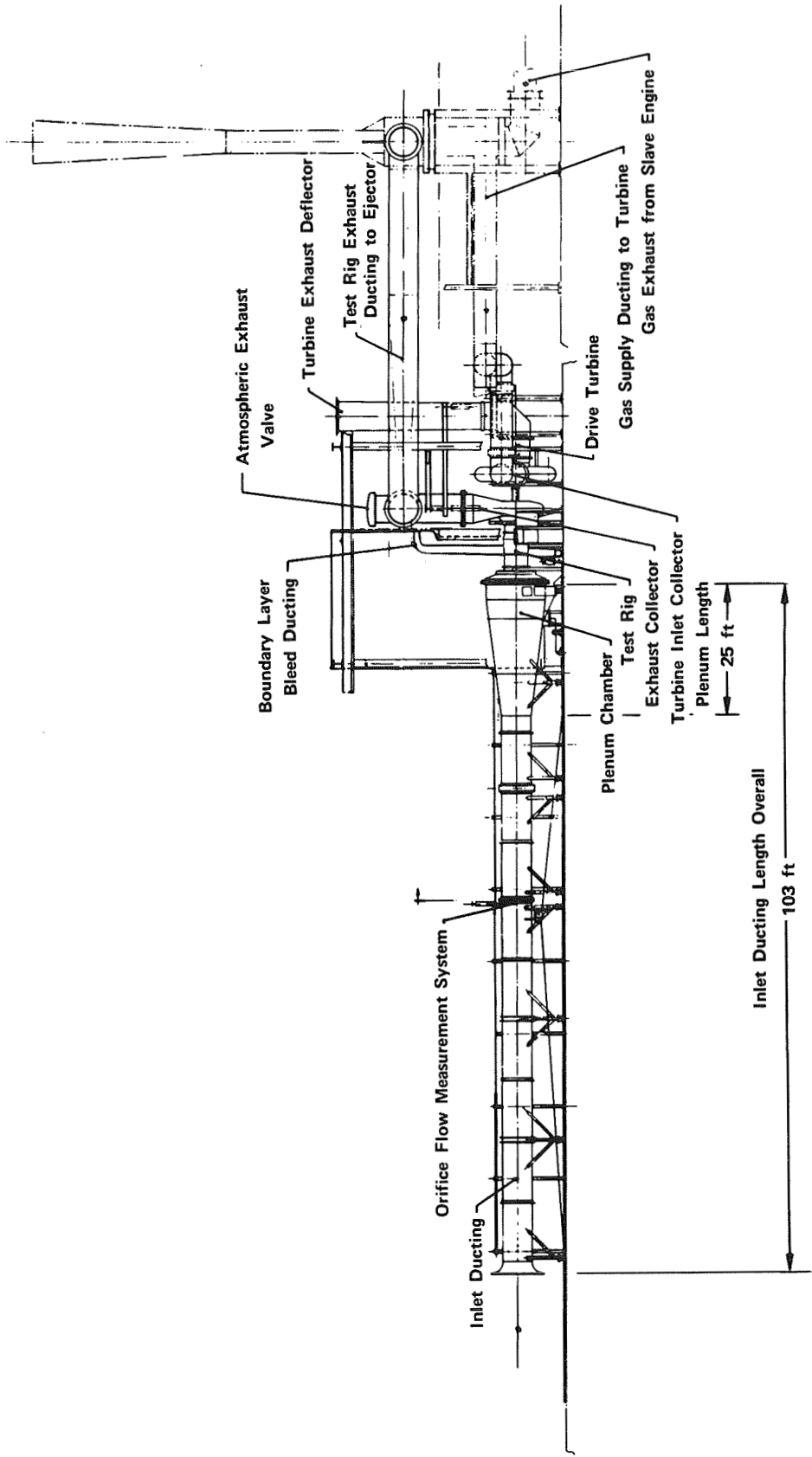


Figure 1. Compressor Research Facility

FD 10891B

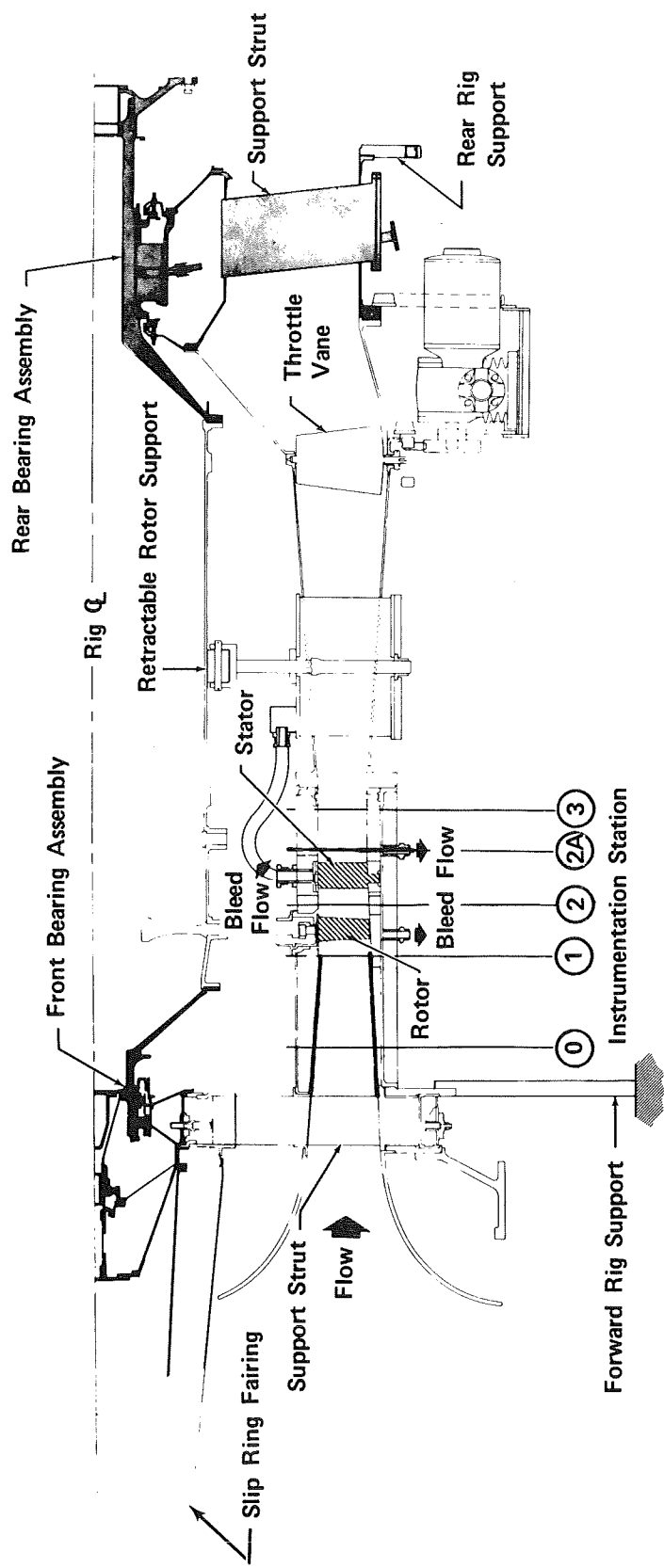


Figure 2. Single Stage Compressor Rig

FD 14681B

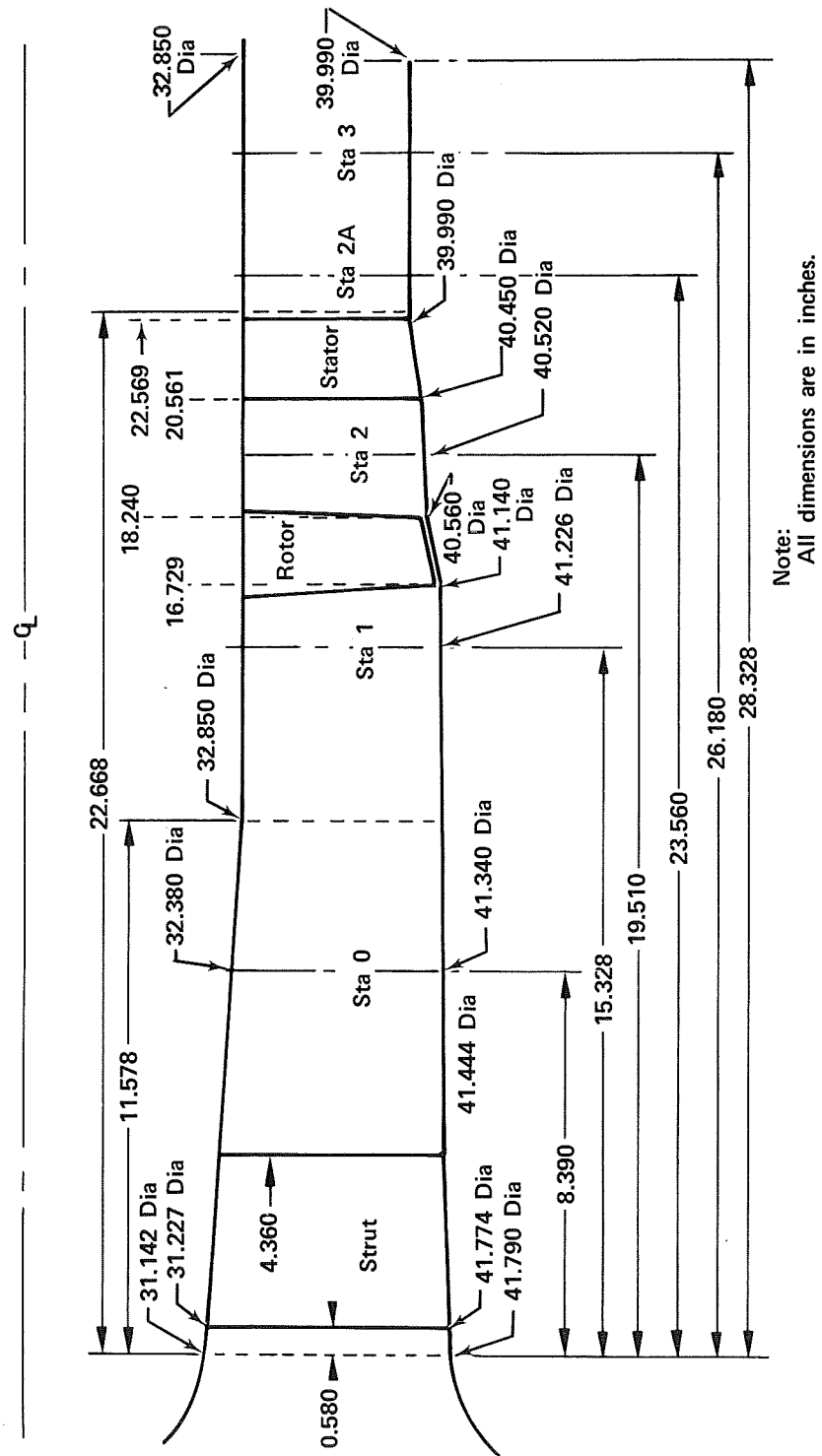


Figure 3. Flowpath Dimensions

FD 34364

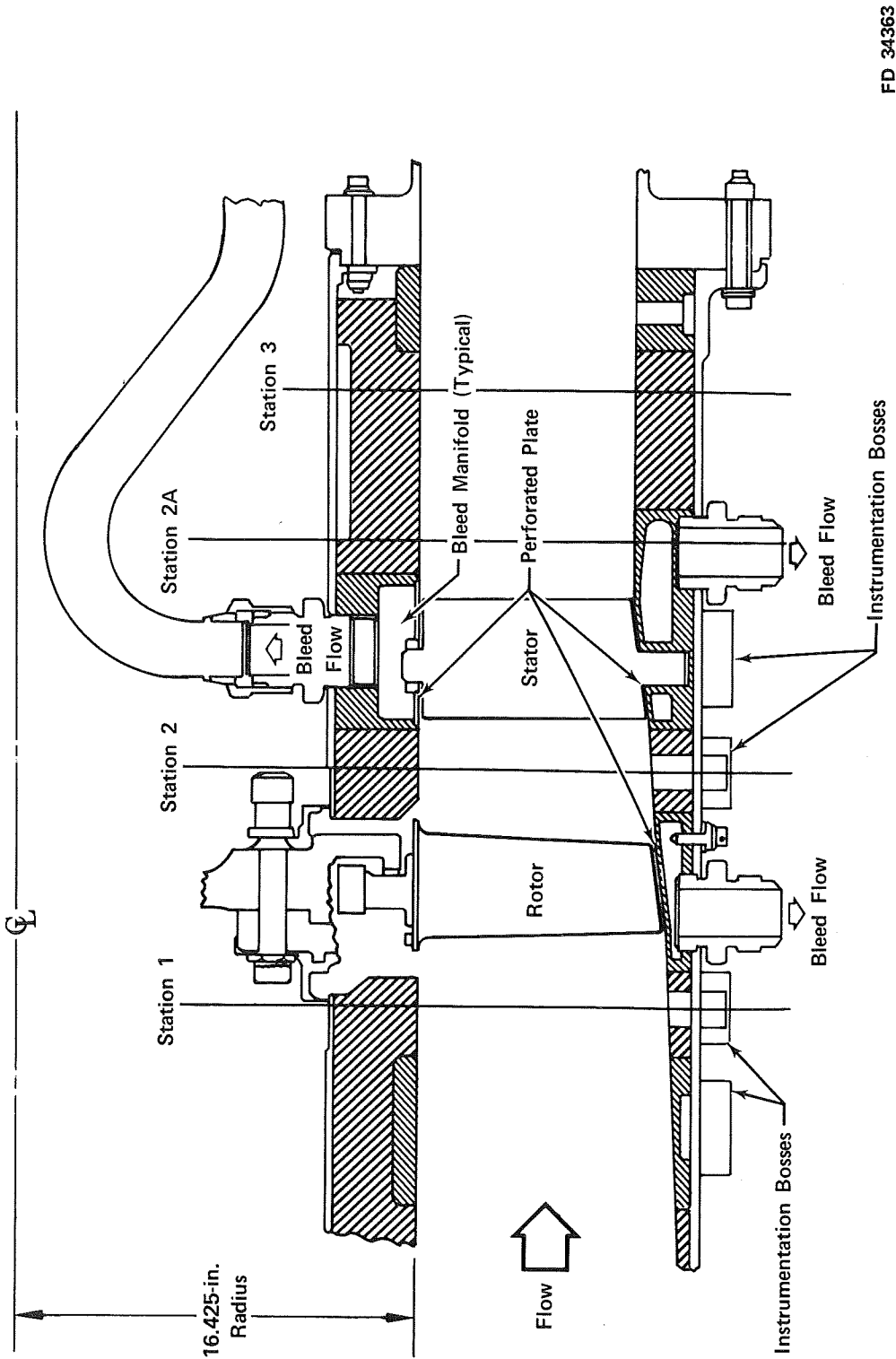
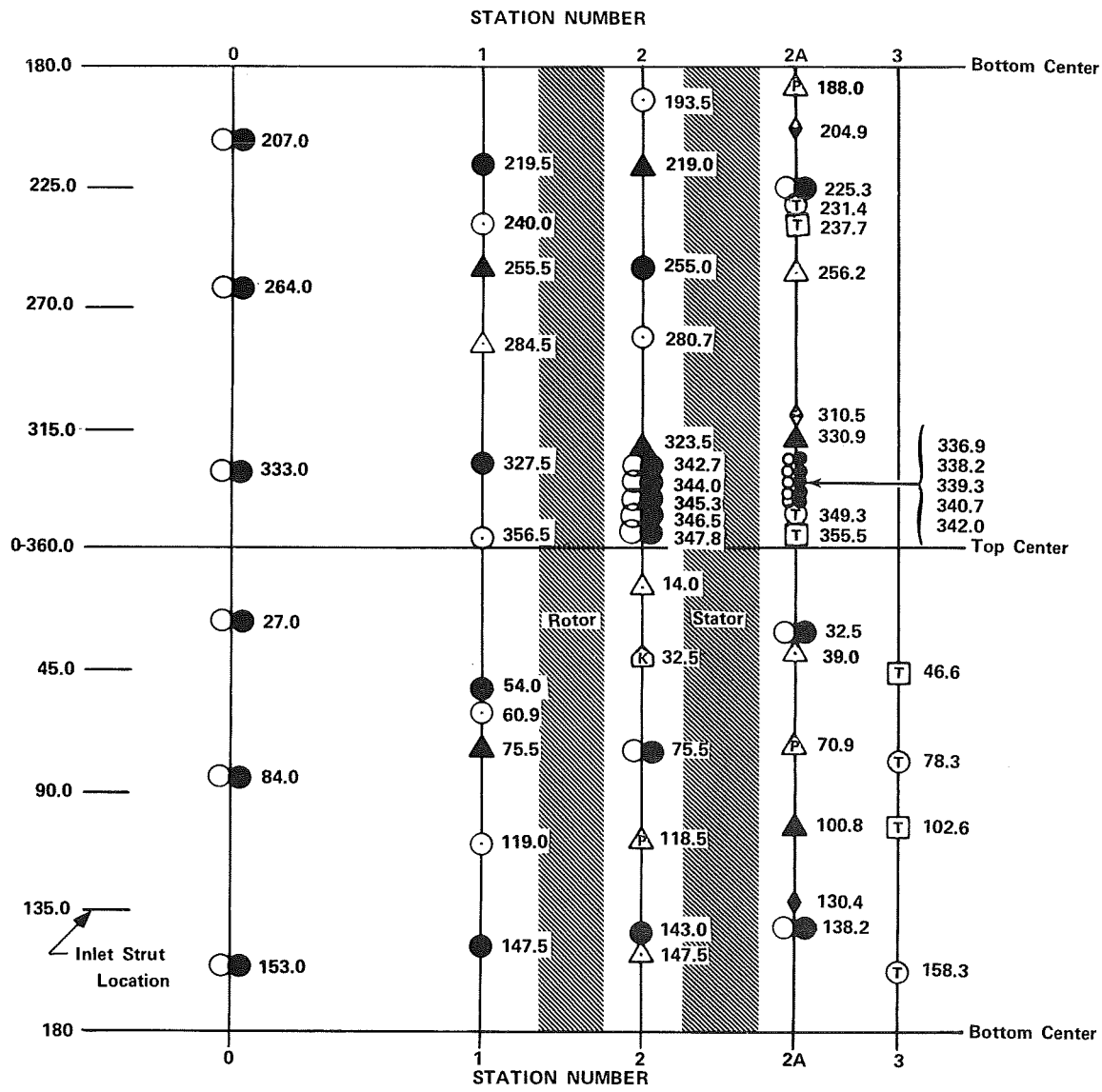


Figure 4. Boundary Layer Bleed System



**Symbol Definition**

- Inner Wall Static
- Outer Wall Static
- △ Traverse Probe - 20° Wedge
- ▲ Traverse Probe - 8° Wedge
- Kistler - 10% Span

- ▲ Total Pressure Radial Rake - 10, 30, 50, 70 and 90% Span
- ◆ Circumferential Total Pressure Rake - 15, 50 and 95% Span
- ◆ Circumferential Total Pressure Rake - 10, 70 and 90% Span
- ◆ Circumferential Total Pressure Rake - 5, 30 and 85% Span
- (T) Total Temperature Radial Rake - 10, 30, 70 and 90% Span
- [T] Total Temperature Radial Rake - 5, 15, 50, 85 and 95% Span

**Note:**

All measurements in degrees

FD 34366

Figure 5. Instrumentation Layout

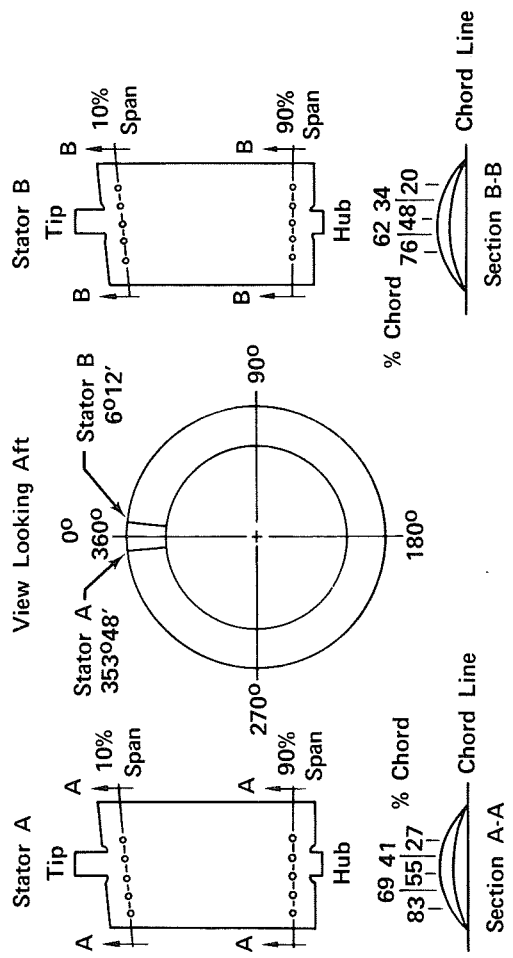


Figure 6. Stator Static Pressure Instrumentation

ID 34362

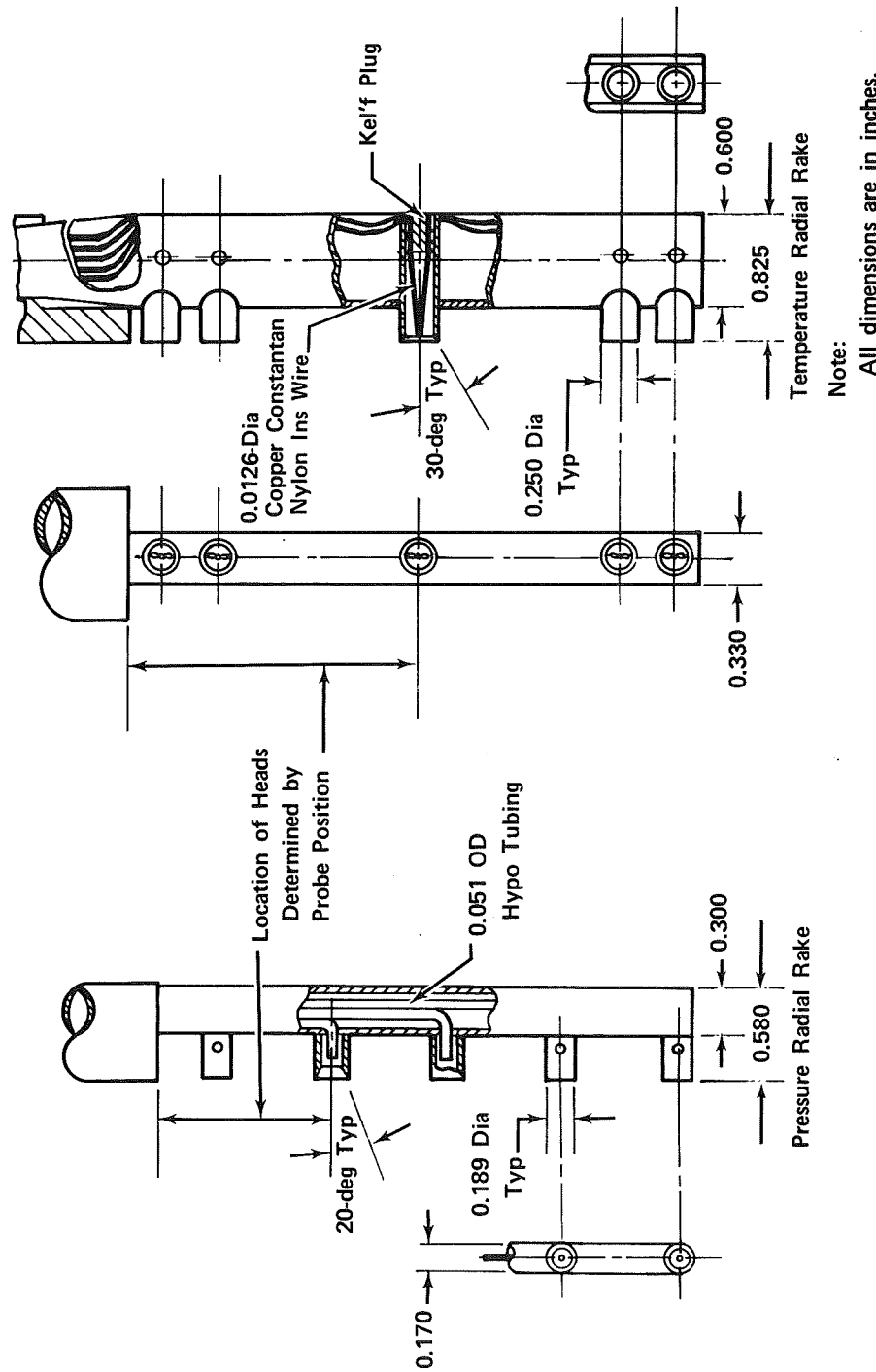
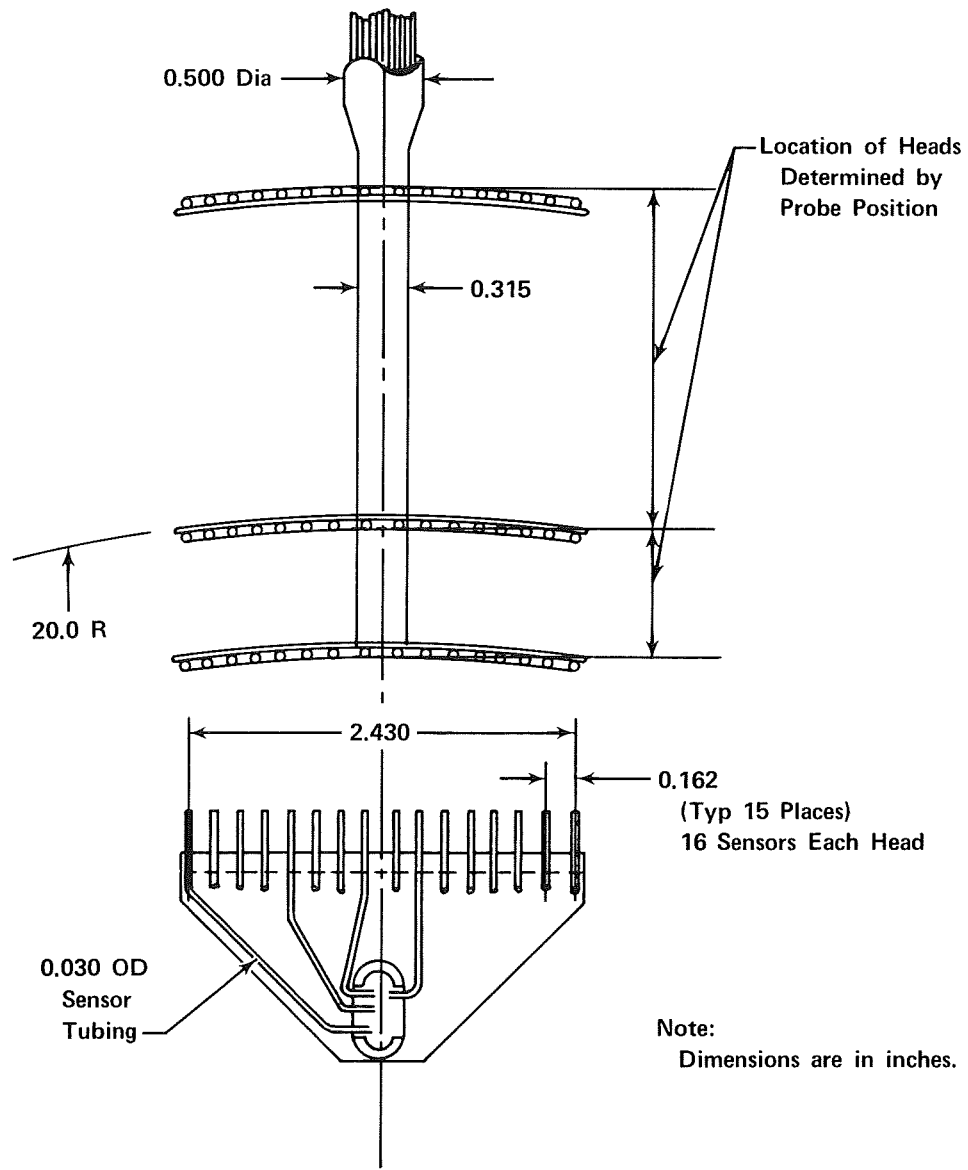


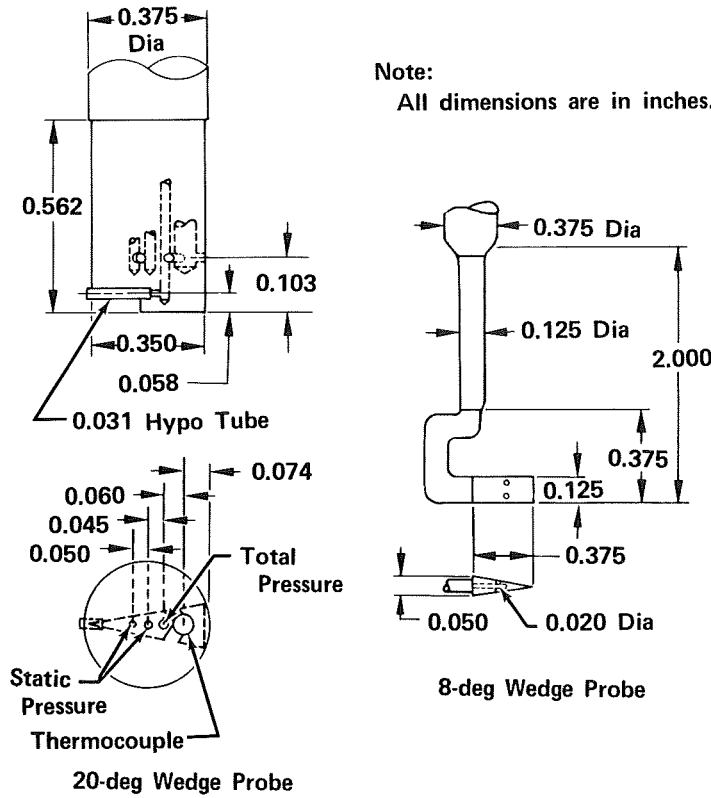
Figure 7. Total Pressure and Temperature Rakes

FD 34361



FD 34365

Figure 8. Circumferential Total Pressure Rake



FD 18483B

Figure 9. Wedge Traverse Probes

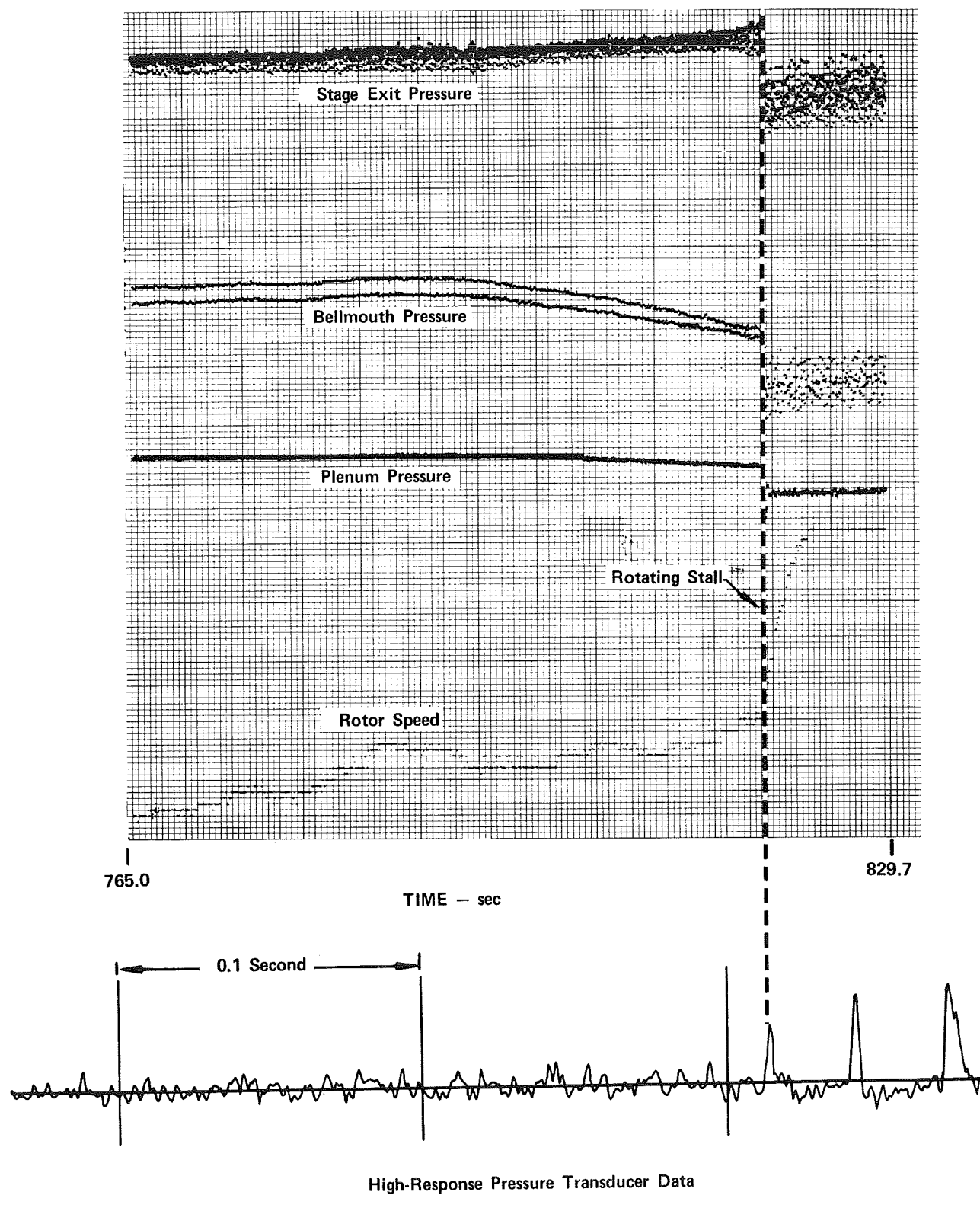


Figure 10. Typical Stall Transient Data

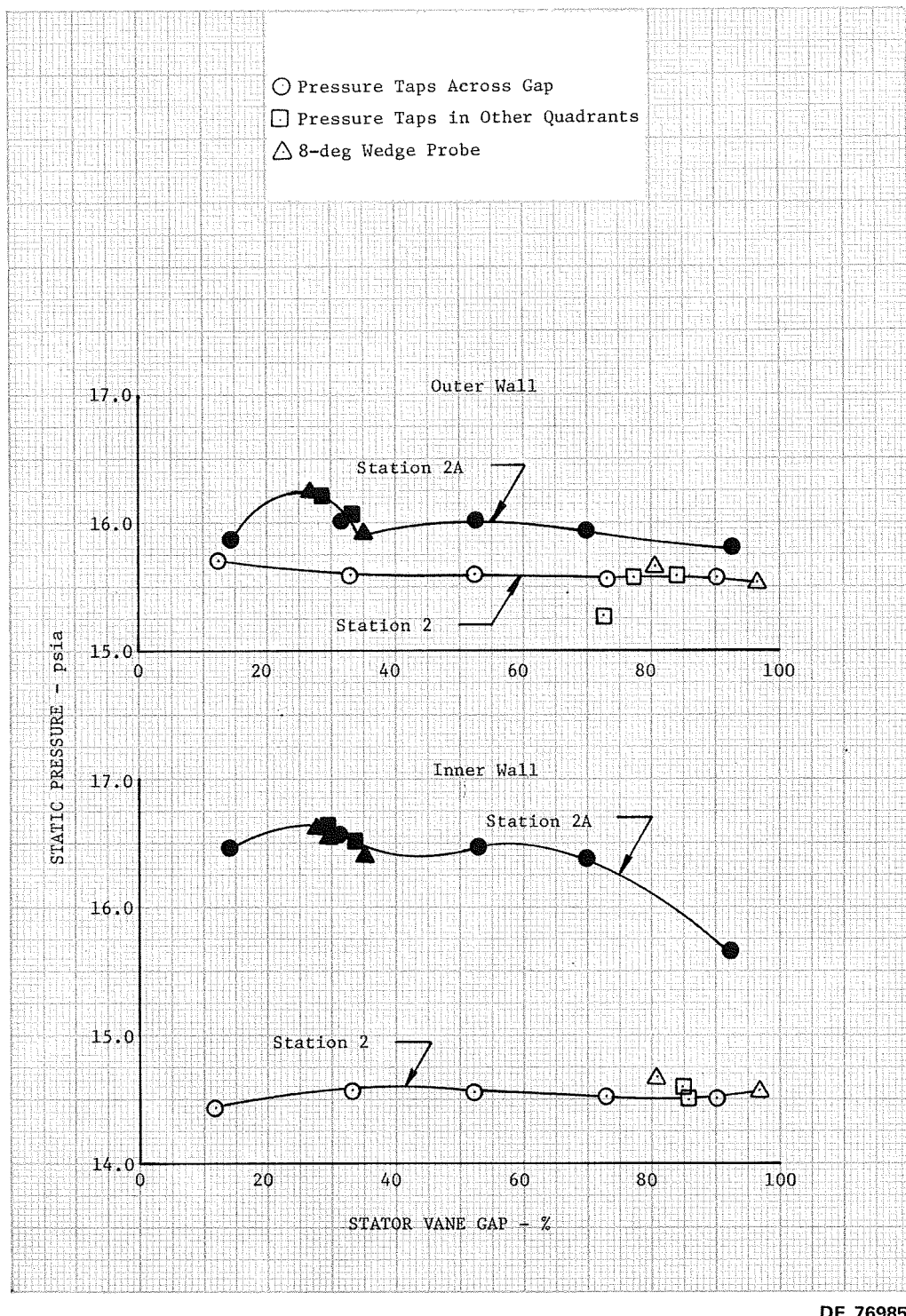


Figure 11. Comparison of Stator Inlet and Exit Wall  
Static Pressures at Near Design Flow Conditions

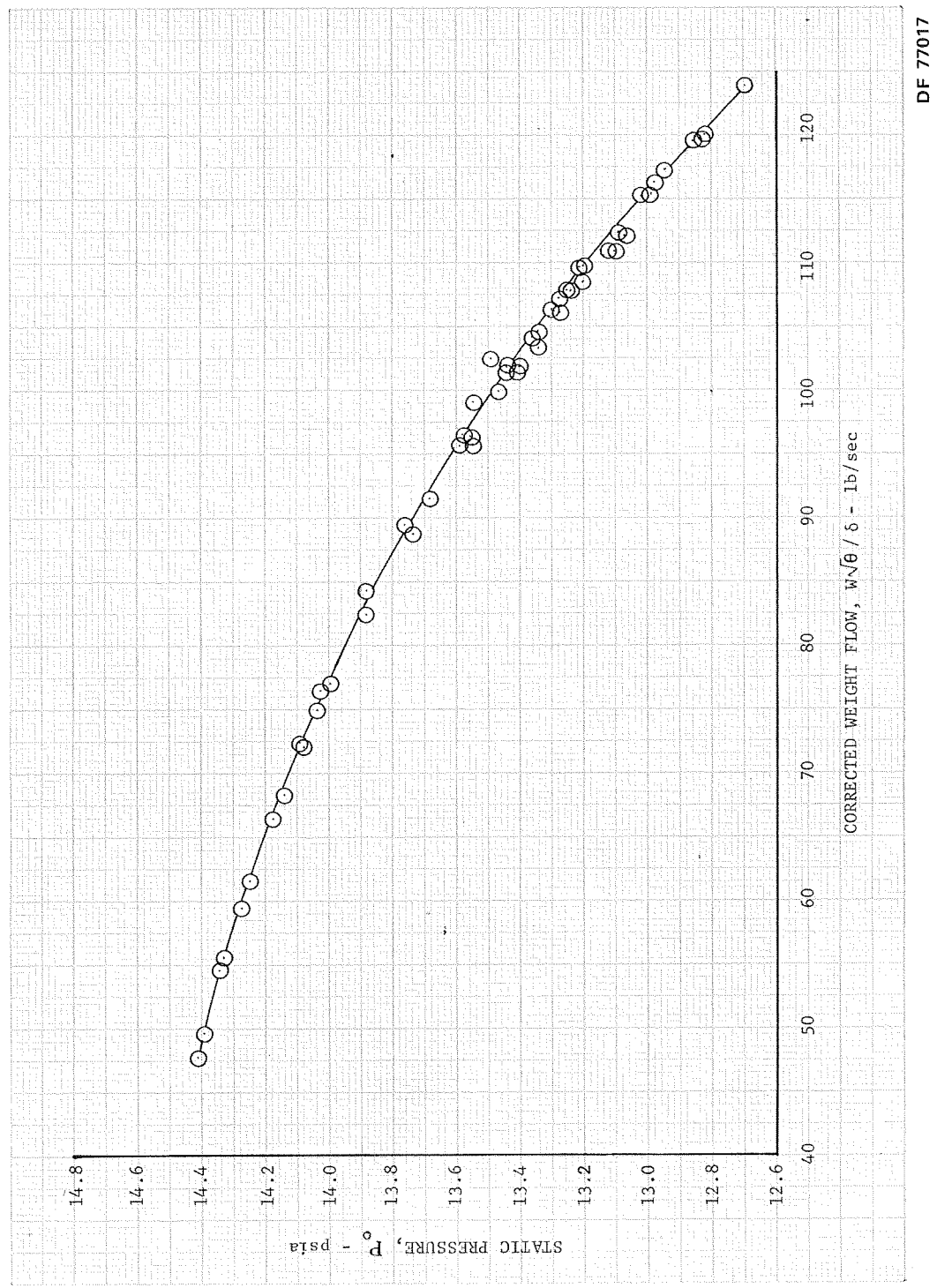
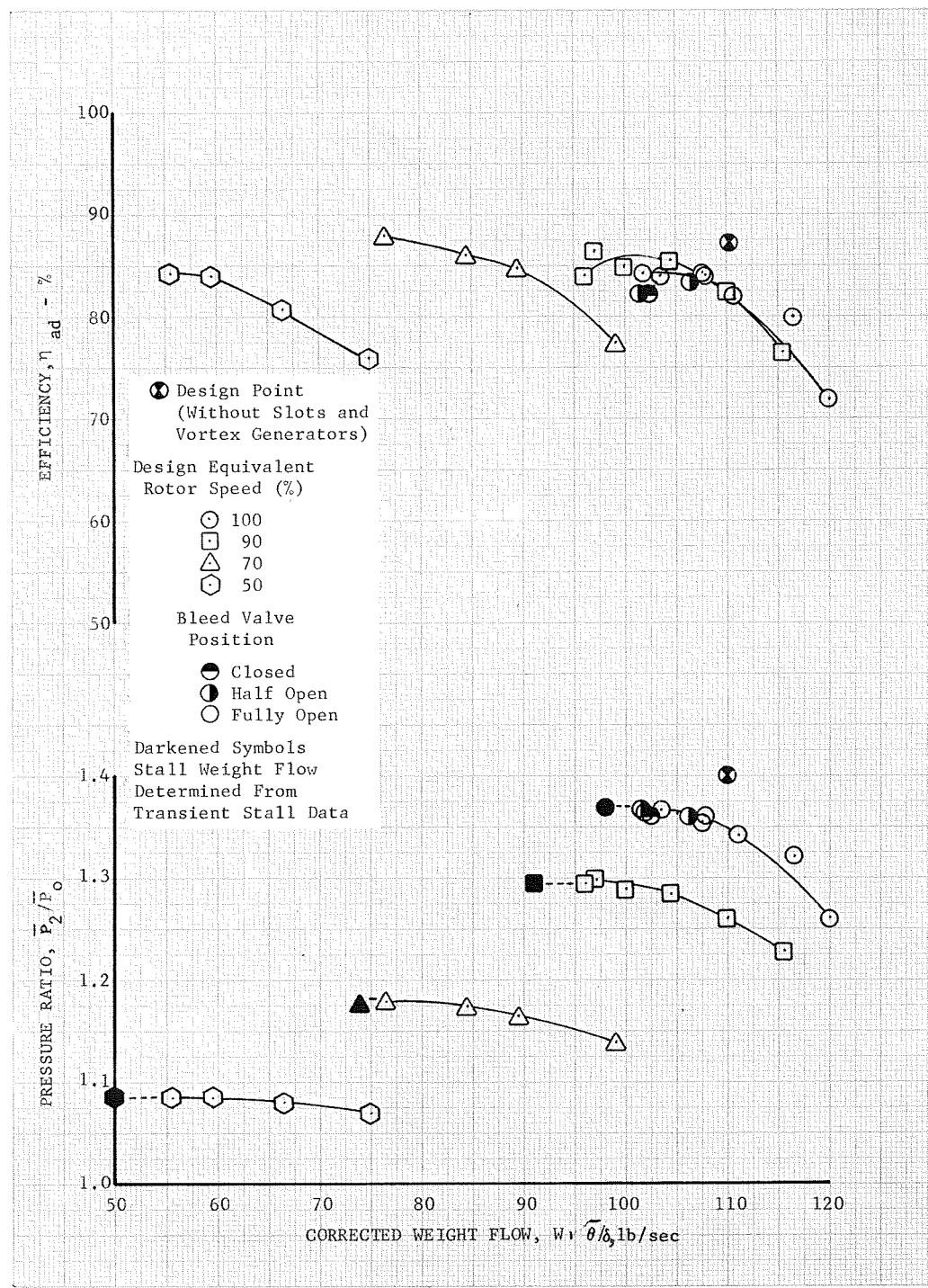


Figure 12. Station 0 Corrected Static Pressure vs Corrected Weight Flow



DF 76996

Figure 13. Overall Performance - Rotor

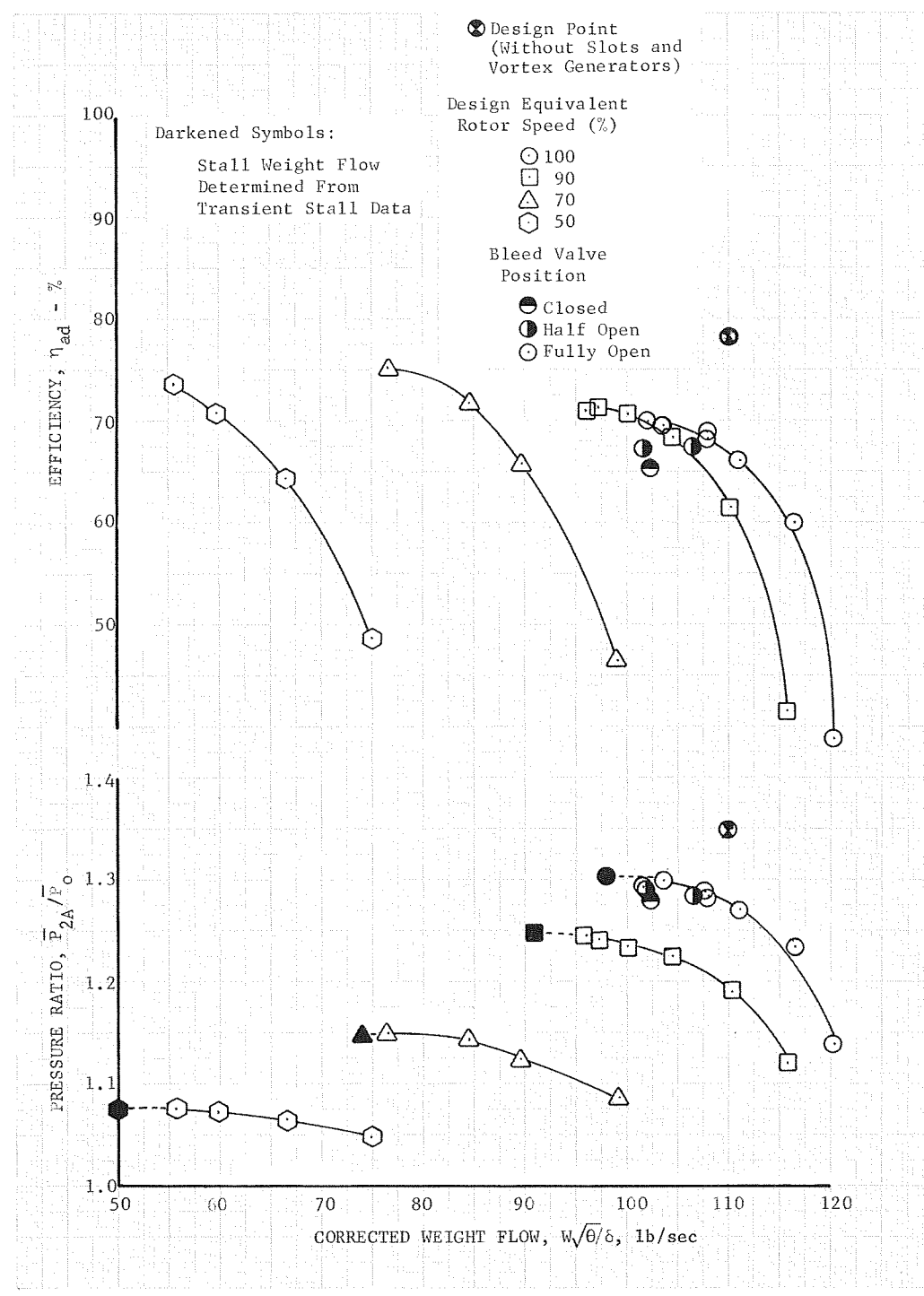


Figure 14. Overall Performance - Stage

DF 76995

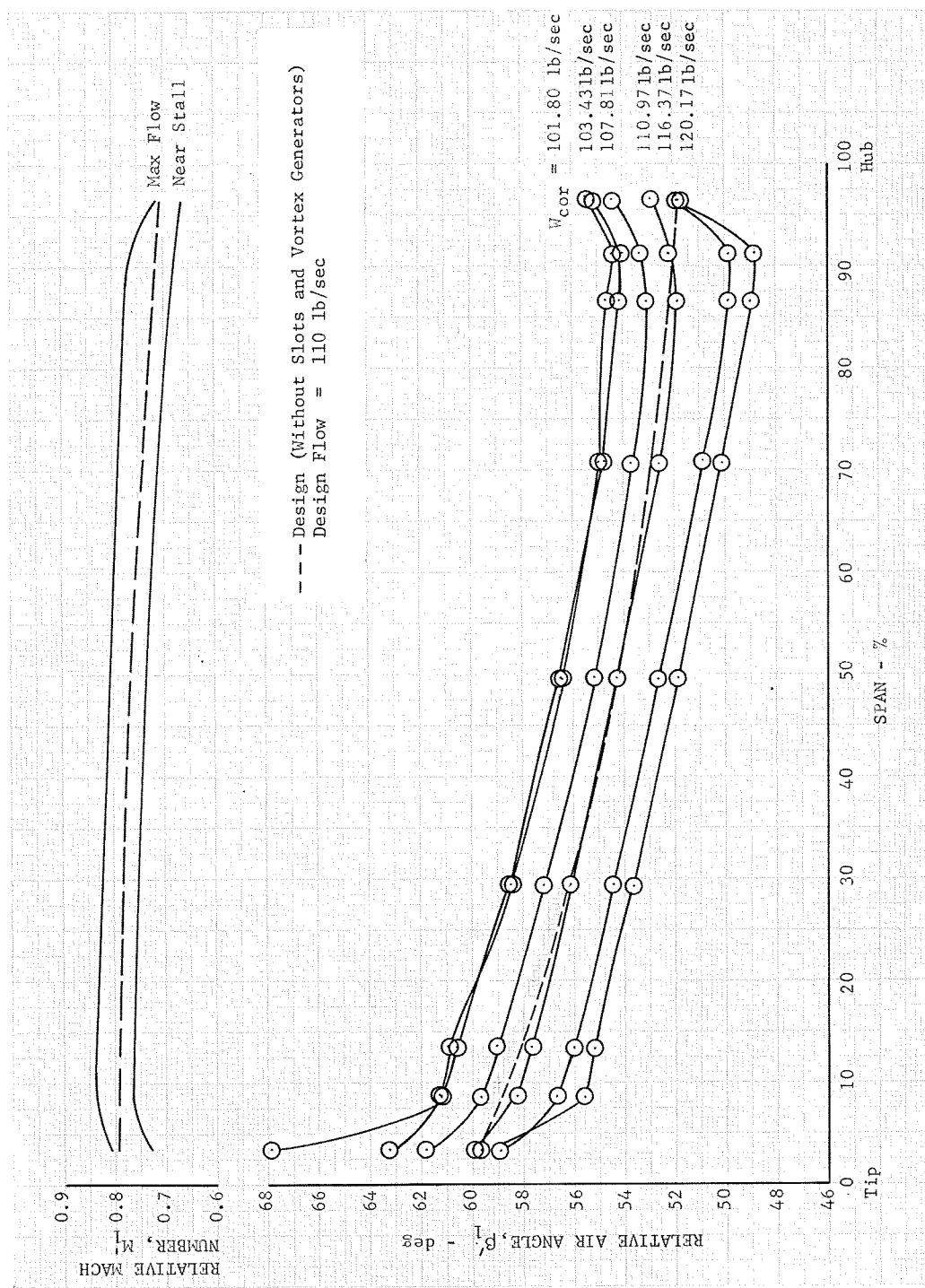
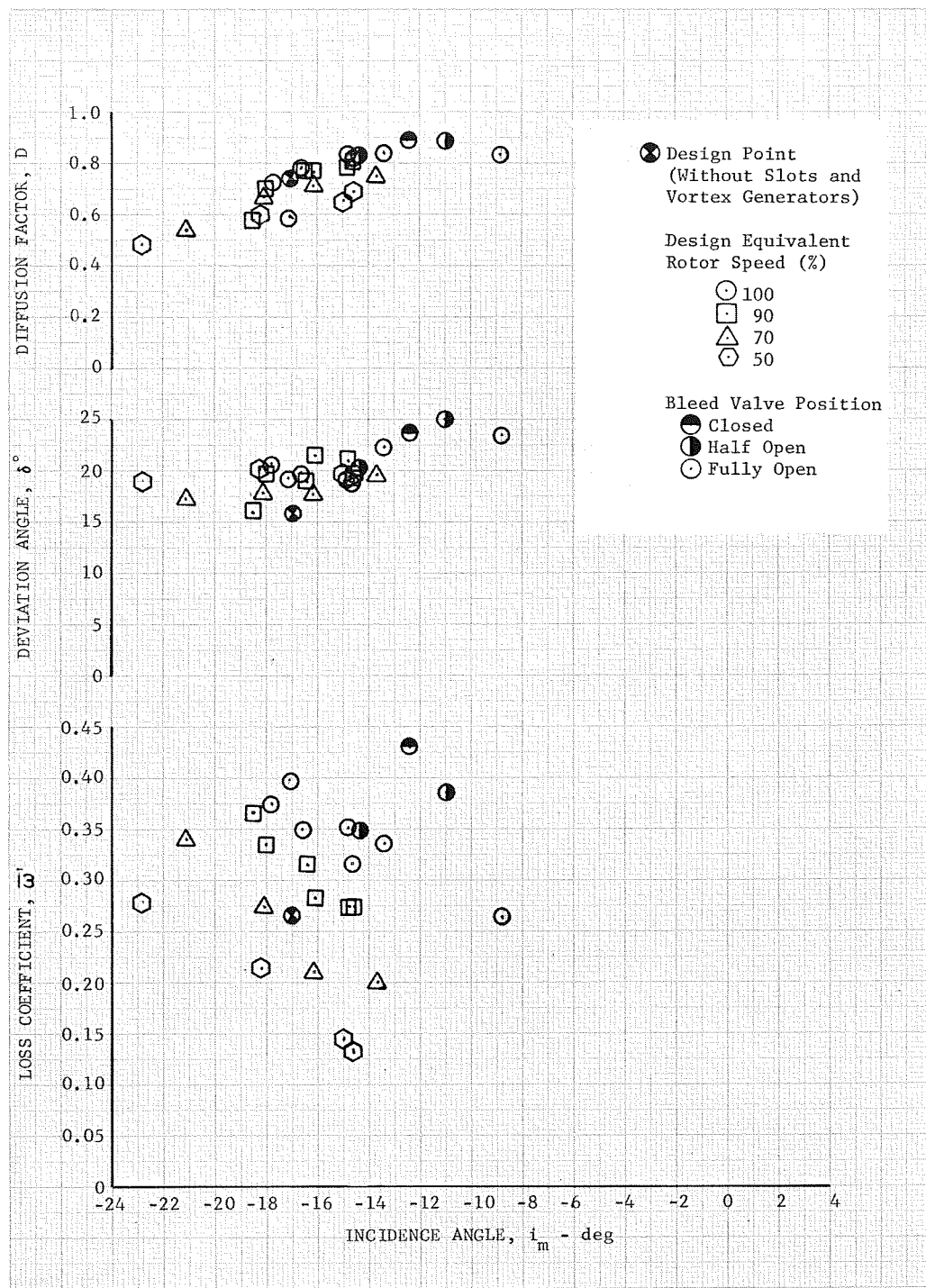


Figure 15. Rotor Inlet Relative Air Angle and Mach Number Distributions - Design Equivalent Rotor Speed

DF 77018



DF 76988

Figure 16. Rotor Blade Element Performance -  
 5% Span From Tip

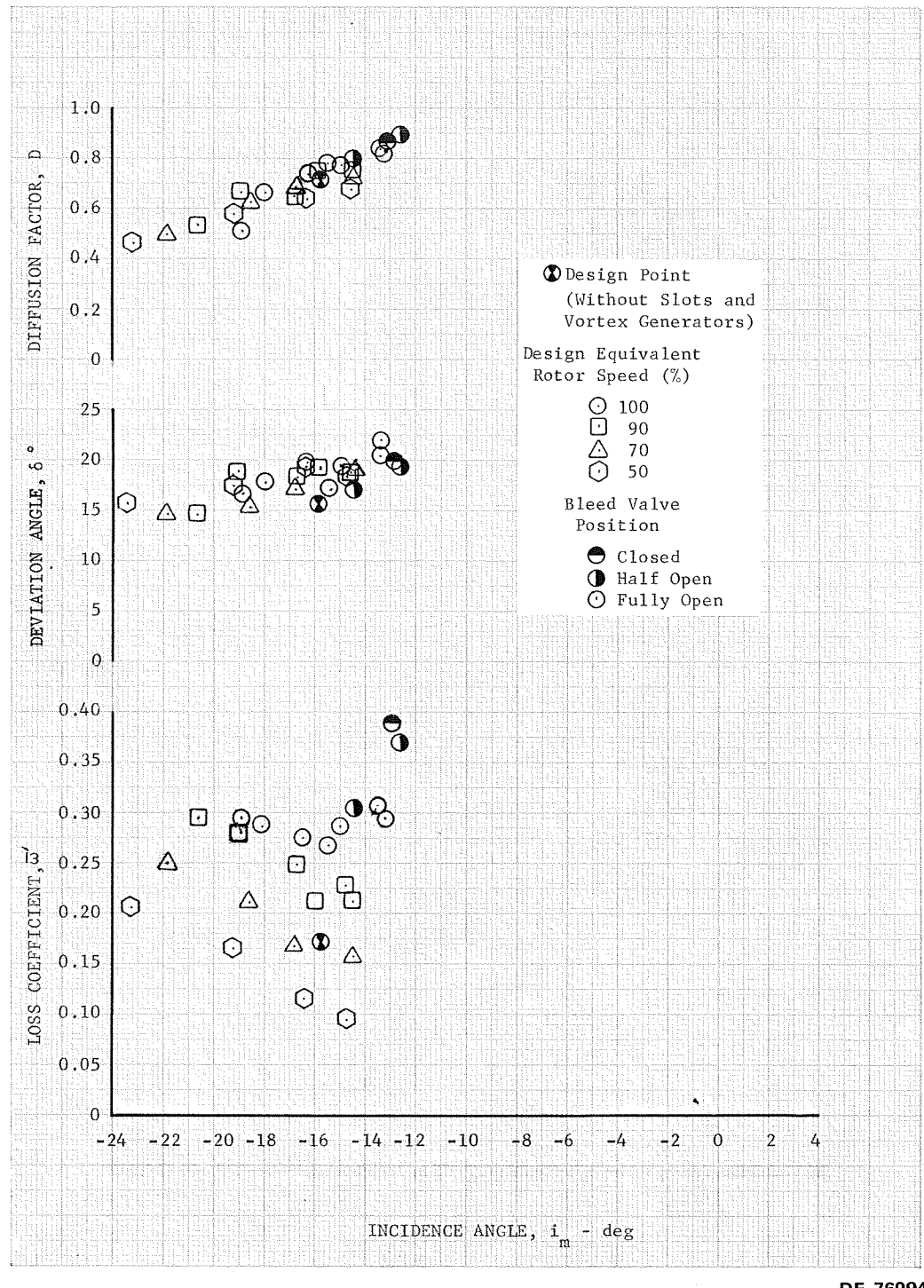
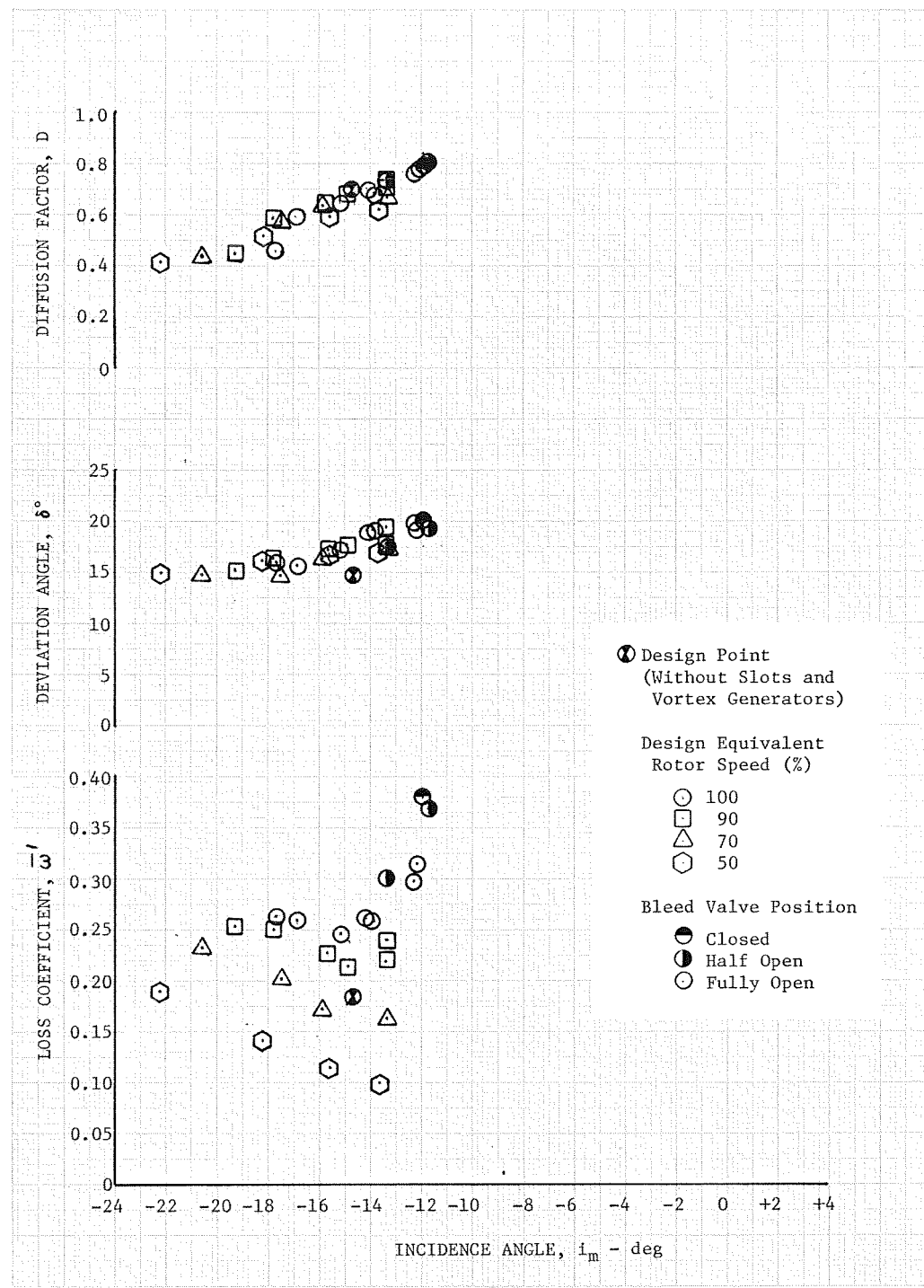
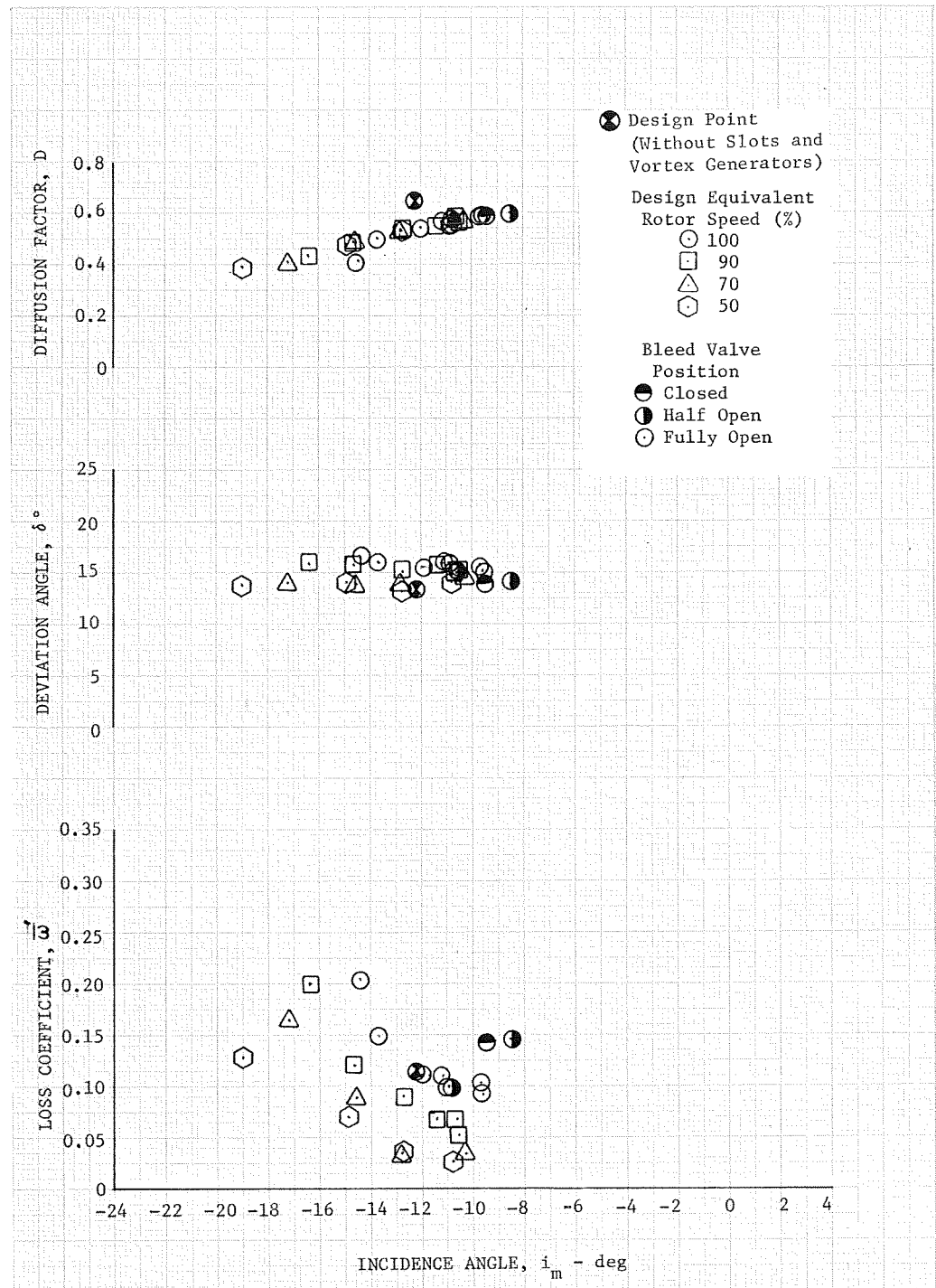


Figure 17. Rotor Blade Element Performance -  
10% Span From Tip



DF 76993

Figure 18. Rotor Blade Element Performance -  
15% Span From Tip



DF 76992

Figure 19. Rotor Blade Element Performance -  
30% Span From Tip

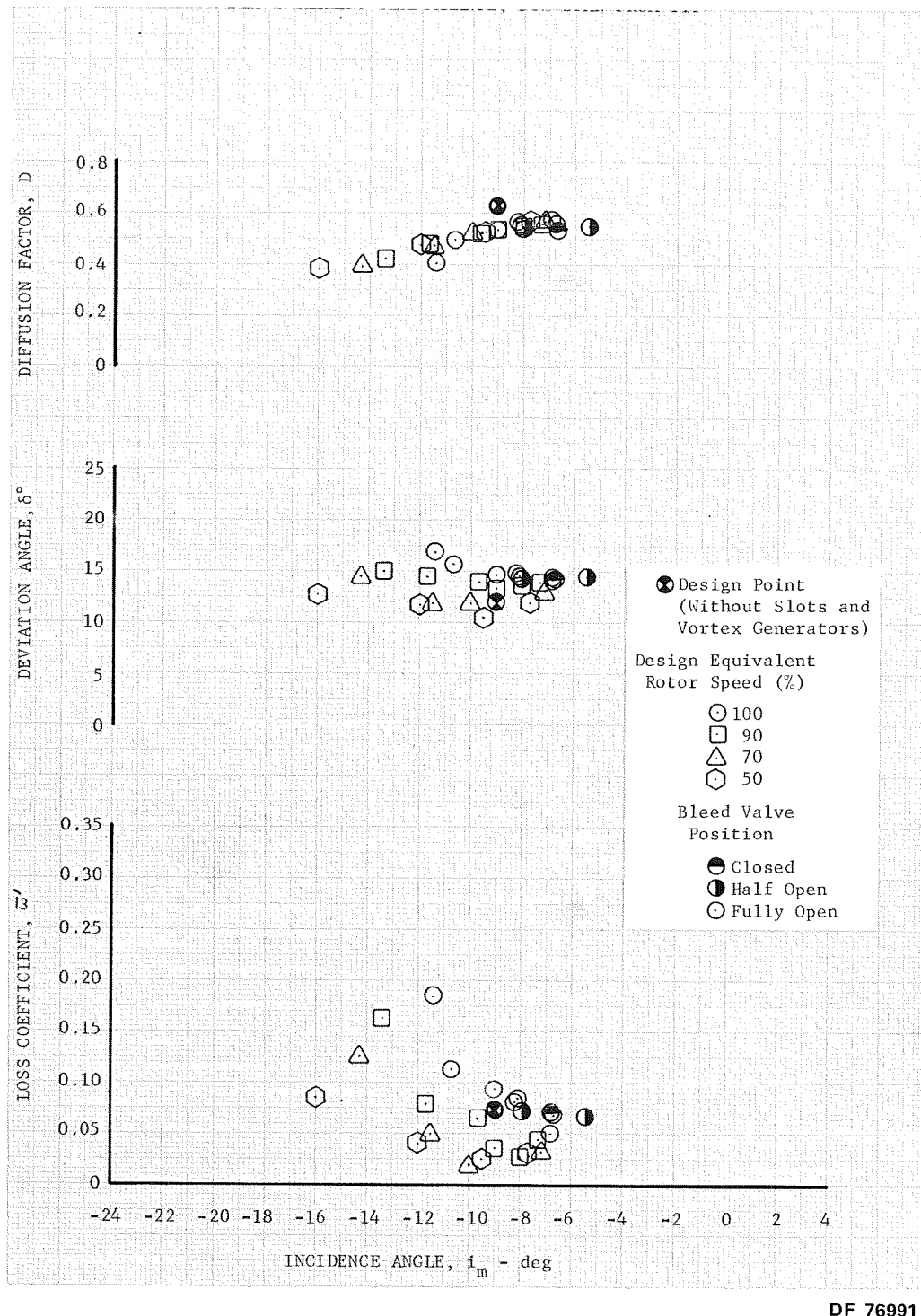


Figure 20. Rotor Blade Element Performance -  
50% Span From Tip

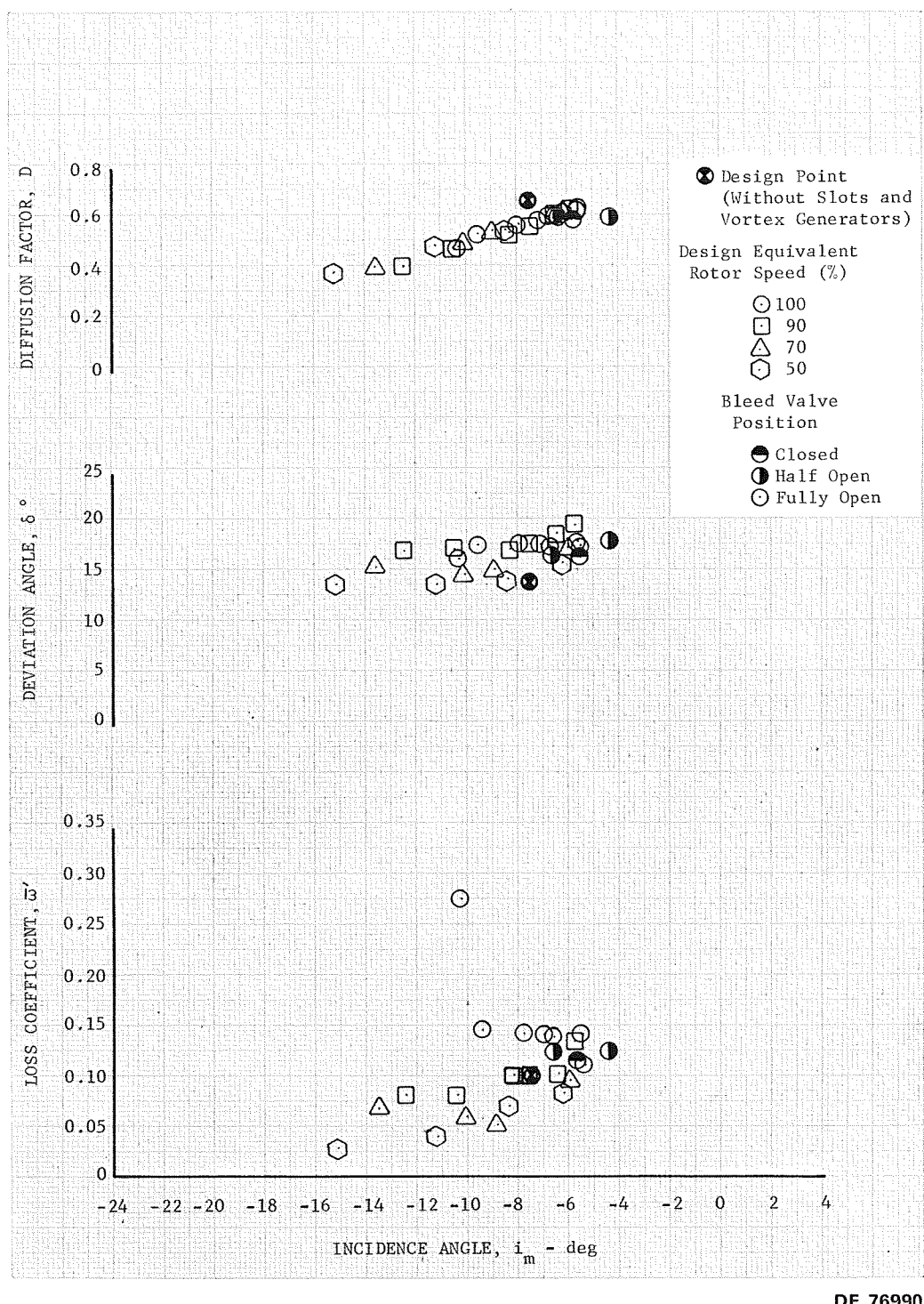


Figure 21. Rotor Blade Element Performance -  
70% Span From Tip

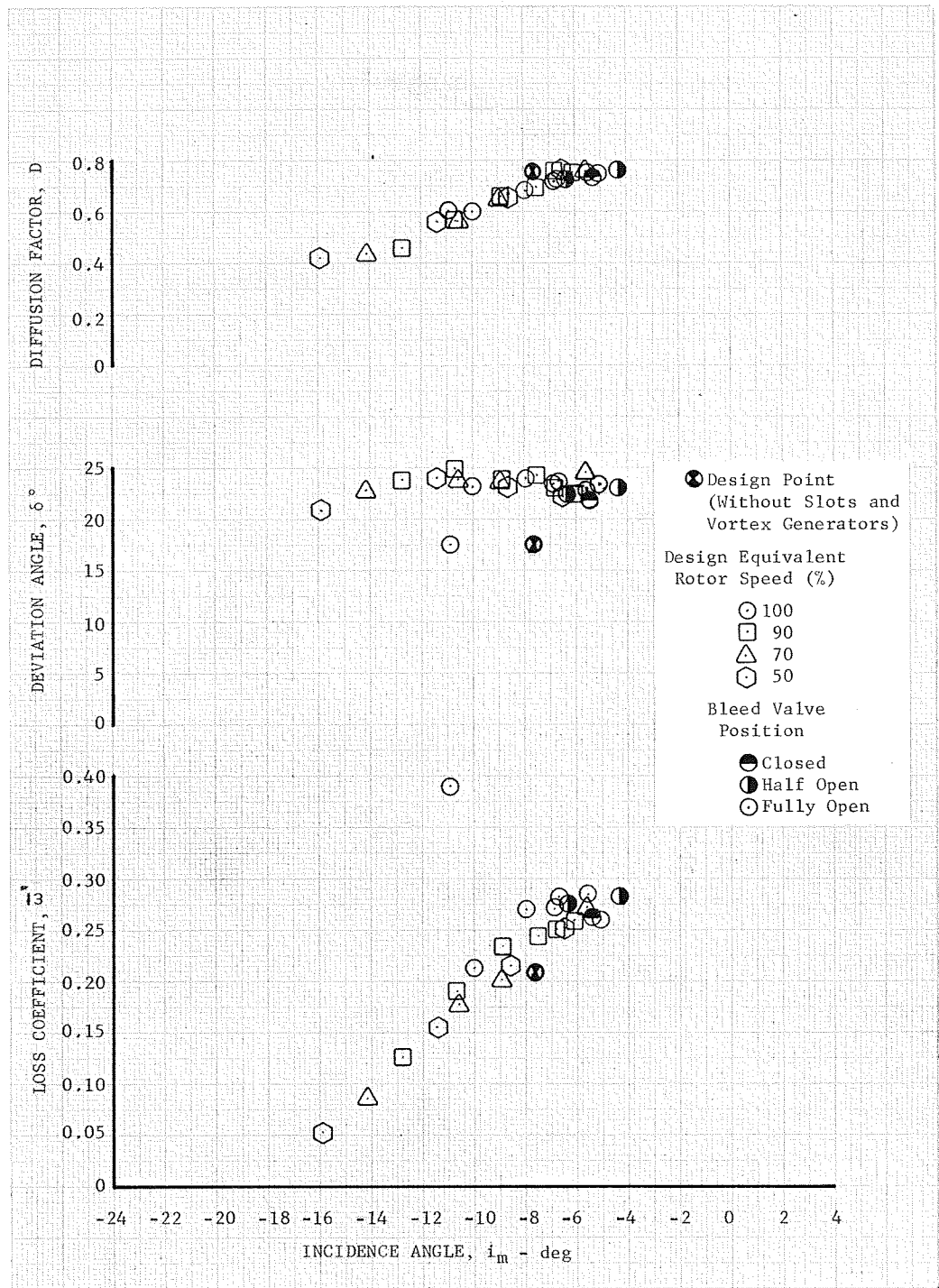
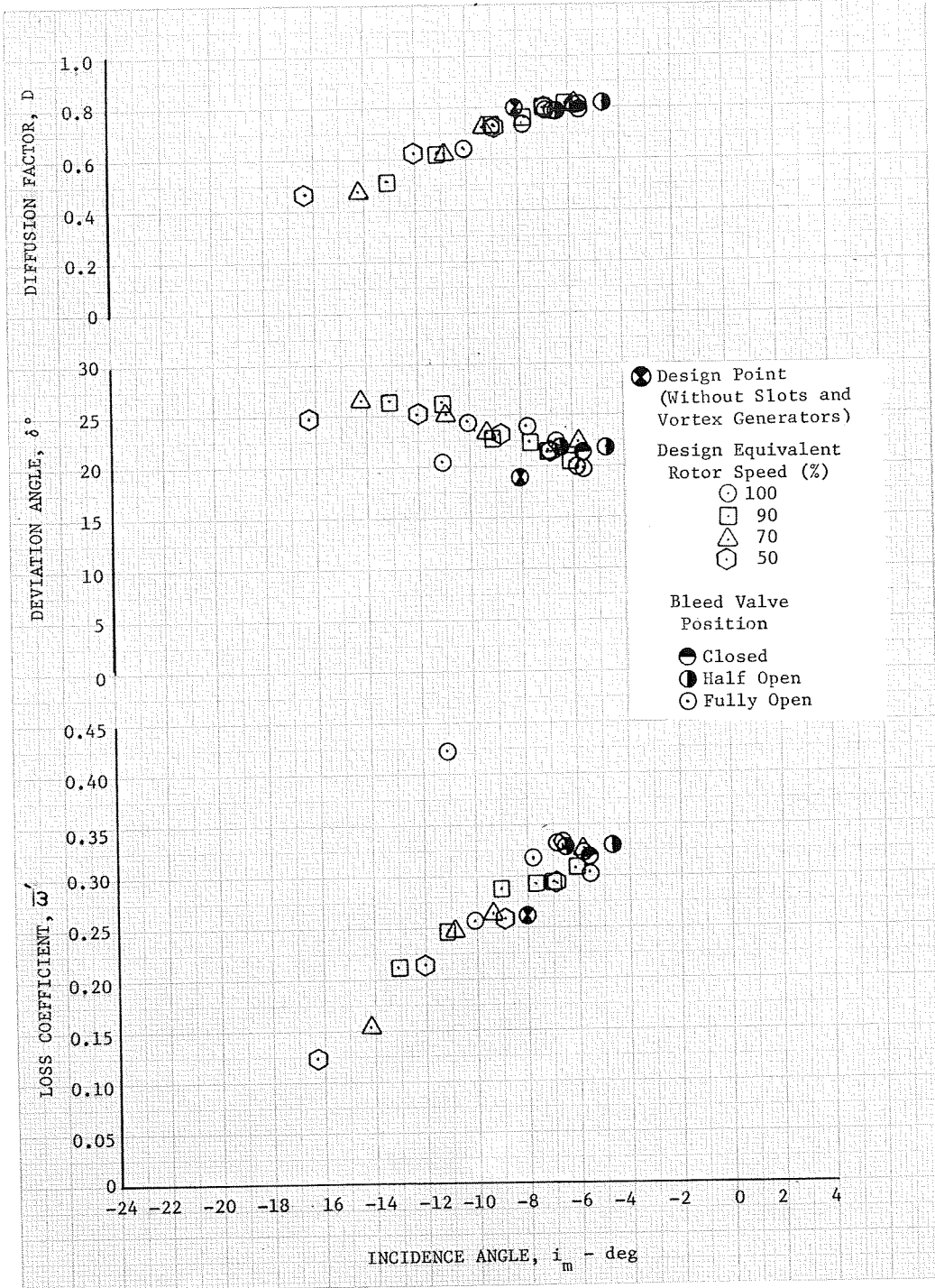
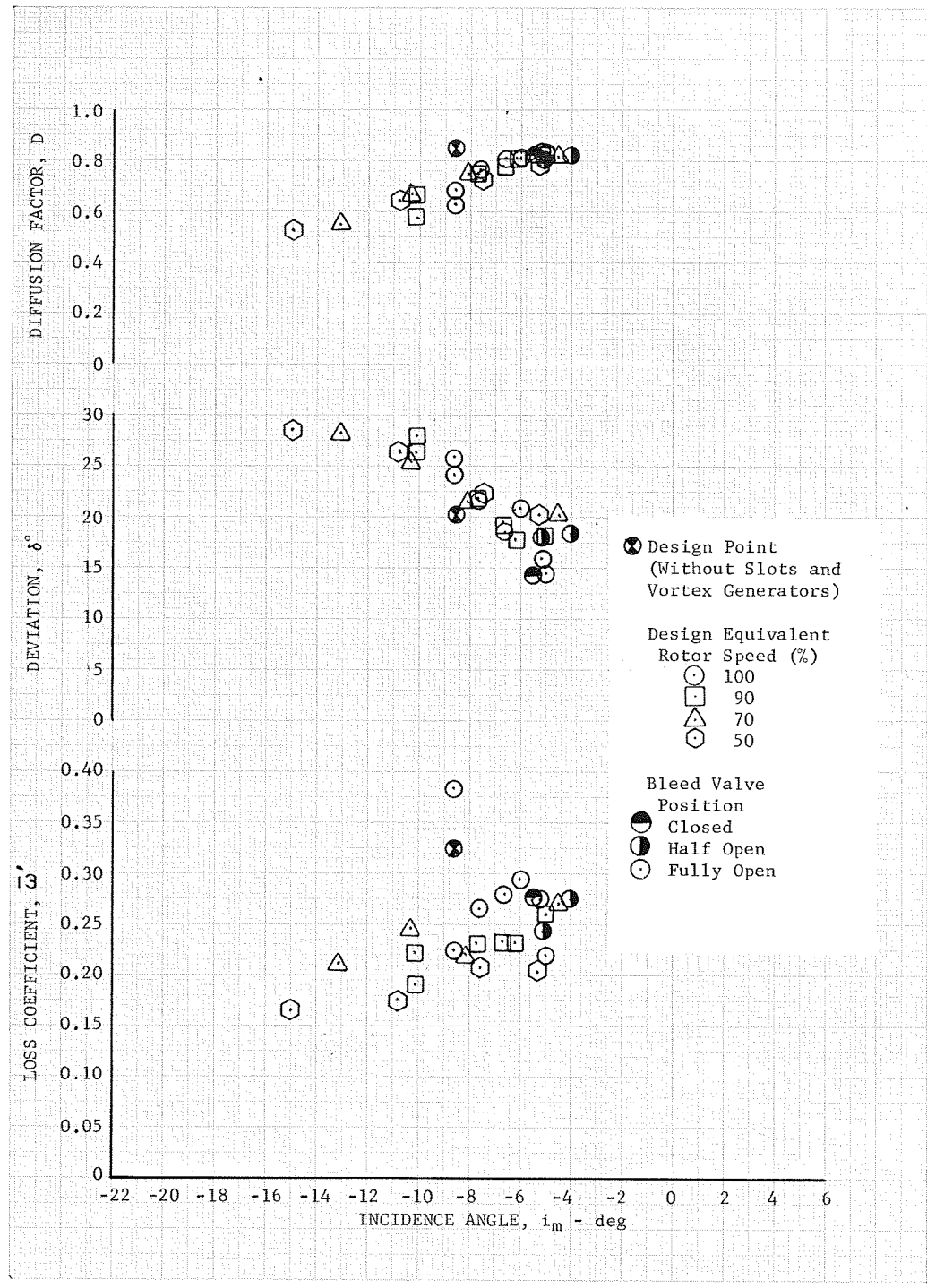


Figure 22. Rotor Blade Element Performance - 85% Span From Tip



DF 76987

Figure 23. Rotor Blade Element Performance -  
90% Span From Tip



DF 76989

Figure 24. Rotor Blade Element Performance -  
95% Span From Tip

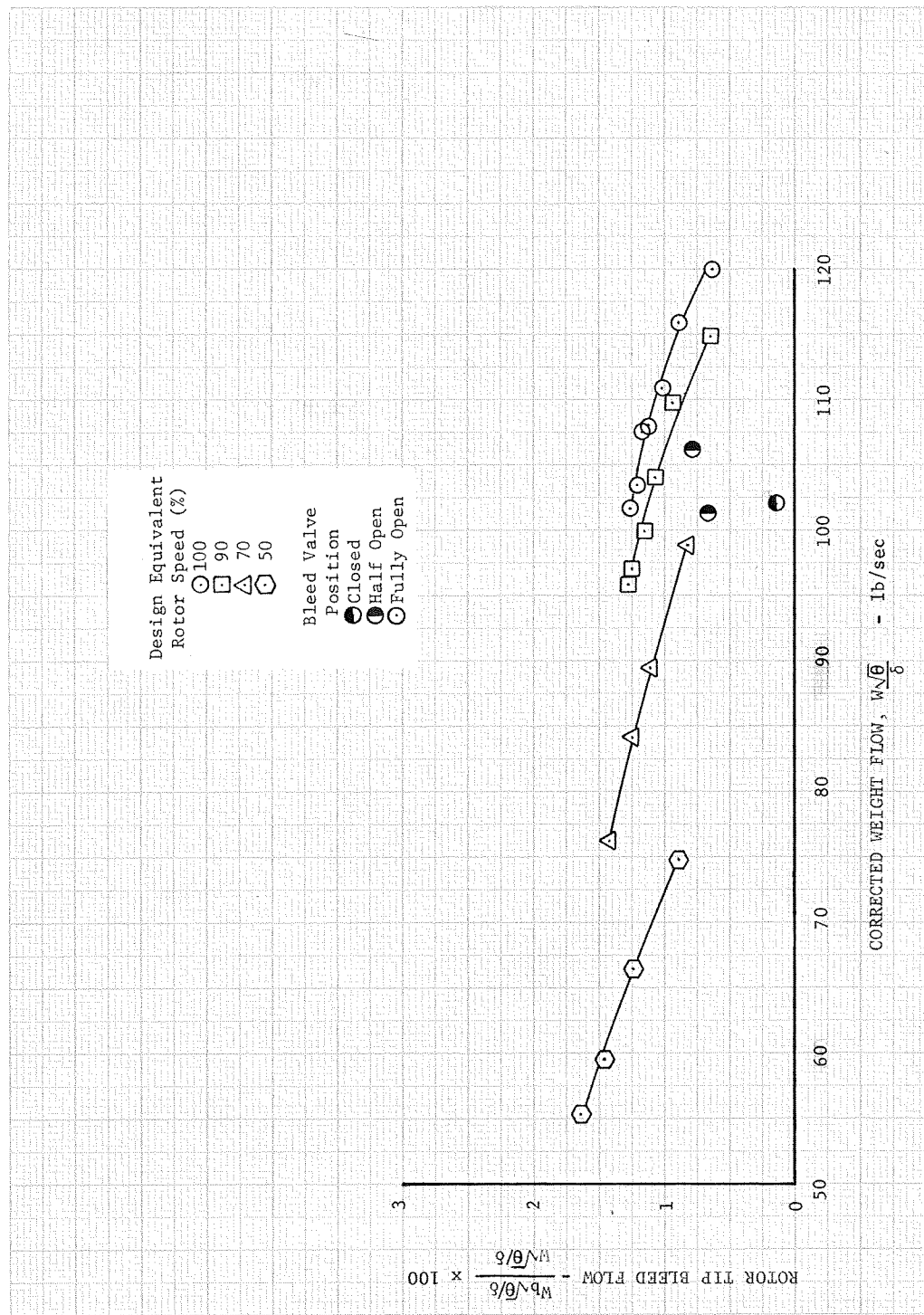
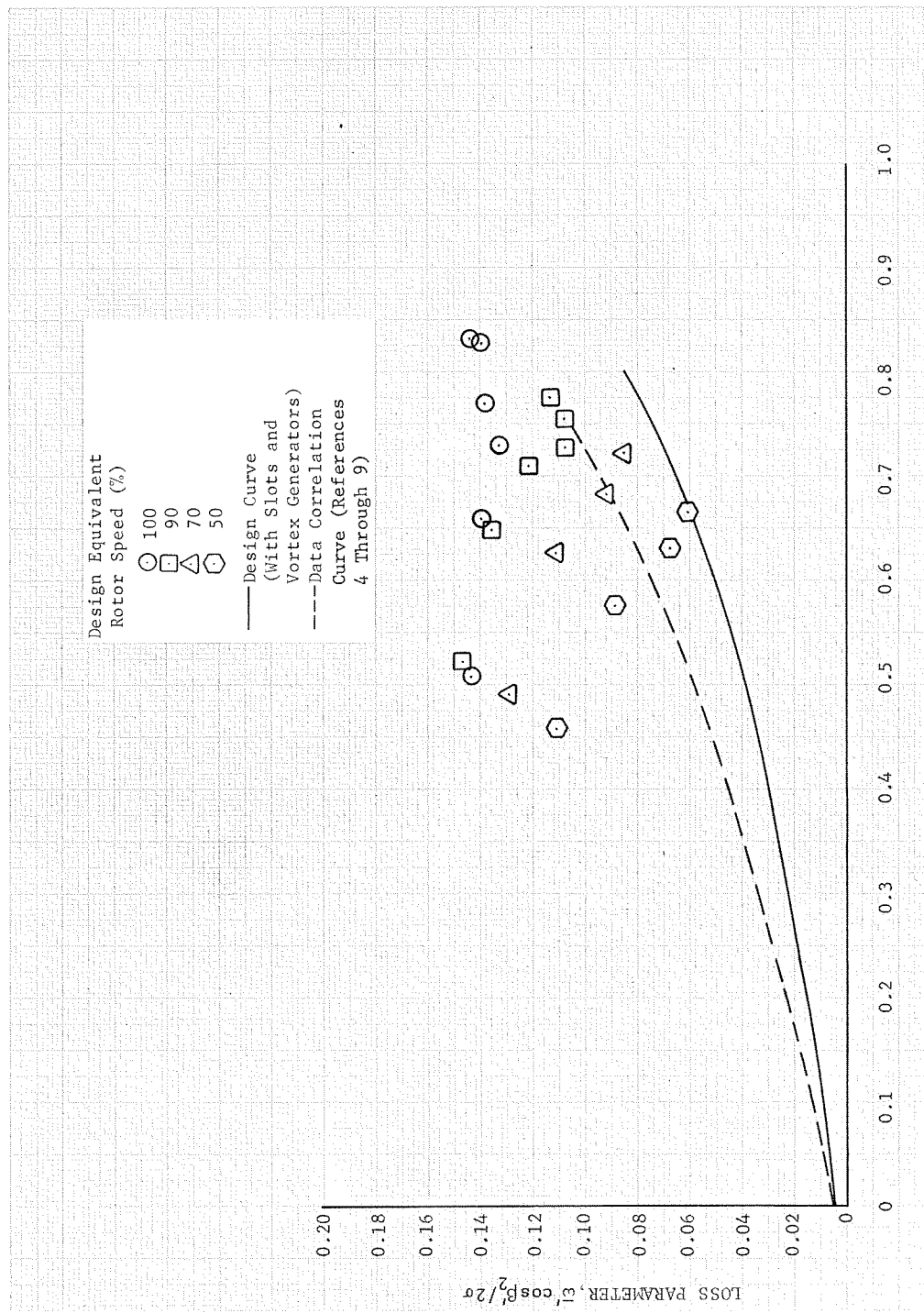


Figure 25. Variation of Rotor Tip Bleed Flow With Equivalent Rotor Speed and Corrected Flow



DF 77011

Figure 26. Rotor Loss Parameter vs Diffusion Factor - 10% Span From Tip

DF 77013

Figure 27. Rotor Loss Parameter vs Diffusion Factor - 30% Span From Tip

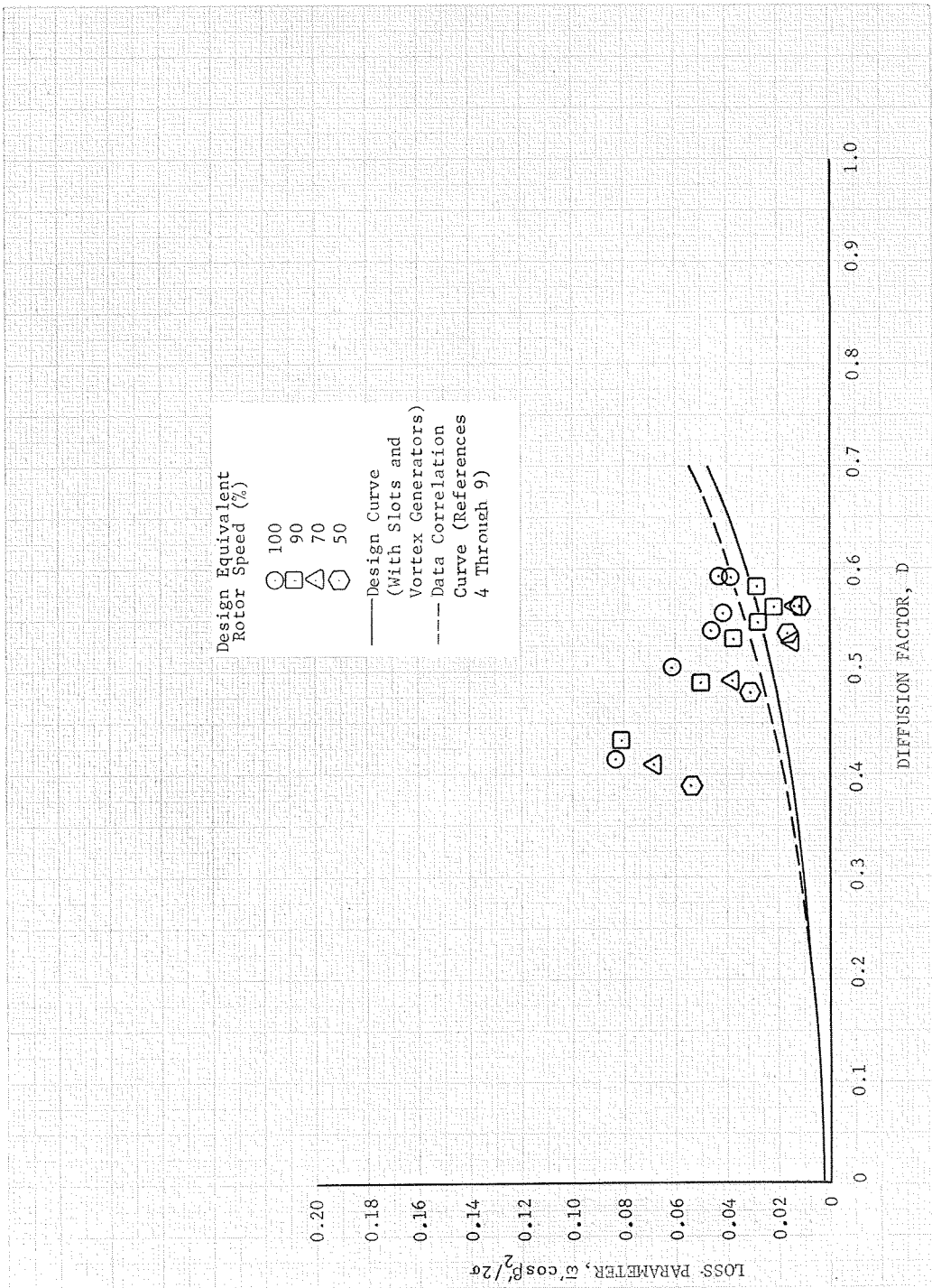
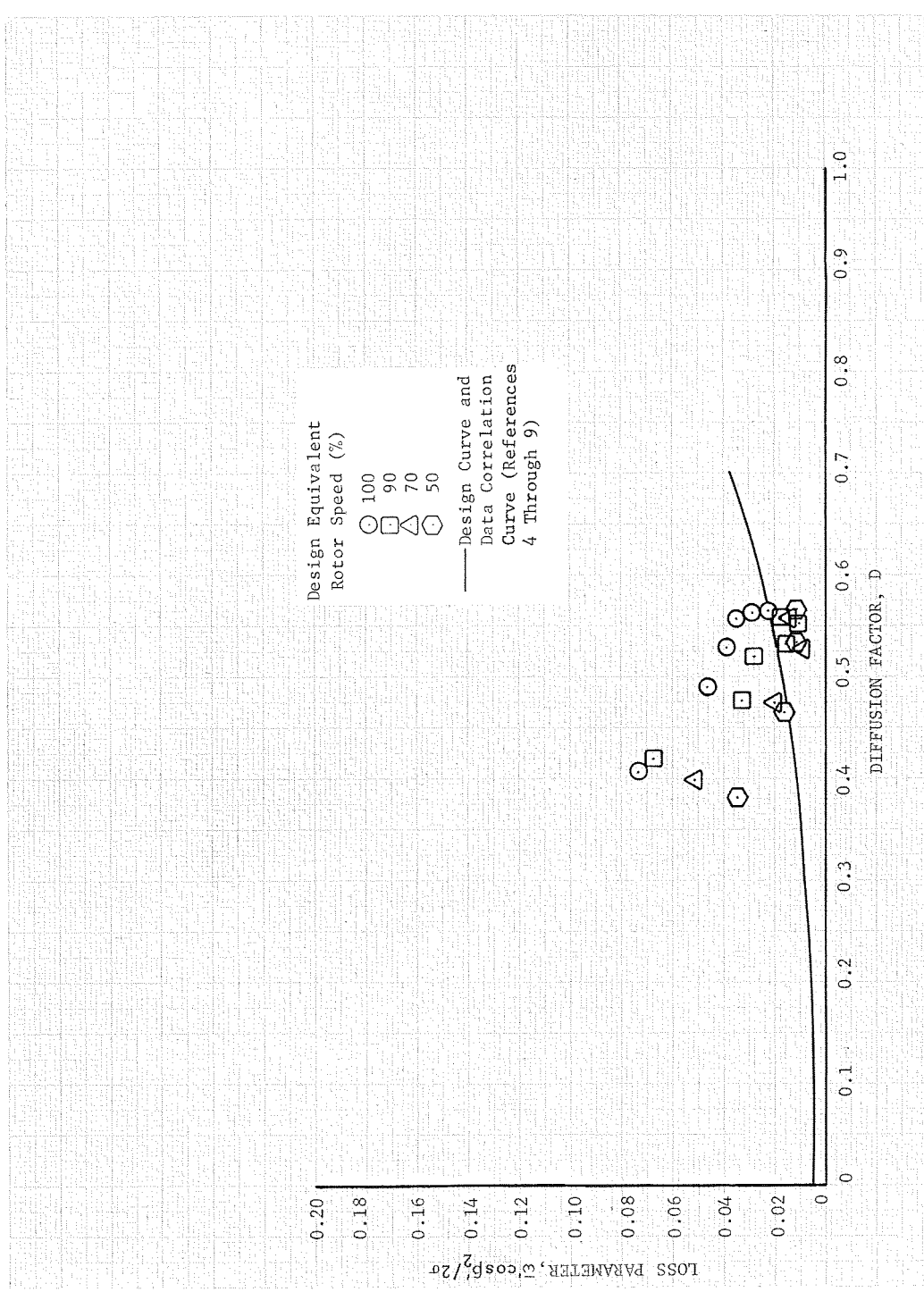
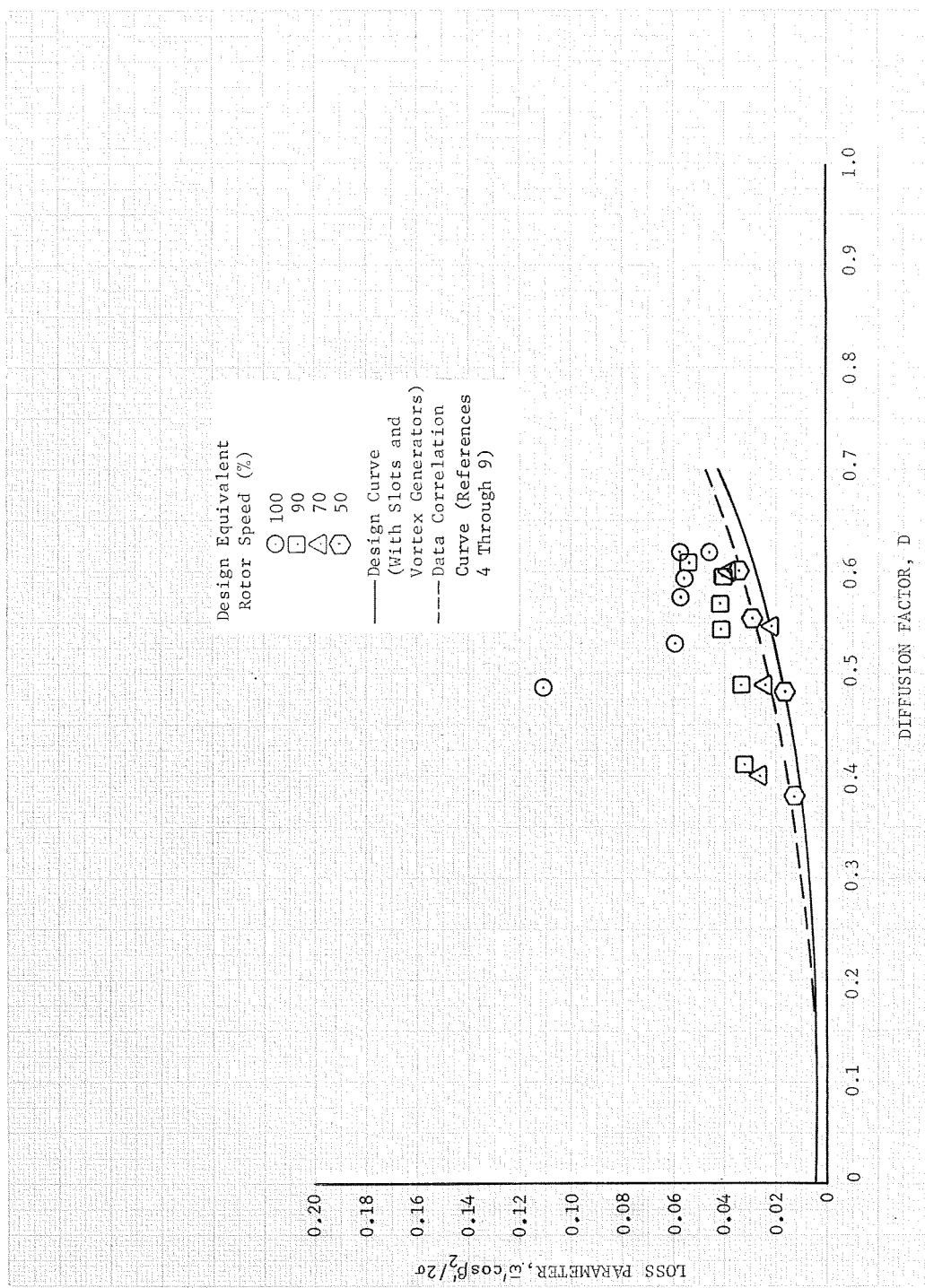


Figure 28. Rotor Loss Parameter vs Diffusion Factor - 50% Span From Tip



DF 77015

Figure 29. Rotor Loss Parameter vs Diffusion Factor - 70% Span From Tip



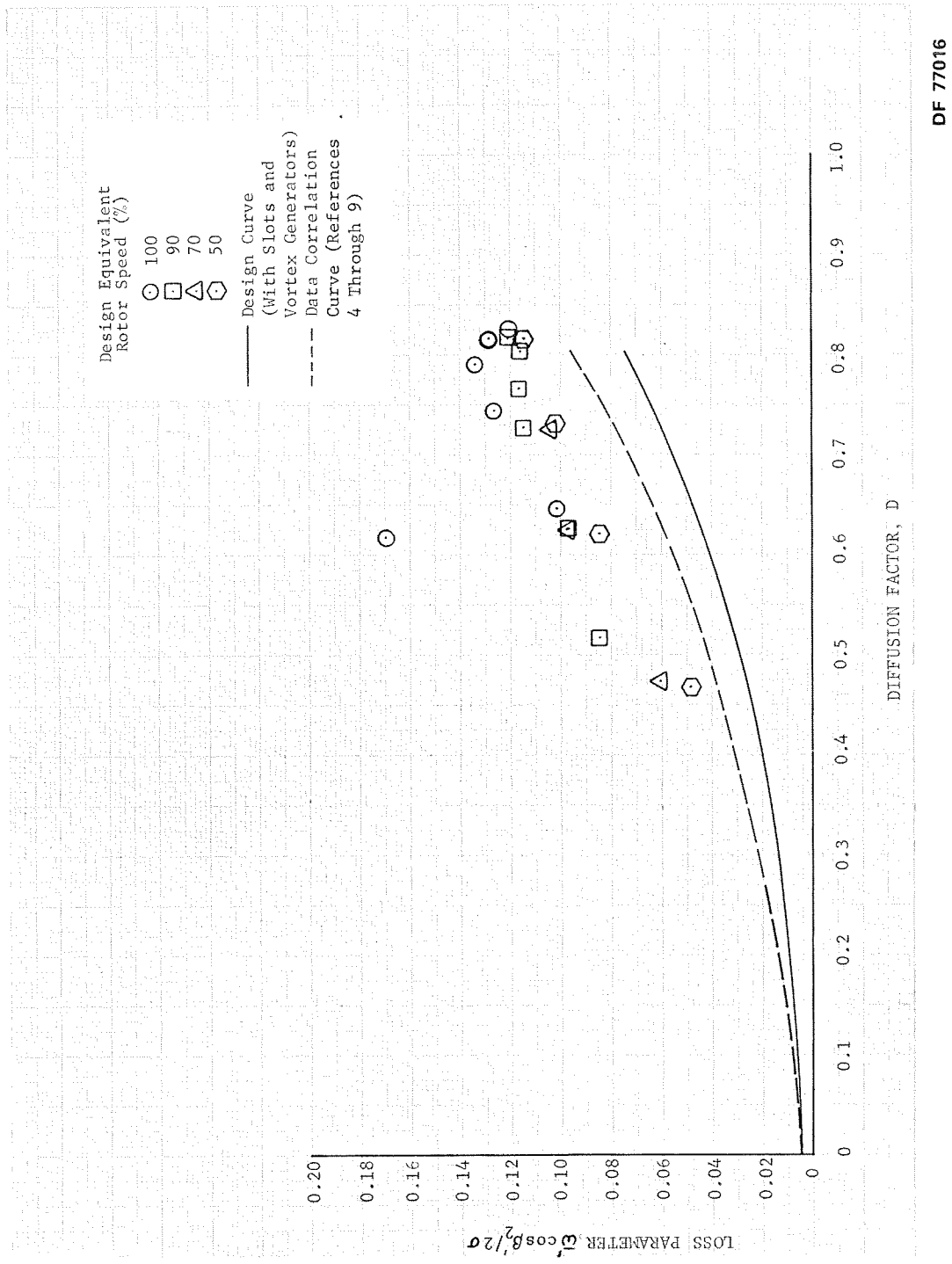
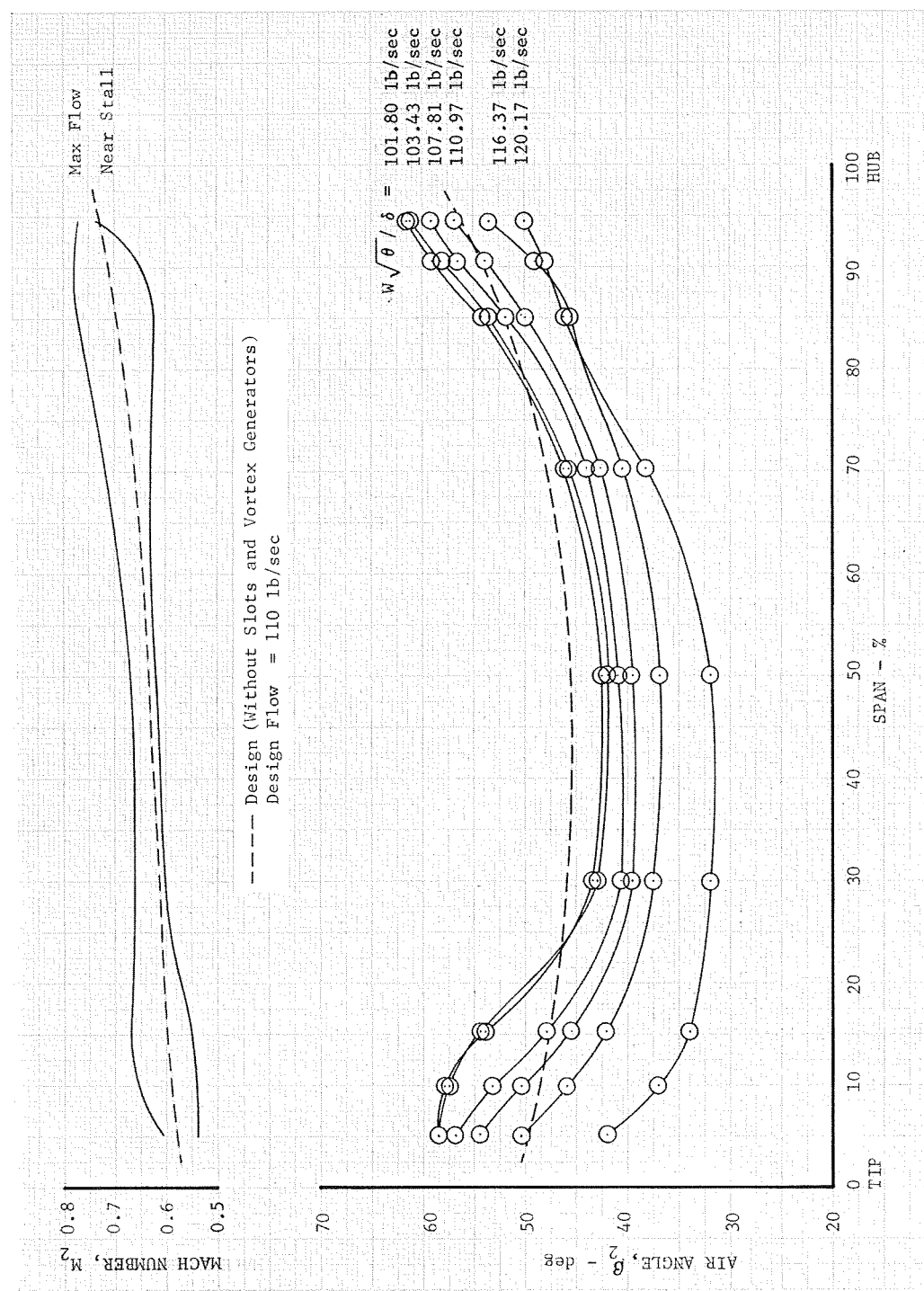


Figure 30. Rotor Loss Parameter vs Diffusion Factor - 90% Span From Tip

DF 77019

Figure 31. Stator Inlet Air Angle and Mach Number Distribution - Design Equivalent Rotor Speed



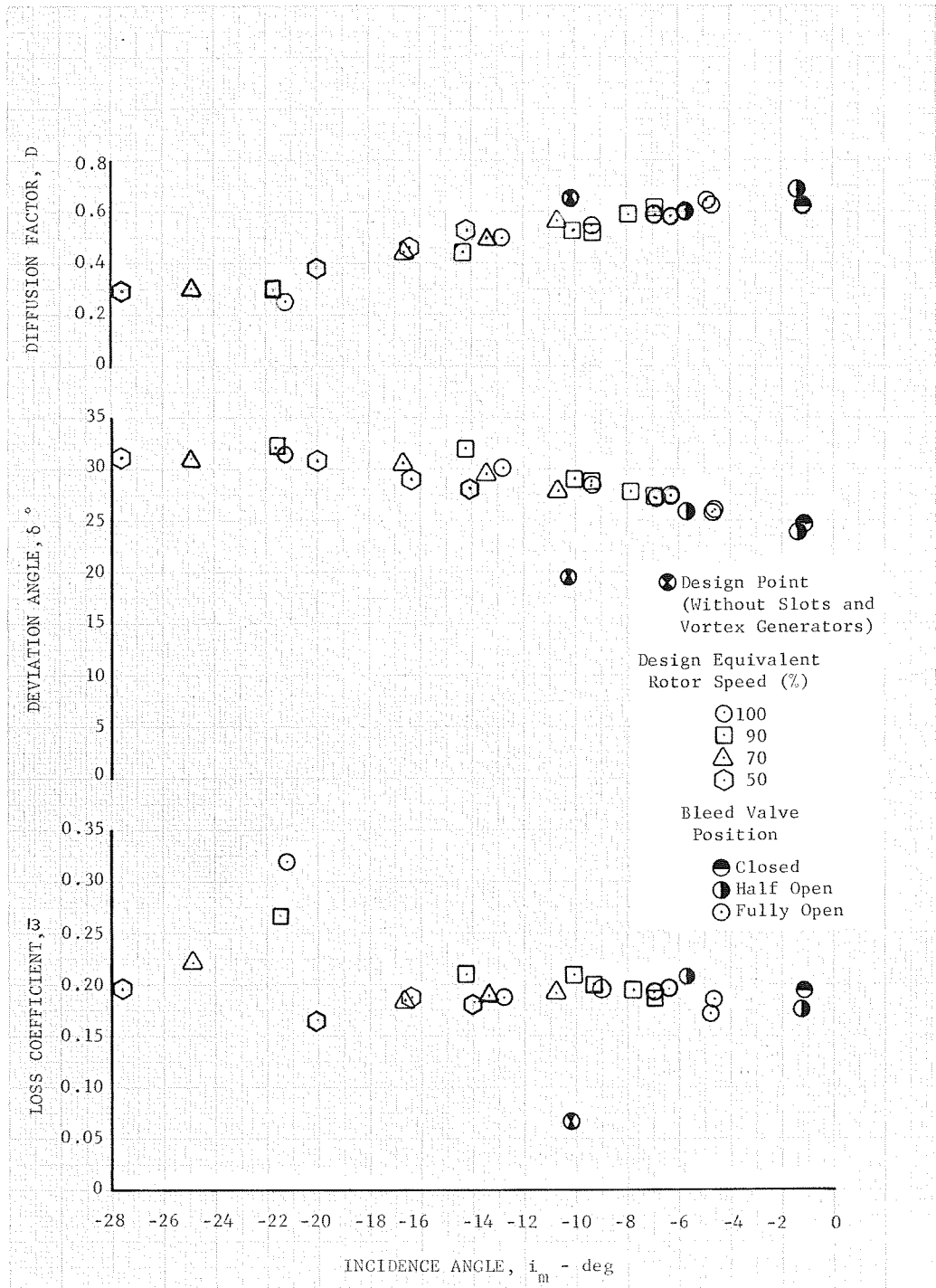


Figure 32. Stator Blade Element Performance -  
5% Span From Tip

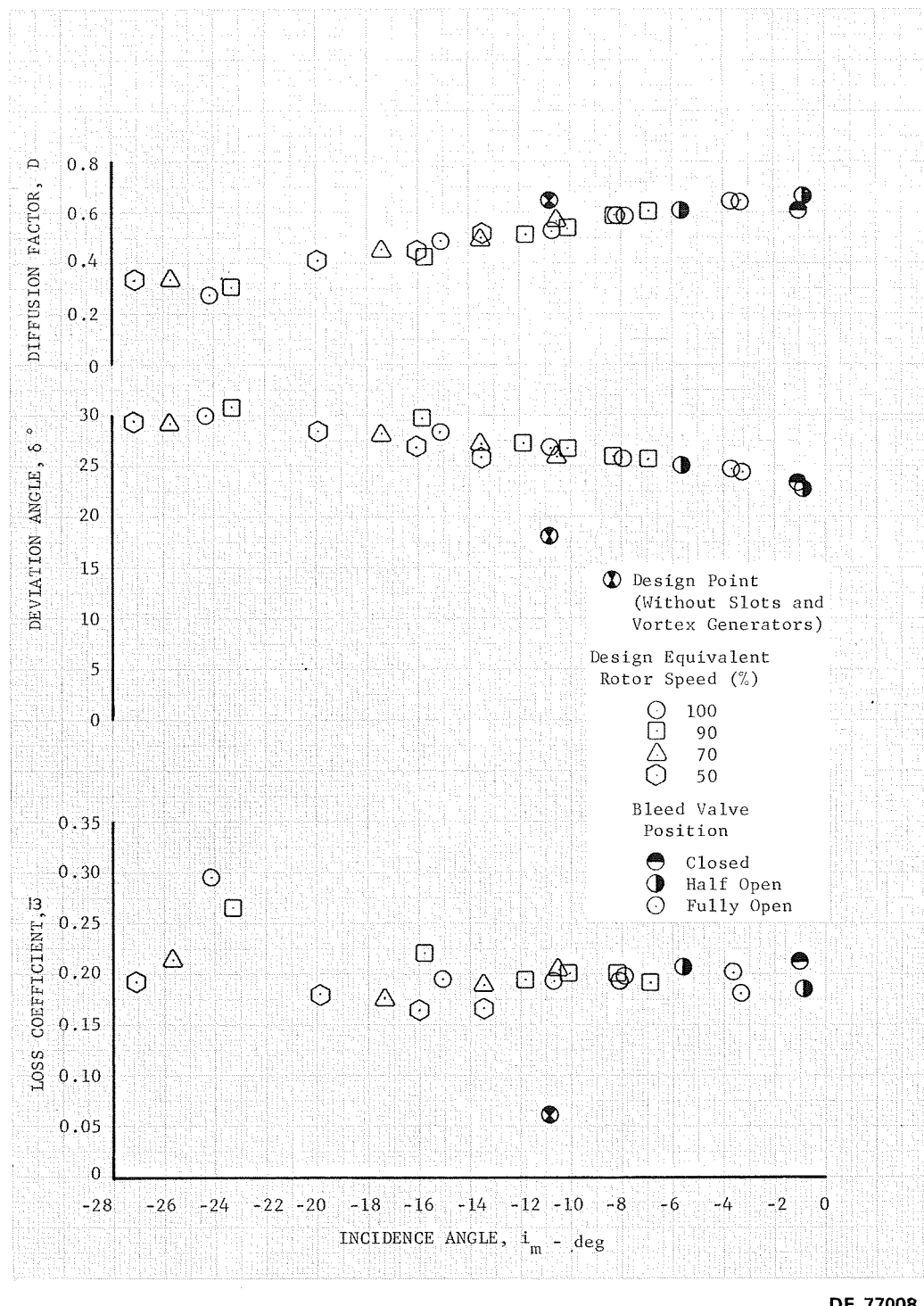


Figure 33. Stator Blade Element Performance - 10% Span From Tip

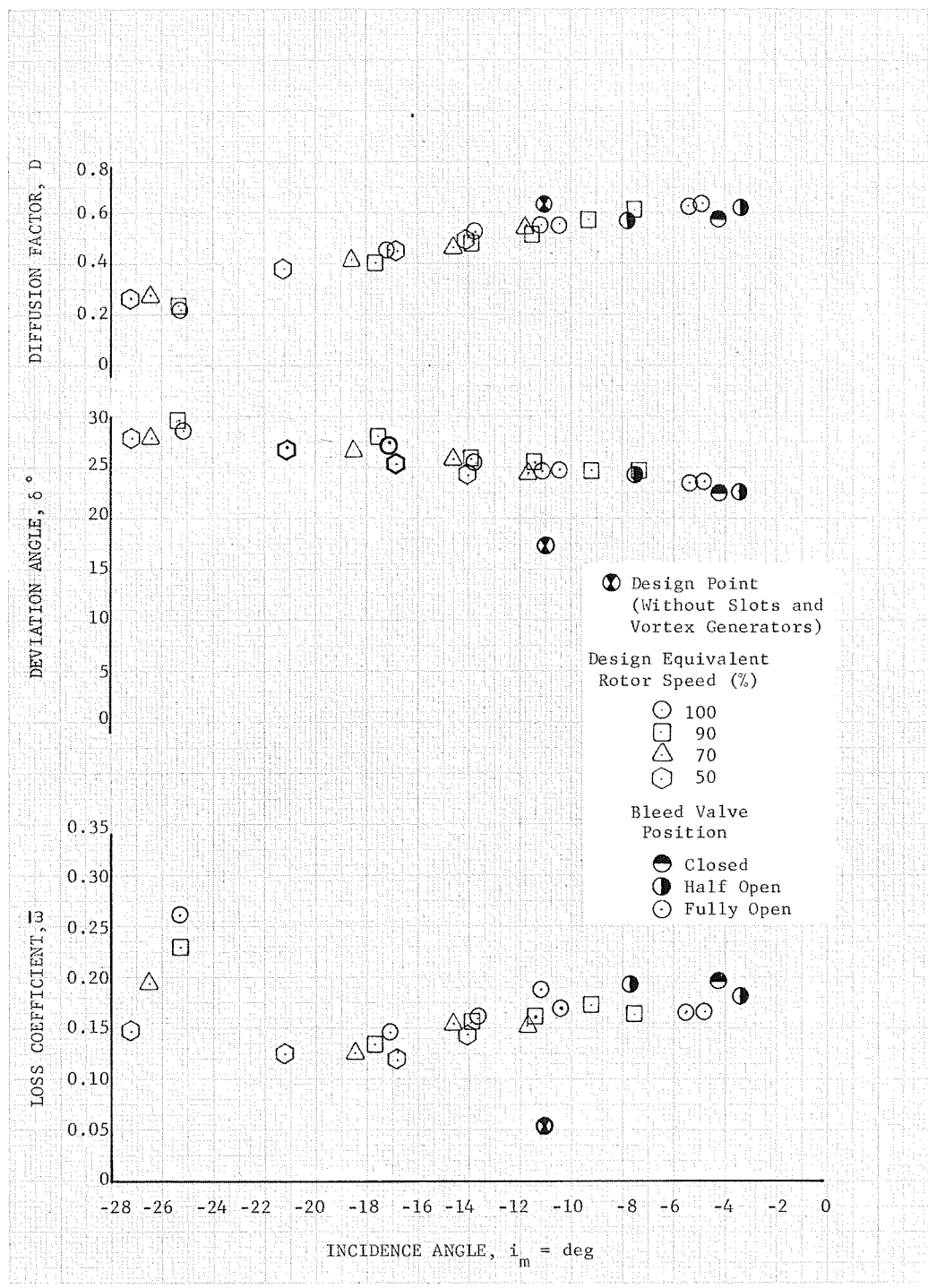
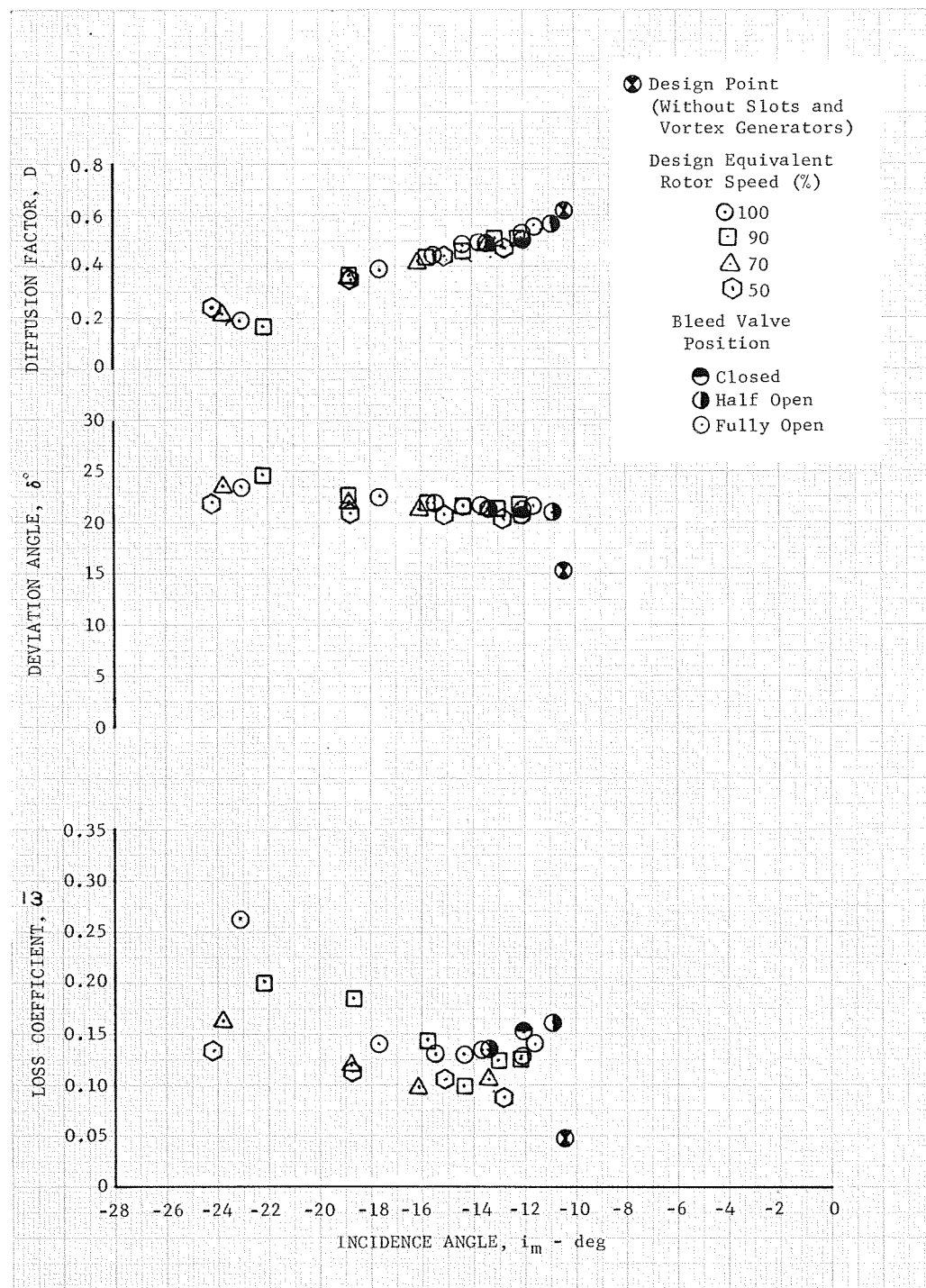


Figure 34. Stator Blade Element Performance -  
15% Span From Tip



DF 77005

Figure 35. Stator Blade Element Performance -  
30% Span From Tip

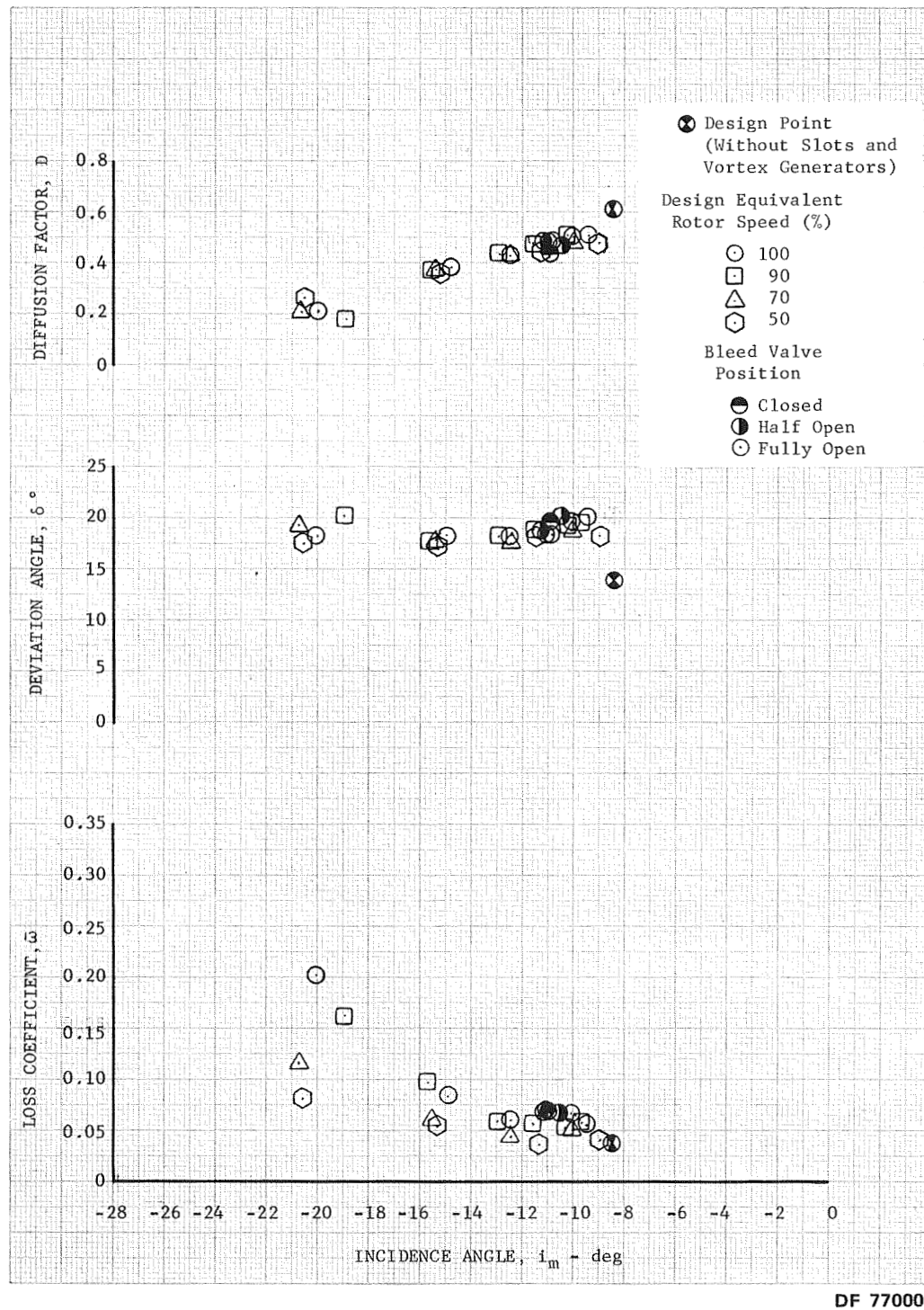


Figure 36. Stator Blade Element Performance -  
50% Span From Tip

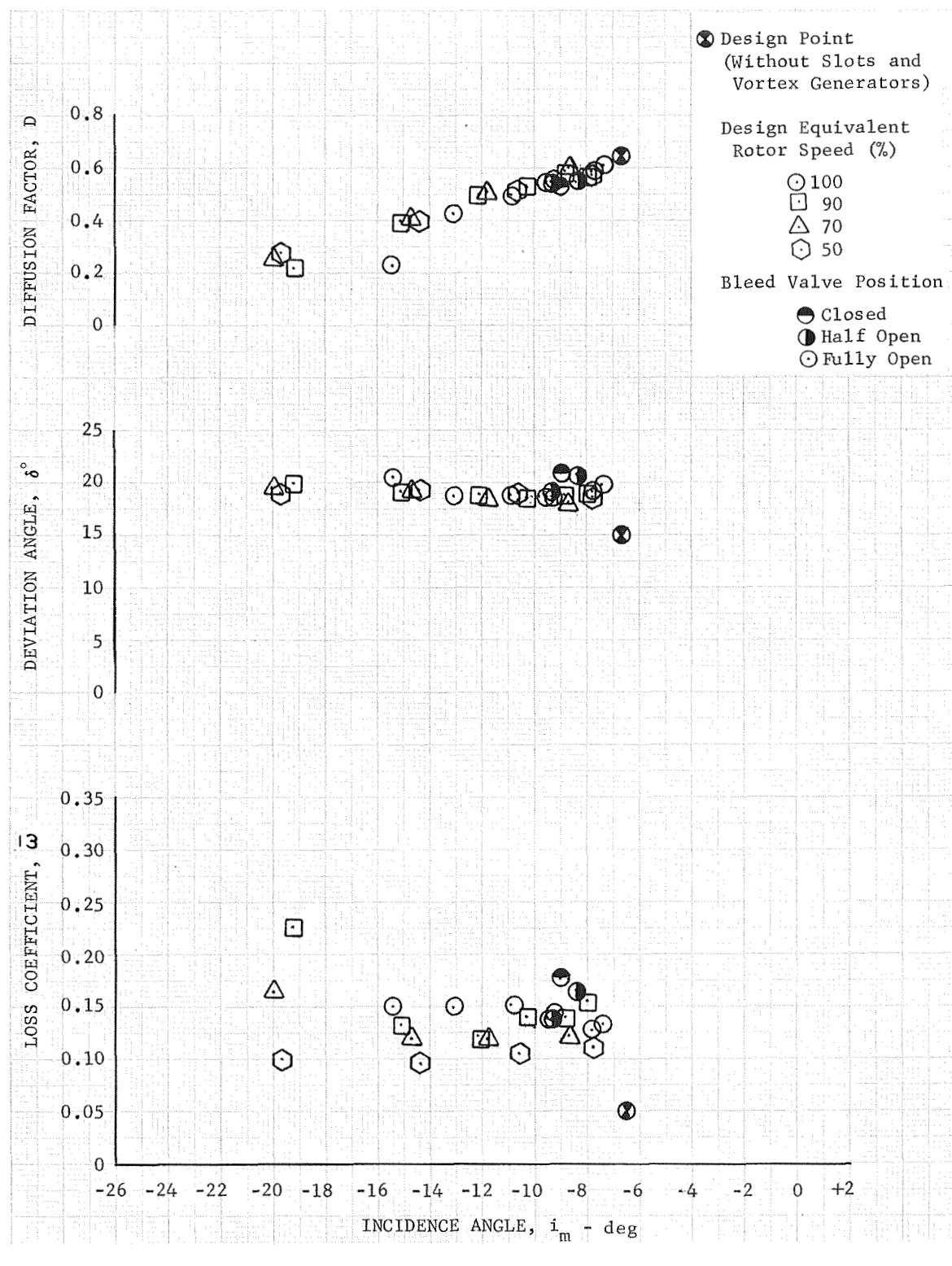


Figure 37. Stator Blade Element Performance -  
70% Span From Tip

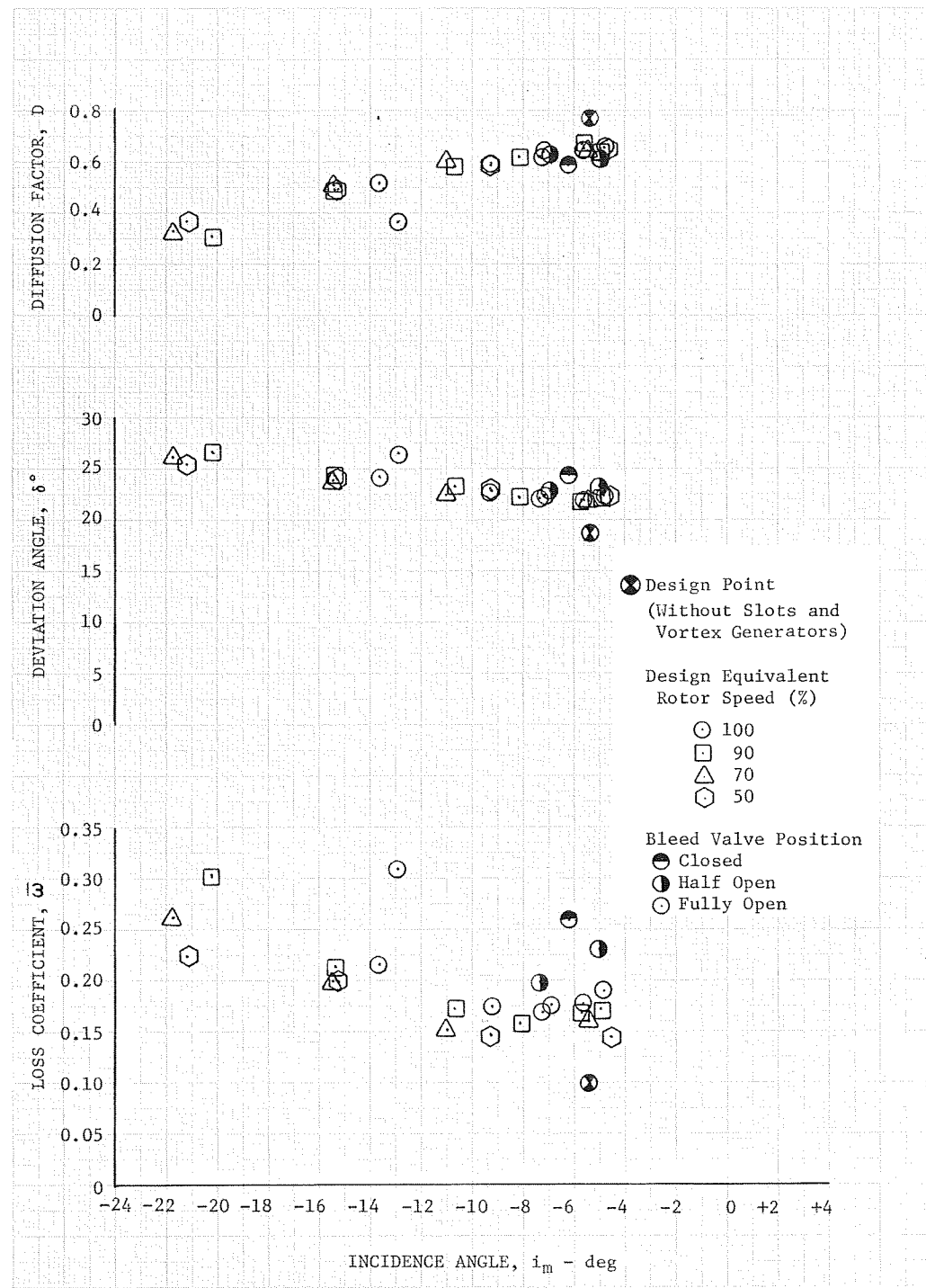


Figure 38. Stator Blade Element Performance -  
85% Span From Tip

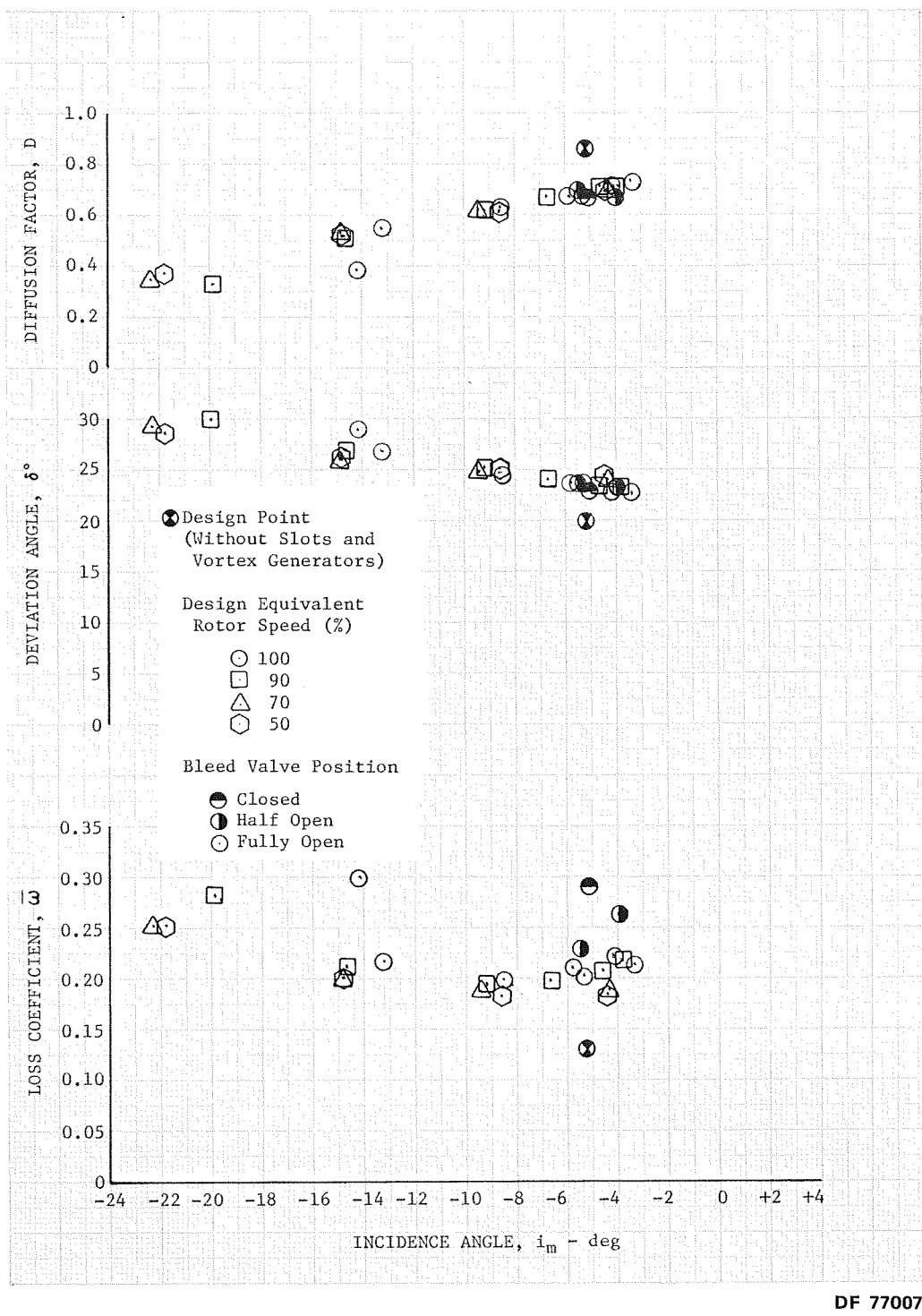
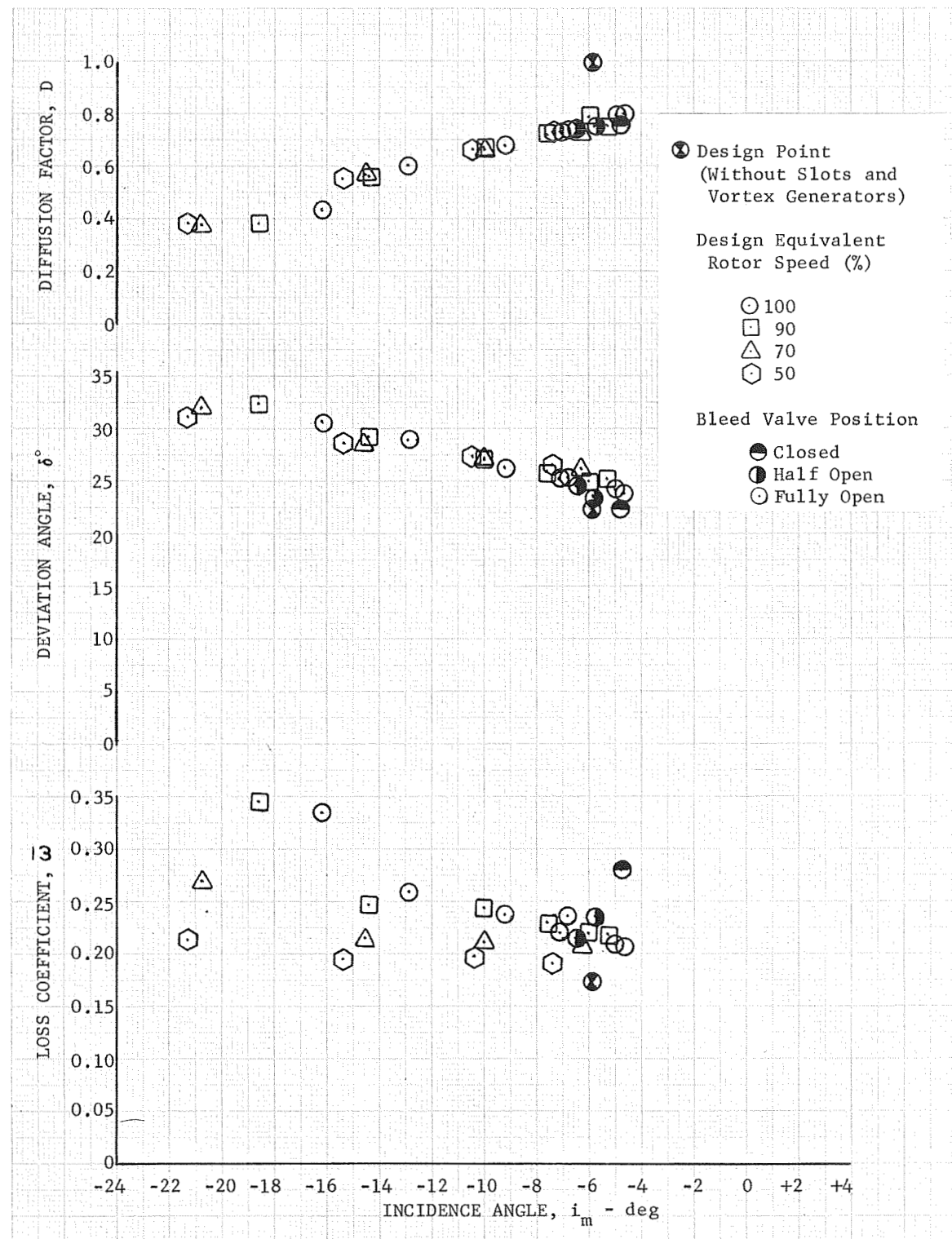


Figure 39. Stator Blade Element Performance - 90% Span From Tip



DF 77002

Figure 40. Stator Blade Element Performance -  
95% Span From Tip

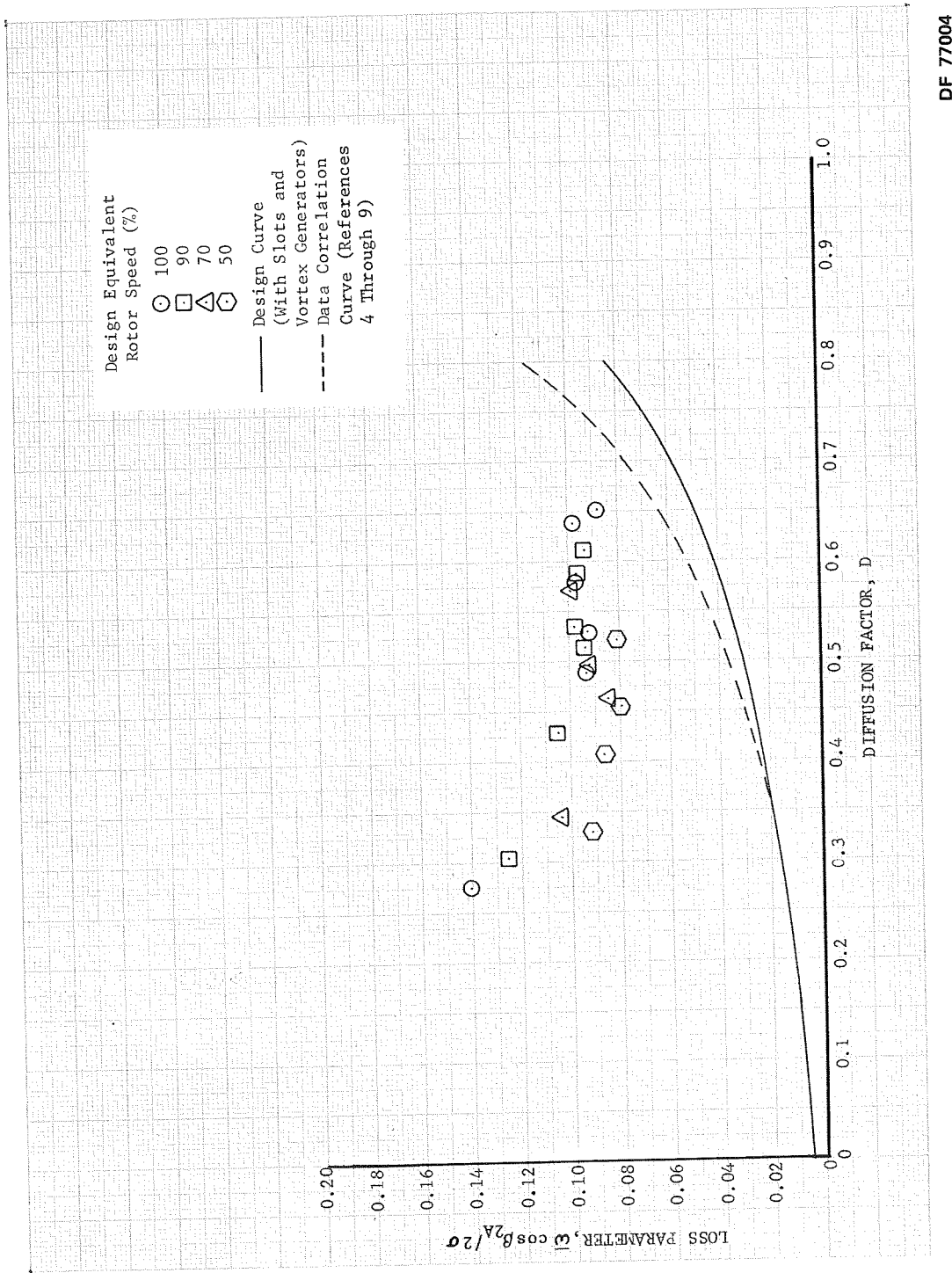


Figure 41. Stator Loss Parameter vs Diffusion Factor - 10% Span From Tip

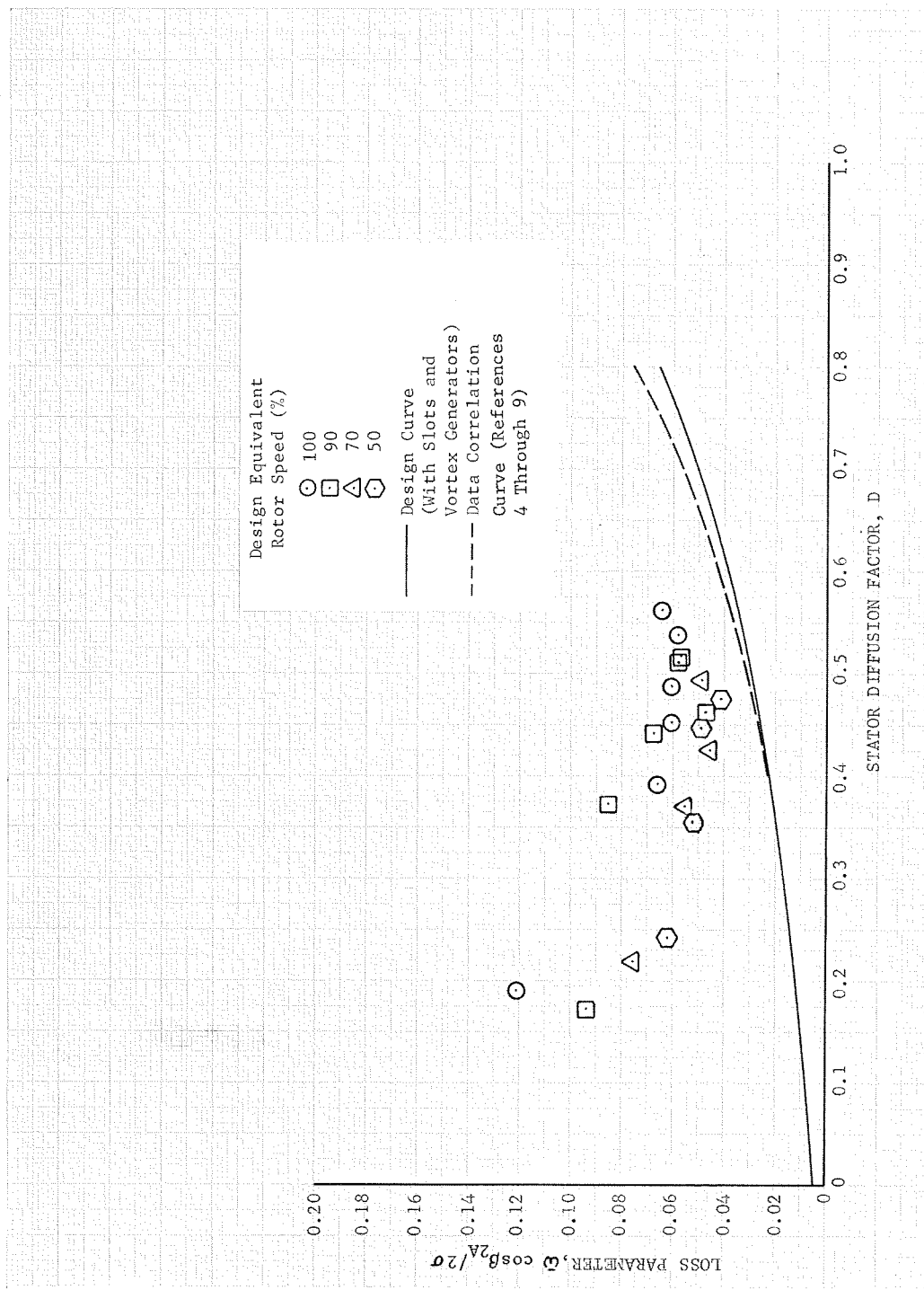


Figure 42. Stator Loss Parameter vs Diffusion Factor - 30% Span From Tip

**DF 76997**

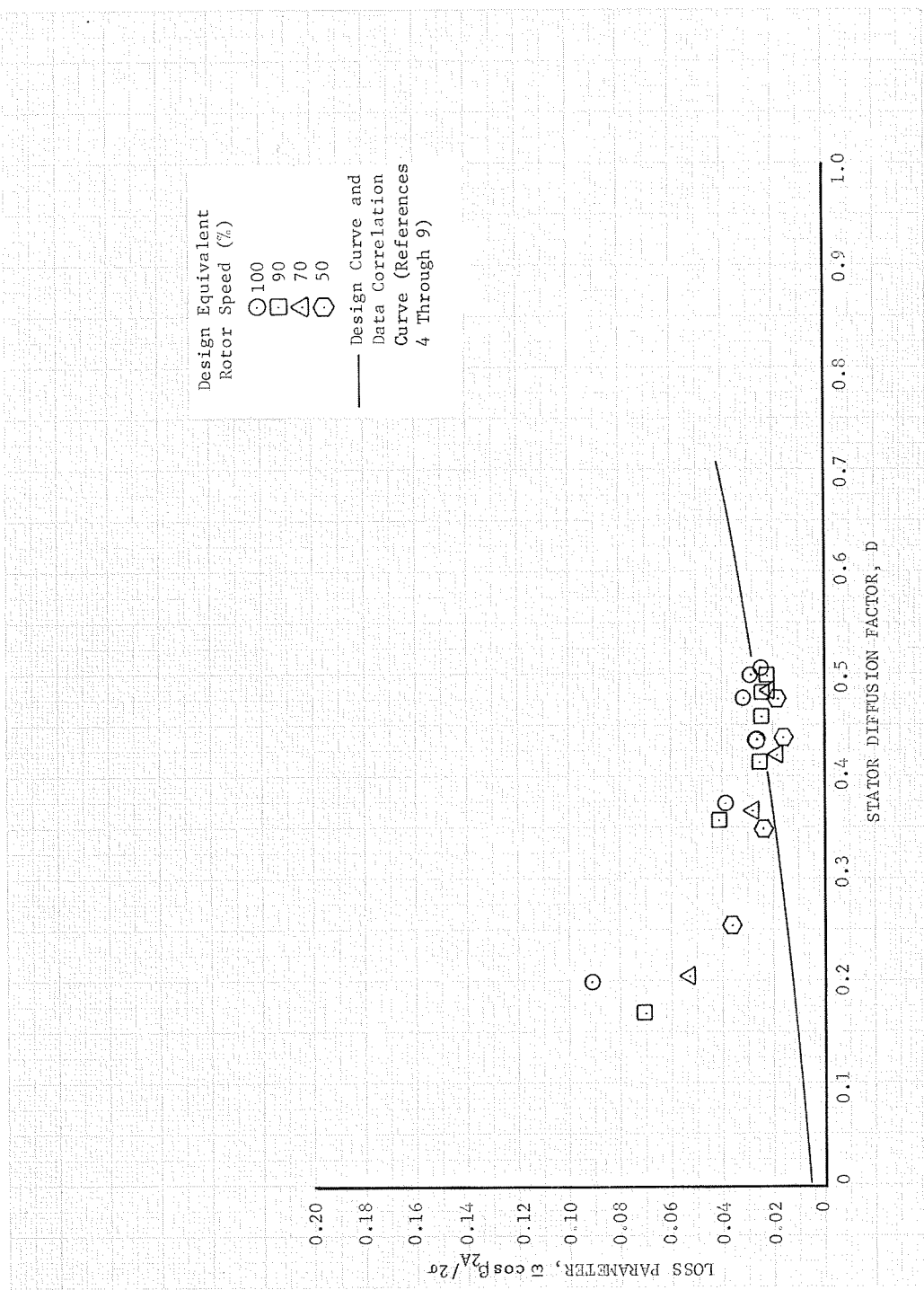
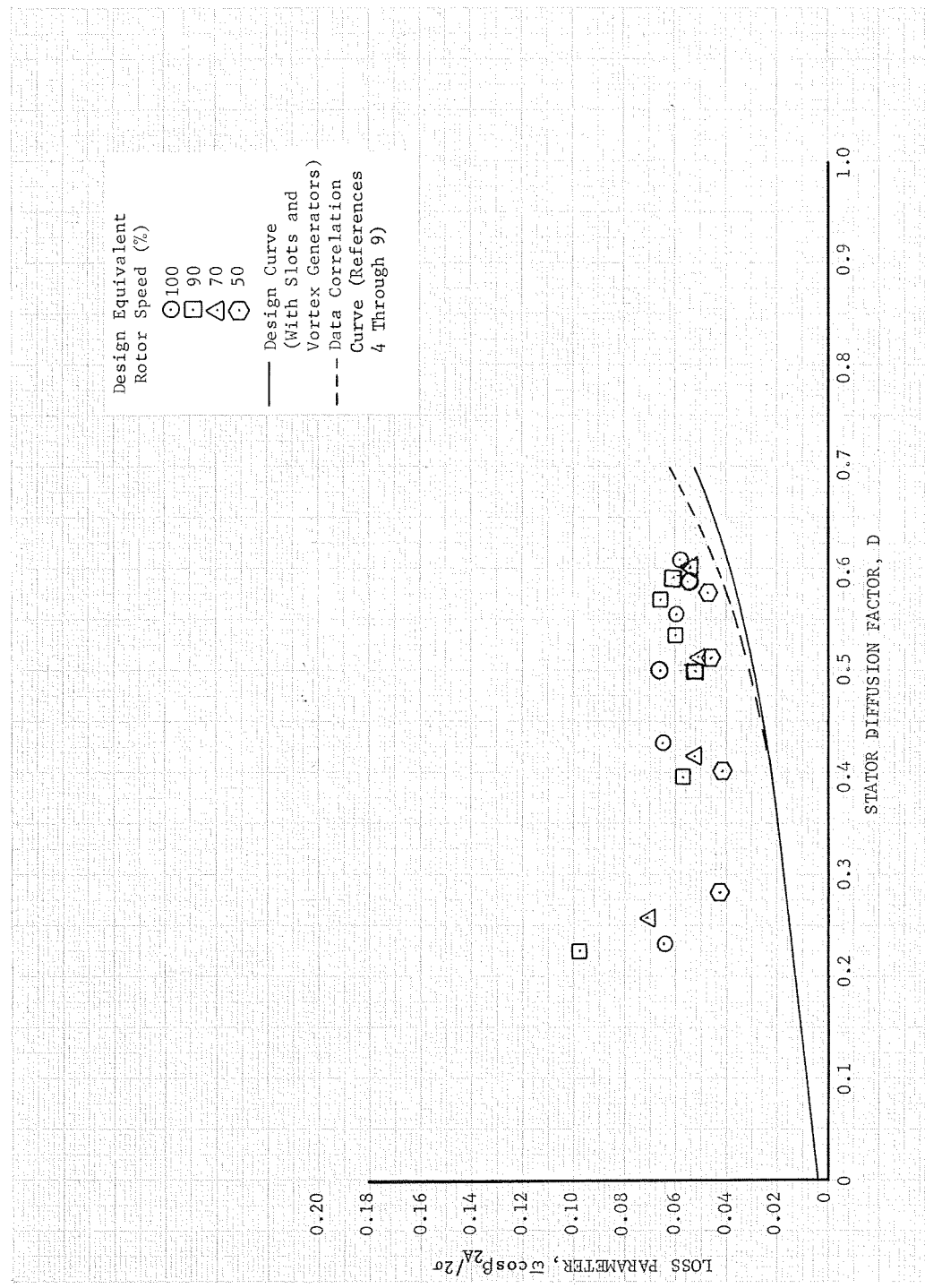
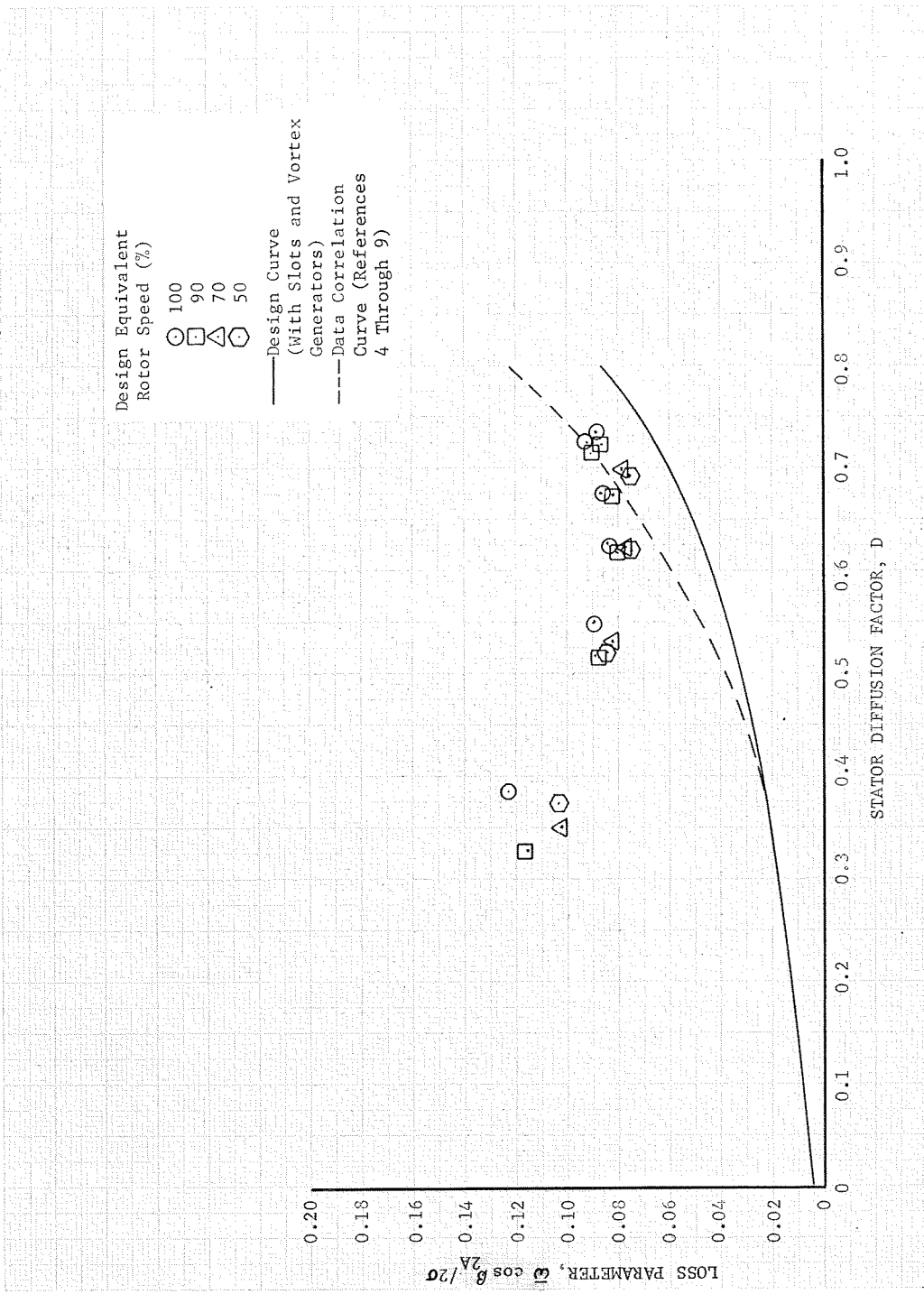


Figure 43. Stator Loss Parameter vs Diffusion Factor - 50% Span From Tip



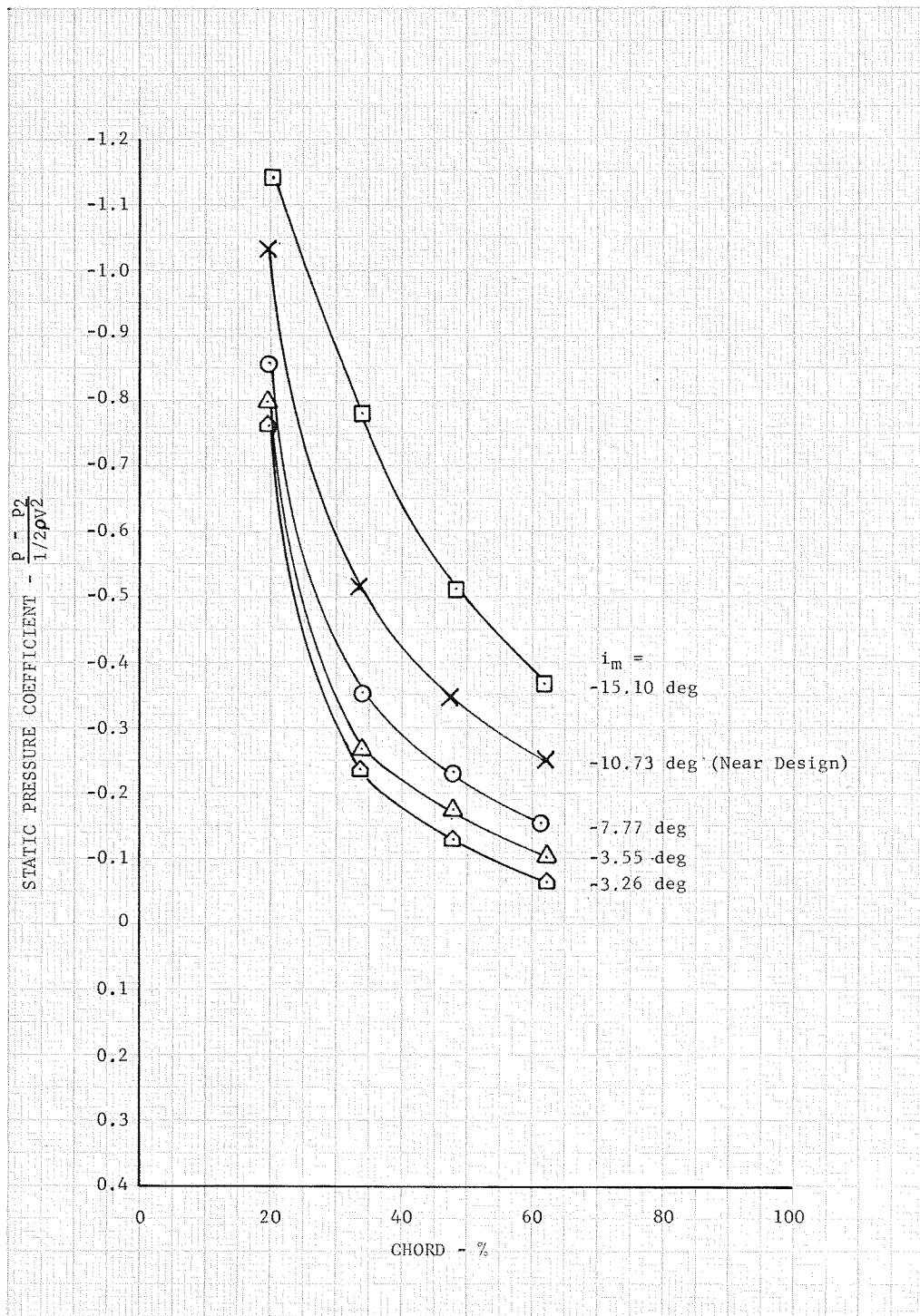
DF 76998

Figure 44. Stator Loss Parameter vs Diffusion Factor - 70% Span From Tip



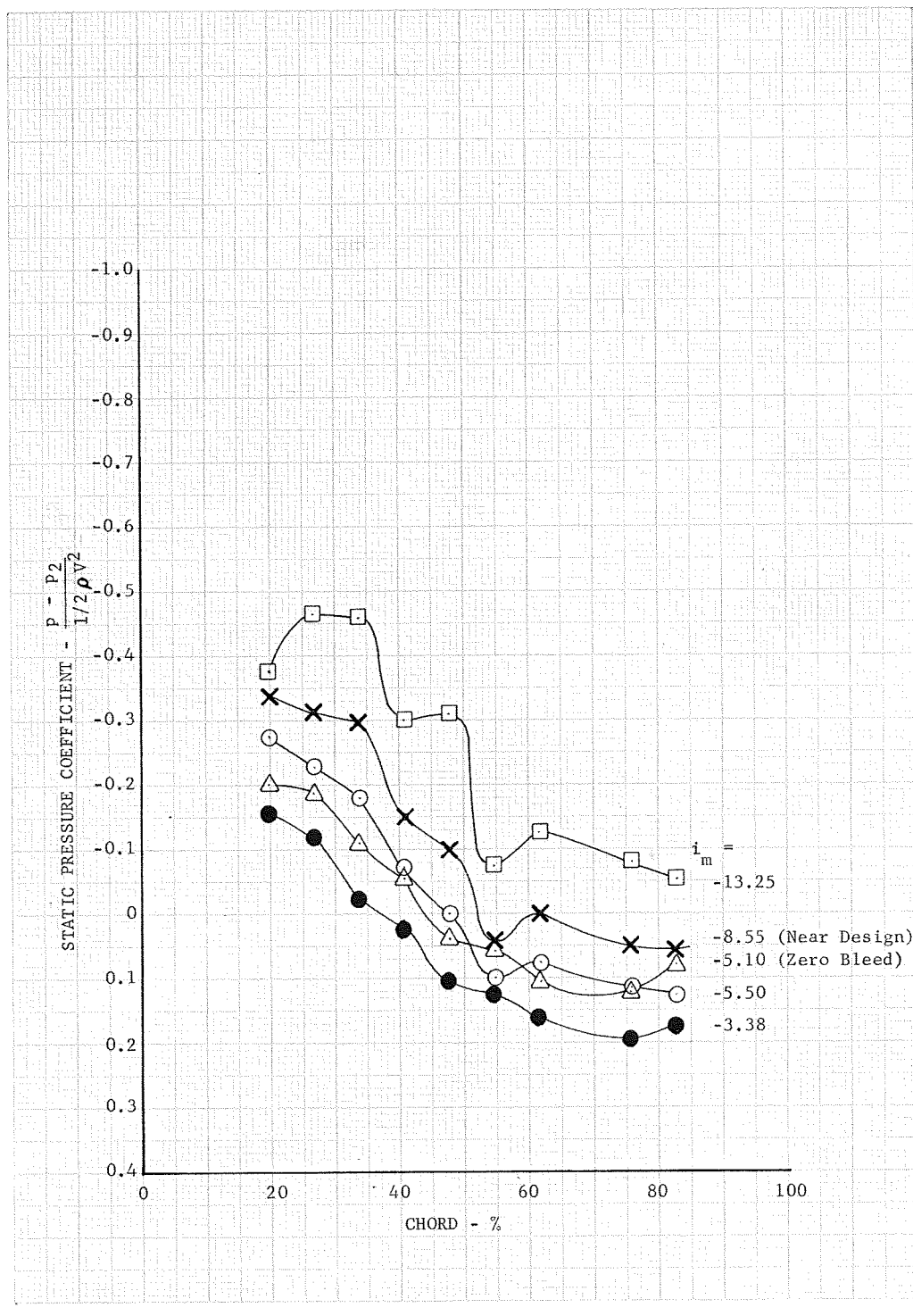
DF 76999

Figure 45. Stator Loss Parameter vs Diffusion Factor - 90% Span From Tip



DF 77020

Figure 46. Stator Static Pressure Coefficients, 10% Span From Tip, 100% Design Equivalent Rotor Speed



DF 77010

Figure 47. Stator Static Pressure Coefficients, 90% Span From Tip, 100% Design Equivalent Rotor Speed

APPENDIX A  
DEFINITION OF SYMBOLS  
AND PERFORMANCE VARIABLES

$A_A$	Flowpath annular area, ft <sup>2</sup>
$a_o'$	Inlet relative stagnation velocity of sound, ft/sec
$c$	Chord length, in.
$C_p$	Static pressure coefficient
$d$	Diameter
$D$	Diffusion factor
$i_m$	Incidence angle, deg (based on equivalent circular arc meanline)
$M$	Absolute Mach number
$N$	Rotor speed, rpm
$o$	Minimum blade passage gap, in.
$o^*$	Critical blade passage gap, in.
$P$	Total pressure, psia
$p$	Static pressure, psia
$t$	Blade maximum thickness, in.
$T$	Total temperature, °R
$T_s$	Static temperature, °R
$U$	Rotor speed, ft/sec
$V$	Velocity, ft/sec
$W$	Actual flowrate, lb <sub>m</sub> /sec
$\beta$	Air angle, deg from axial direction
$\gamma$	Ratio of specific heats
$\gamma^{\circ}$	Blade-chord angle, deg from axial direction
$\delta$	Ratio of total pressure to NASA standard sea level pressure of 14.694 psia
$\delta^{\circ}$	Deviation angle, deg
$\eta_{ad}$	Adiabatic efficiency
$\theta$	Ratio of total temperature to NASA standard sea level temperature of 518.7°R

$\kappa$	Blade metal angle, deg from axial direction (based on equivalent circular arc meanline)
$\rho$	Density, $\text{lb}_f \text{ sec}^2/\text{ft}^4$
$\sigma$	Solidity, c/S
$\phi$	Blade camber angle, $\kappa_1 - \kappa_2$ , deg
$\bar{\omega}$	Loss coefficient
$\bar{\omega} \cos \beta / 2\sigma$	Loss parameter

Subscripts:

0	Guide vane inlet
1	Rotor inlet
2	Rotor exit
2A	Stator exit
3	Stator exit (1.0 chord length downstream from Station 2A)
f	Force
fs	Free stream value
id	Isentropic condition
L	Local
m	Mean or mass
le	Leading edge
te	Trailing edge
s	Static condition
z	Axial component
$\theta$	Tangential component

Superscripts:

'	Related to rotor blade
-	Mass average value

## Definition of Overall Performance Variables

**Pressure Ratio:**

$$\begin{array}{ll} \text{Rotor: } \frac{\bar{P}_2}{\bar{P}_1} & \text{Stage: } \frac{\bar{P}_{2A}}{\bar{P}_1} \end{array}$$

**Corrected Flow**

$$W\sqrt{\theta}/\delta$$

**Corrected Specific Flow:**

$$\frac{W\sqrt{\theta}}{\delta A_A}$$

**Equivalent Rotor Speed:**

$$N/\sqrt{\theta}$$

**Adiabatic Efficiency:**

$$\begin{array}{ll} \text{Rotor: } \frac{(\bar{P}_2/\bar{P}_1)^{\frac{\gamma-1}{\gamma}} - 1}{T_2/518.7 - 1} & \text{Stage: } \frac{(\bar{P}_{2A}/\bar{P}_1)^{\frac{\gamma-1}{\gamma}} - 1}{T_{2A}/518.7 - 1} \end{array}$$

**Adiabatic Efficiency:**

$$\text{Rotor: } \eta_{ad} = \frac{[(\bar{P}_2/\bar{P}_1)^{\frac{\gamma-1}{\gamma}} - 1]}{T_2/518.7 - 1}$$

**Polytropic Efficiency:**

$$\text{Rotor: } \eta_p = \frac{\frac{\gamma-1}{\gamma} \ln (\bar{P}_2/\bar{P}_1)}{\ln(T_2/518.7)} \quad \text{Stator: } \eta_p = \frac{\frac{\gamma-1}{\gamma} \ln (\bar{P}_{2A}/\bar{P}_2)}{\ln(T_{2A}/T_{s2})}$$

## Definition of Blade Element Performance Variables

Incidence Angle:

$$\text{Rotor: } i_m = \beta'_1 - \kappa_{1e} \quad \text{Stator: } i_m = \beta_2 - \kappa_{1e}$$

Diffusion Factor:

$$\text{Rotor: } D = 1 - \frac{V'_2}{V'_1} + \frac{d_2 V'_{\theta 2} - d_1 V'_{\theta 1}}{(d_1 + d_2) V'_1 \sigma}$$

$$\text{Stator: } D = 1 - \frac{V_{2A}}{V'_2} + \frac{d_2 V'_{\theta 2} - d_{2A} V'_{\theta 2A}}{(d_2 + d_{2A}) V'_2 \sigma}$$

Deviation Angle:

$$\text{Rotor: } \delta^\circ = \beta'_2 - \kappa_{te} \quad \text{Stator: } \delta^\circ = \beta_{2A} - \kappa_{te}$$

Loss Coefficient:

$$\text{Rotor: } \bar{\omega}' = \frac{\bar{P}'_{2id} - \bar{P}'_2}{\bar{P}'_1 - \bar{P}_1}$$

where:

$$\bar{P}'_{2id} = \bar{P}'_1 \left\{ 1 + \frac{\gamma - 1}{2} \left( \frac{U_2^2}{a_{01}^2} \right) \left[ 1 - \left( \frac{d_1}{d_2} \right)^2 \right] \right\} \frac{\gamma}{\gamma - 1}$$

$$\bar{P}' \text{ is found from } p/\bar{P}' = \left[ 1 + \frac{\gamma - 1}{2} M'^2 \right] \frac{\gamma}{\gamma - 1}$$

and  $M'$  is calculated using trigonometric functions and the measurements of  $U$ ,  $\beta$ ,  $P$ , and  $p$ .

$$\text{Stator: } \bar{\omega} = \frac{\bar{P}_{21} - \bar{P}_A}{\bar{P}_{21} - \bar{P}_2}$$

where:

$\bar{P}_{21}$  = the wake rake freestream total pressure

Stator Static Pressure Coefficient:

$$C_p = \frac{p_L - p_2}{1/2 \rho_2 V_2^2}$$

## APPENDIX B TABULATED PERFORMANCE

Rotor and stator blade element design data are presented in tables B-1 and B-2. The overall performance, rotor performance, and the rotor and stator bleed flow rates are presented in table B-3. Table B-4 presents blade element data for each test point. Definitions of velocity diagram and performance variables as tabulated in the computer printouts are presented in Appendix A. The span locations in table B-4 correspond to design streamlines.

Table B-1. Rotor 5 Blade Element Design Data Along Design Streamlines

GEOMETRY DATA

Airfoil: NACA 65(A = 1.0)  
No. of Blades: 60

Aspect Ratio: 1.820  
Chord Length: 2.21 in.

Percent Span From Tip  
Leading Trailing

Edge	Edge	$\kappa_{le}$	$\kappa_{te}$	$\phi$	$\gamma^o$	$0/0^*$	$\sigma$	$t/c$
96.41	94.75	60.40	-31.00	91.40	14.70	1.039	1.276	0.078
91.20	89.25	59.90	-22.60	82.50	18.65	1.060	1.258	0.076
86.77	84.80	59.70	-17.00	76.70	21.35	1.079	1.243	0.074
70.84	69.00	60.37	-2.40	62.77	28.99	1.142	1.197	0.068
50.30	49.40	63.22	7.00	56.22	35.11	1.194	1.143	0.060
29.94	29.75	68.07	9.85	58.22	38.96	1.229	1.093	0.052
13.65	14.40	72.80	10.40	62.40	41.60	1.266	1.060	0.046
9.22	10.00	74.35	10.20	64.15	42.28	1.277	1.050	0.044
3.41	4.70	76.60	9.65	66.95	43.13	1.293	1.040	0.042

VELOCITY DIAGRAM DATA

Equivalent Rotor Speed: 4210 rpm

Corrected Weight Flow: 110 lb/sec

Percent Span From Tip  
Leading Trailing

Edge	Edge	$V'_{le}$	$V'_{zle}$	$V'_{\theta le}$	$\beta'_{le}$	$U'_{le}$	$V'_{te}$	$V'_{zle}$	$V'_{\theta te}$	$\beta'_{te}$	$U'_{te}$
96.39	94.83	775.3	479.3	608.8	51.77	608.8	384.2	373.9	-69.0	-10.8	610.6
92.31	89.41	781.5	481.2	614.9	51.94	614.9	418.9	419.6	-31.5	-5.1	618.2
87.50	84.37	788.8	483.7	622.5	52.13	622.5	447.1	447.1	2.5	-0.1	625.6
71.70	69.38	811.8	491.1	646.6	52.79	646.6	503.3	494.1	93.5	10.8	646.8
50.24	49.48	838.7	490.8	679.6	54.15	679.6	529.9	500.6	73.0	19.1	675.3
28.85	29.59	857.4	475.6	712.6	56.19	712.4	529.6	485.0	209.5	23.2	703.7
13.10	14.86	866.5	454.7	736.8	58.21	736.5	510.2	458.6	219.0	25.2	724.7
8.65	9.88	868.7	448.1	743.3	58.74	743.2	497.8	444.7	217.5	25.7	731.7
3.37	4.91	870.8	441.4	751.4	59.61	751.3	481.3	427.7	214.0	26.2	738.8

DESIGN PERFORMANCE DATA

Pressure Ratio: 1.401

Efficiency = 87.3%

Percent Span from Tip  
Leading Trailing

Edge	Edge	$\Delta\beta$	$M'_{le}$	$i_m$	$D_F$	$\bar{\omega}$	Loss Parameter	$\delta^o$	$P_{te}$ psia	$T_{te}$ R
96.39	94.83	62.57	0.708	-8.63	0.851	0.325	0.125	20.20	20.684	587.9
92.31	89.41	57.04	0.714	-8.06	0.801	0.262	0.104	19.00	20.801	586.0
87.50	84.37	52.23	0.721	-7.57	0.759	0.210	0.085	17.70	20.882	583.8
71.70	69.38	41.99	0.742	-7.51	0.663	0.101	0.041	13.80	20.828	578.1
50.24	49.48	35.05	0.766	-9.07	0.632	0.074	0.030	12.00	20.603	575.0
28.85	29.59	32.99	0.784	-12.21	0.650	0.115	0.048	13.30	20.479	576.6
13.10	14.86	33.01	0.790	-14.79	0.692	0.187	0.080	14.80	20.335	579.5
8.65	9.88	33.04	0.791	-15.86	0.715	0.221	0.095	15.50	20.263	581.0
3.37	4.91	33.41	0.793	-16.99	0.745	0.264	0.114	16.60	20.184	583.0

Table B-2. Stator 5 Blade Element Design Data  
Along Design Streamlines

GEOMETRY DATA

Airfoil: NACA 65(A = 1.0)  
No. of Blades: 58

Aspect Ratio: 1.689  
Chord Length: 2.182 in.  
Thickness, t/c = 0.090

Percent Span From Tip  
Leading Trailing

Edge	Edge	$\kappa_{1e}$	$\kappa_{te}$	$\phi$	$\gamma^c$	0/0*	$\sigma$
94.74	94.90	66.30	-22.42	88.72	21.90	1.311	1.214
90.13	90.40	62.35	-20.42	82.77	20.87	1.255	1.200
84.87	85.00	59.20	-18.60	77.80	20.23	1.201	1.187
70.39	70.10	53.65	-15.12	68.77	19.32	1.126	1.151
50.66	49.80	51.95	-13.80	65.75	19.13	1.101	1.105
30.92	30.00	55.03	-15.17	70.20	19.95	1.131	1.063
15.79	15.00	59.20	-17.22	76.42	21.10	1.188	1.032
10.53	10.00	61.10	-18.15	79.25	21.57	1.212	1.021
5.13	5.00	63.30	-19.40	82.70	22.00	1.238	1.010

VELOCITY DIAGRAM DATA

Percent Span From Tip  
Leading Trailing

Edge	Edge	$V_{1e}$	$V_{z1e}$	$V_{\theta 1e}$	$\beta_{1e}$	$V_{te}$	$V_{zte}$	$V_{\theta te}$	$\beta_{te}$
94.73	94.40	784.5	388.7	679.5	60.41	283.5	278.5	0.0	0.0
89.86	88.38	782.8	427.9	655.0	57.01	381.0	373.5	0.0	0.0
84.59	82.84	778.9	463.6	626.0	53.58	439.0	441.5	0.0	0.0
70.03	68.49	759.9	520.4	554.0	46.77	509.5	507.5	0.0	0.0
50.73	48.88	732.8	531.2	504.5	43.53	515.0	515.5	0.0	0.0
30.83	28.71	708.6	503.6	498.0	44.59	507.0	506.5	0.0	0.0
15.81	13.87	683.3	454.7	509.0	48.17	496.5	495.5	0.0	0.0
10.54	8.54	671.6	427.8	516.5	50.33	492.5	491.5	0.0	0.0
5.01	5.18	660.3	395.6	527.5	53.12	490.0	489.0	0.0	0.0

DESIGN PERFORMANCE DATA

Stage Pressure Ratio: 1.353  
Stage Efficiency: 78.1%

Percent Span From Tip  
Leading Trailing

Edge	Edge	$\Delta\beta$	$M_{1e}$	$i_m$	$D_F$	Loss Parameter	$\bar{\omega}$	$P_{te}$ psia	$\delta^\circ$
94.73	94.40	60.41	0.690	- 5.89	0.999	0.422	0.174	18.310	22.40
89.86	88.38	57.01	0.690	- 5.19	0.864	0.316	0.132	19.035	20.30
84.59	82.84	53.58	0.688	- 5.42	0.775	0.237	0.100	19.560	18.50
70.03	68.49	46.77	0.674	- 6.73	0.649	0.116	0.050	20.190	15.00
50.73	48.88	43.53	0.649	- 8.42	0.610	0.079	0.036	20.200	13.80
30.83	28.71	44.59	0.626	-10.44	0.618	0.094	0.044	20.045	15.27
15.81	13.87	48.17	0.600	-11.03	0.636	0.118	0.057	19.810	17.20
10.54	8.54	50.33	0.588	-10.77	0.646	0.129	0.063	19.700	18.20
5.01	5.18	53.12	0.576	-10.18	0.654	0.137	0.068	19.630	19.40

Table B-3. Overall Performance, Rotor 5-Stator 5

$\eta_{ad}$	Corrected Weight Flow lb/sec	Rotor Tip Bleed Flow lb/sec	Stator Hub & Tip Bleed Flow lb/sec	$P_2/P_o$	Rotor $\eta_{ad}$ %	$\eta_p$ %	$P_{2A}/P_o$	Stage $\eta_{ad}$ %	$\eta_p$ %	
50% Design Equivalent Rotor Speed										
74.89	0.65	0.868	1.29	1.723	1.0723	0.7611	0.7635	.1.0458	0.4862	0.4894
66.54	0.80	1.202	1.85	2.780	1.0812	0.8079	0.8100	1.0645	0.6447	0.6478
59.72	0.85	1.423	2.05	3.433	1.0864	0.8399	0.8418	1.0725	0.7076	0.7105
55.56	0.89	1.602	2.15	3.870	1.0864	0.8425	0.8444	1.0751	0.7345	0.7372
70% Design Equivalent Rotor Speed										
99.11	0.75	6.757	1.29	1.302	1.1421	0.7760	0.7802	1.0835	0.4645	0.4705
89.55	0.98	1.094	2.31	2.580	1.1642	0.8477	0.8509	1.1258	0.6570	0.6627
84.36	1.04	1.233	2.57	3.046	1.1740	0.8616	0.8647	1.1437	0.7179	0.7232
76.47	1.08	1.412	2.74	3.583	1.1775	0.8824	0.8851	1.1500	0.7516	0.7565
90% Design Equivalent Rotor Speed										
115.65	0.72	0.623	1.15	0.994	1.2283	0.7648	0.7716	1.1198	0.4149	0.4242
110.23	1.01	0.916	2.46	2.232	1.2591	0.8229	0.8286	1.1900	0.6156	0.6250
104.51	1.11	1.062	2.90	2.775	1.2846	0.8544	0.8595	1.2240	0.6841	0.6930.
99.94	1.14	1.141	3.10	3.102	1.2876	0.8508	0.8561	1.2357	0.7074	0.7160
97.15	1.19	1.225	3.19	3.284	1.2976	0.8635	0.8685	1.2420	0.7131	0.7218
95.88	1.20	1.252	3.24	3.379	1.2940	0.8409	0.8466	1.2453	0.7110	0.7199

Table B-3. Overall Performance, Rotor 5-Stator 5 (Continued)

Corrected Weight Flow lb/sec	Rotor Tip Bleed Flow lb/sec	Stator Hub & Tip Bleed Flow lb/sec	$P_2/P_o$	Rotor $\eta_{ad}$ %	$\eta_p$ %	$P_{2A}/P_o$	Stage $\eta_{ad}$ %	$\eta_p$ %
120.17	0.76	0.632	1.07	0.890	1.2628	0.7189	0.7280	1.1365
116.37	1.03	0.885	2.68	2.303	1.3208	0.8018	0.8095	1.2336
110.97	1.12	1.009	3.12	2.812	1.3416	0.8203	0.8276	1.2699
107.81	1.20	1.113	3.28	3.042	1.3576	0.8390	0.8459	1.2845
107.66	1.22	1.133	3.35	3.112	1.3562	0.8422	0.8488	1.2854
106.26	0.76	0.715	2.05	1.929	1.3602	0.8343	0.8414	1.2854
103.43	1.23	1.189	3.47	3.355	1.3679	0.8393	0.8463	1.2997
102.28	0.12	0.117	0.28	0.274	1.3628	0.8230	0.8306	1.2810
101.80	1.26	1.238	3.49	3.428	1.3673	0.8427	0.8495	1.2994
101.47	0.67	0.660	1.96	1.932	1.3671	0.8225	0.8302	1.2956

Nomenclature Used for Blade Element Data Tabulation

Exit Percent Span from Tip	PCT SPAN
Exit Diameter	DIA
Absolute Flow Angle	BETA
Relative Flow Angle	BETA (PR)
Absolute Velocity	V
Axial Velocity	VZ
Absolute Tangential Velocity	V - THETA
Relative Velocity	V (PR)
Relative Tangential Velocity	V - THETA PR
Rotor Speed	U
Absolute Mach Number	M
Relative Mach Number	M (PR)
Relative Turning Angle	TURN (PR)
Loss Coefficient	UUBAR
Loss Parameter	LOSS PARA
Diffusion Factor	DFAC
Polytropic Efficiency	EFFP
Adiabatic Efficiency	EFF
Incidence	INCID
Deviation	DEVM
Total Pressure	P
Total Temperature	T

Note: Where applicable the appropriate instrumentation station is noted.





















Table B-4. Blade Element Performance (Continued)

PERCENT EQUIVALENT DESIGN SPEED = 90.48		EQUIVALENT ROTOR SPEED = 3809.00		CORRECTED WEIGHT FLOW = 104.51		PRESSURE RATIO = 1.2240	
INLET	PCT SPAN	96.42	91.17	86.46	70.64	49.46	29.30
	DIA	33.150	33.590	33.985	35.310	37.085	38.775
STATION 0	BETA 0	0.000	0.000	0.000	0.000	0.000	0.000
STATION 1	BETA 1	-0.100	-0.100	-0.100	-0.100	-0.100	-0.100
V 0		405.55	405.55	405.55	405.55	405.55	405.55
V 1		420.59	455.18	461.62	458.35	455.61	446.61
VZ 0		405.55	405.55	405.55	405.55	405.55	405.55
VZ 1		420.59	455.18	461.55	458.28	455.33	446.33
V-THETA 0		0.00	0.00	0.00	0.00	0.00	0.00
V-THETA 1		-0.73	-0.75	-0.81	-0.80	-0.79	-0.75
M 0		0.3682	0.3682	0.3682	0.3682	0.3682	0.3682
M 1		0.3822	0.4147	0.4208	0.4177	0.4151	0.4066
TURN		0.10	0.10	0.10	0.10	0.10	0.10
UUBAR		0.2132	0.274	0.0053	-0.0000	-0.0000	-0.0000
DFAC		-0.037	-0.122	-0.138	-0.130	-0.123	-0.101
EFFP		0.2717	0.9098	0.9833	0.9999	1.0000	0.9611
INCID		0.0001	0.0001	0.0001	0.0001	0.0001	0.0001
DEVM		0.100	0.100	0.100	0.100	0.100	0.100
P 0		14.694	14.694	14.694	14.694	14.694	14.694
P 1		14.414	14.658	14.687	14.694	14.694	14.682
T 0		518.700	518.700	518.700	518.700	518.700	518.700
T 1		518.700	518.700	518.700	518.700	518.700	518.700
ROTOR 5	PCT SPAN	95.01	90.00	85.01	70.01	50.01	30.01
	DIA	33.233	33.617	34.000	35.150	36.684	38.218
STATION 1	BETA 1	-0.100	-0.100	-0.100	-0.100	-0.100	-0.100
STATION 2	BETA 2	56.280	53.180	48.520	41.550	39.090	39.270
BETA(PR) 1		52.679	50.846	50.786	52.051	53.580	55.326
BETA(PR) 2		-9.659	-0.333	6.417	14.411	20.961	24.911
V 1		420.59	455.18	461.62	458.35	455.61	446.61
V 2		743.52	701.02	686.08	683.03	657.46	640.43
VZ 1		420.59	455.18	461.55	458.28	455.33	446.33
VZ 2		412.76	420.10	454.40	510.99	510.00	495.45
V-THETA 1		-0.73	-0.75	-0.81	-0.80	-0.79	-0.75
V-THETA 2		618.43	561.15	513.97	452.88	414.32	405.09
V(PR) 1		653.7	720.5	730.1	745.3	767.1	784.7
V(PR) 2		416.0	426.2	457.3	527.9	546.6	481.1
VTHETA PR1		-551.7	-555.1	-565.6	-587.6	-617.1	-645.2
VTHETA PR2		66.1	2.4	-51.1	-131.3	-195.4	-230.1
U 1		550.95	558.26	564.83	586.85	616.35	644.44
U 2		552.33	558.71	565.08	584.19	609.68	635.18
M 1		0.3822	0.4147	0.4208	0.4177	0.4151	0.4066
M 2		0.6624	0.6228	0.6102	0.6088	0.5857	0.5692
M(PR) 1		0.6304	0.6568	0.6655	0.6791	0.6989	0.7144
M(PR) 2		0.3724	0.3733	0.4068	0.4705	0.4869	0.4860
TURN(PR)		61.778	51.181	44.365	37.644	32.621	30.425
UUBAR		0.2318	0.2875	0.2329	0.0999	0.0660	0.0907
LOSS PARA		0.0901	0.1145	0.0932	0.0403	0.0268	0.0372
DFAC		0.7452	0.7277	0.6576	0.5464	0.5214	0.5356
EFFP		0.9337	0.8199	0.8346	0.9067	0.9412	0.9163
EFF		0.9307	0.8131	0.8286	0.9032	0.9391	0.9132
INCID		-7.721	-5.052	-8.919	-8.323	-9.657	-12.760
DEVM		21.901	22.667	23.416	16.803	13.943	15.035
P 1		14.414	14.658	14.687	14.694	14.682	14.673
P 2		19.661	19.045	18.880	19.034	18.958	18.883
T 1		518.700	518.700	518.700	518.700	518.700	518.700
T 2		570.390	568.250	565.270	562.770	560.410	561.040
STATOR 5	PCT SPAN	94.40	50.62	85.08	70.31	50.14	22.97
	DIA	33.250	33.520	33.915	34.970	36.410	37.850
STATION 2	BETA 2	56.280	53.180	48.520	41.550	39.090	39.270
STATION 2A	BETA 2A	4.650	4.850	4.710	3.780	4.140	6.730
V 2		743.52	701.02	686.08	683.03	657.46	640.43
V 2A		485.59	484.24	483.42	524.08	553.82	520.43
VZ 2		412.76	420.10	454.40	510.99	510.00	495.45
VZ 2A		484.39	482.50	481.79	522.94	552.37	516.85
V-THETA 2		618.43	561.15	513.97	452.88	414.32	405.09
V-THETA 2A		39.40	40.94	39.70	34.55	39.98	60.99
M 2		0.6624	0.6228	0.6102	0.6088	0.5857	0.5692
M 2A		0.4225	0.4217	0.4221	0.4601	0.4885	0.4575
TURN(PR)		51.630	48.326	43.806	37.753	34.923	32.506
UUBAR		0.2059	0.1956	0.1727	0.1218	0.0571	0.1154
LOSS PARA		0.1003	0.0810	0.0724	0.0527	0.0257	0.0678
DFAC		0.6677	0.6185	0.5868	0.4993	0.4161	0.4414
EFFP		0.5348	0.6338	0.6545	0.6968	0.8186	0.5719
EFF		-0.0000	-0.0000	0.0017	-0.0000*****	-0.0000*****	-0.0000*****
INCID		-10.020	-9.174	-10.684	-12.117	-12.887	-15.794
DEVM		27.076	25.270	23.310	18.900	17.940	21.900
P 21		19.283	18.935	18.763	18.939	18.946	18.808
P 2A		18.152	18.099	18.058	18.437	18.722	18.277
T 2		570.390	568.250	565.270	562.770	560.410	561.040
T 2A		570.390	568.250	565.270	562.770	560.410	562.510



























#### REFERENCES

1. Rockenbach, R. W., "Single Stage Experimental Evaluation of Slotted Rotor and Stator Blading, Part IX - Final Report," NASA CR-54553, PWA FR-2289, 26 September 1968.
2. Rockenbach, R. W., "Single Stage Experimental Evaluation of Compressor Blading with Slots and Wall Flow Fences," NASA CR-72635 PWA FR-3597.
3. Rockenbach, R. W., J. A. Brent, and B. A. Jones, "Single Stage Experimental Evaluation of Compressor Blading with Slots and Vortex Generators, Part I - Design of Stages 4 and 5," NASA CR-72626, PWA FR-3461.
4. Linder, C. G., and B. A. Jones, "Single Stage Experimental Evaluation of Slotted Rotor and Stator Blading, Part III - Data and Performance for Slotted Rotor 1," NASA CR-54546, PWA FR-2110, February 1967.
5. Linder, C. G., and B. A. Jones, "Single Stage Experimental Evaluation of Slotted Rotor and Stator Blading, Part IV - Data and Performance for Slotted Rotor 2," NASA CR-54547, PWA FR-2111, February 1967.
6. Linder, C. G., and B. A. Jones, "Single Stage Experimental Evaluation of Slotted Rotor and Stator Blading, Part V - Data and Performance for Slotted Rotor 3 - Slotted Stator 2," NASA CR-54547, PWA FR-2285, August 1967.
7. Linder, C. G., and B. A. Jones, "Single Stage Experimental Evaluation of Slotted Rotor and Stator Blading, Part VI - Data and Performance for Slotted Stator 1," NASA CR-54549, PWA FR-2286, July 1967.
8. Linder, C. G., and B. A. Jones, "Single Stage Experimental Evaluation of Slotted Stator 2," NASA CR-54550, PWA FR-2287, September 1967.
9. Linder, C. G., and B. A. Jones, "Single Stage Experimental Evaluation of Slotted Rotor and Stator Blading, Part VIII - Data and Performance for Slotted Stator 3," NASA CR-54551, PWA FR-2288, October 1967.
10. Aerodynamic Design of Axial Flow Compressors (Revised), NASA SP-36, 1965.

Distribution List

Contract NAS3-10481

1. NASA-Lewis Research Center  
21000 Brookpark Road  
Cleveland, Ohio 44135  
Attention:  

Report Control Office	MS 5-5	1
Technical Utilization Office	MS 3-19	1
Library	MS 60-3	2
Fluid System Components Division	MS 5-3	1
Pump and Compressor Branch	MS 5-9	6
Dr. B. Lubarsky	MS 3-3	1
A. Ginsburg	MS 5-3	1
M. J. Hartmann	MS 5-9	1
W. A. Benser	MS 5-9	1
D. M. Sandercock	MS 5-9	1
L. J. Herrig	MS 7-1	1
T. F. Gelder	MS 5-9	1
C. L. Ball	MS 5-9	1
L. Reid	MS 5-9	1
L. W. Schopen	MS 77-3	1
S. Lieblein	MS 100-1	1
C. L. Meyer	MS 60-4	1
J. H. Povolny	MS 60-4	1
A. W. Goldstein	MS 7-1	1
J. J. Kramer	MS 7-1	1
W. L. Beede	MS 5-3	1
C. H. Voit	MS 5-3	1
E. E. Bailey	MS 5-9	1
2. NASA Scientific and Technical Information Facility  
P. O. Box 33  
College Park, Maryland 20740  
Attention: NASA Representative 6
3. FAA Headquarters  
800 Independence Ave., S. W.  
Washington, D. C. 20553  
Attention: Brig. General J. C. Maxwell 1

4.	NASA Headquarters Washington, D. C. 20546 Attention: N. F. Rekos (RAP)	1
5.	U. S. Army Aviation Material Laboratory Fort Eustes, Virginia Attention: John White	1
6.	Headquarters Wright Patterson AFB, Ohio 45433 Attention: J. L. Wilkins, SESOS S. Kobelak, APTP R. P. Carmichael, SESSP	1 1 1
7.	Department of Navy Bureau of Weapons Washington, D. C. 20525 Attention: Robert Brown, RAPP14	1
8.	Department of Navy Bureau of Ships Washington, D. C. 20360 Attention: G. L. Graves	1
9.	NASA-Langley Research Center Technical Library Hampton, Virginia 23365 Attention: Mark R. Nichols John V. Becker	1 1
10.	Boeing Company Commercial Airplane Division P. O. Box 3991 Seattle, Washington 98124 Attention: C. J. Schott MS80-66	1
11.	Douglas Aircraft Company 3855 Lakewood Boulevard Long Beach, California 90801 Attention: J. E. Merriman Technical Information Center Cl-250	1
12.	Pratt & Whitney Aircraft Florida Research & Development Center P. O. Box 2691 West Palm Beach, Florida 33402 Attention: R. A. Schmidtke H. D. Stetson J. M. Silk R. W. Röckenbach B. A. Jones B. S. Savin J. A. Fligg	1 1 1 1 1 1 1 1

- |     |   |                       |
|-----|---|-----------------------|
| 13. | Pratt & Whitney Aircraft<br>400 Main Street<br>East Hartford, Connecticut<br>Attention: R. E. Palatine<br>M. J. Keenan<br>A. A. Mikolajczak<br>Library (UARL)                               | 1<br>1<br>1<br>1<br>1 |
| 14. | Allison Division, GMC<br>Department 8894, Plant 8<br>P. O. Box 894<br>Indianapolis, Indiana 46206<br>Attention: J. N. Barney<br>R. J. Loughery<br>Library<br>J. L. Dillard                  | 1<br>1<br>1<br>1      |
| 15. | Northern Research and Engineering<br>219 Vassar Street<br>Cambridge 39, Massachusetts<br>Attention: K. Ginwala  | 1                     |
| 16. | General Electric Company<br>Flight Propulsion Division<br>Cincinnati 15, Ohio<br>Attention: J. Ringrose H-79<br>L. H. Smith H-50<br>Technical Information Center N-32<br>Marlen Miller H-50 | 1<br>1<br>1<br>1      |
| 17. | General Electric Company<br>1000 Western Avenue<br>West Lynn, Massachusetts<br>Attention: L. H. King - Bldg. 2-40<br>Dr. C. W. Smith Library<br>Bldg. 2-40M                                 | 1<br>1                |
| 18. | Curtiss-Wright Corporation<br>Wright Aeronautical<br>Woodridge, New Jersey<br>Attention: S. Lombardo  | 1                     |
| 19. | Air Research Manufacturing Company<br>402 South 36th Street<br>Phoenix, Arizona 85034<br>Attention: Robert O. Bullock   | 1                     |
| 20. | Air Research Manufacturing Company<br>8951 Sepulveda Boulevard<br>Los Angeles, California 90009<br>Attention: Linwood C. Wright   | 1                     |

- |     |  |   |
|-----|--|---|
| 21. | Union Carbide Corporation<br>Nuclear Division<br>Oak Ridge Gaseous Diffusion Plant<br>P. O. Box "P"<br>Oak Ridge, Tennessee 37830<br>Attention: R. G. Jordon<br>D. W. Burton, K-1001, K-25 | 1 |
| 22. | Avco Corporation<br>Lycoming Division<br>550 South Main Street<br>Stratford, Connecticut<br>Attention: Clause W. Bolton  | 1 |
| 23. | Continental Aviation & Engineering Corp.<br>12700 Kercheval<br>Detroit, Michigan 48215<br>Attention: Eli H. Benstein   | 1 |
| 24. | Solar<br>San Diego, California 92112<br>Attention: P. A. Pitt  | 1 |
| 25. | Goodyear Atomic Corporation<br>Box 628<br>Piketon, Ohio<br>Attention: C. O. Langebrake   | 1 |
| 26. | Iowa State University of<br>Science and Technology<br>Ames, Iowa 50010<br>Attention: Professor George K. Serovy<br>Dept. of Mechanical Engineering   | 1 |
| 27. | Hamilton Standard Division of<br>United Aircraft Corporation<br>Windsor Locks, Connecticut<br>Attention: Mr. Carl Rohrbach<br>Head of Aerodynamics and Hydrodynamics                       | 1 |
| 28. | Westinghouse Electric Corporation<br>Small Steam and Gas Turbine Engineering B-4<br>Lester Branch<br>P. O. Box 9175<br>Philadelphia, Pennsylvania 19113<br>Attention: Mr. S. M. DeCorso    | 1 |
| 29. | J. Richard Joy<br>Supervisor, Analytical Section<br>Williams Research Corporation<br>P. O. Box 95<br>Walled Lake, Michigan   | 1 |

30. Raymond S. Poppe  
Building 541, Dept. 80-91  
Lockheed Missile and Space Company  
P. O. Box 879  
Mountain View, California 94040 1
31. James D. Raisbeck  
The Boeing Company  
224 N. Wilkinson  
Dayton, Ohio 45402 1
32. James Furlong  
Chrysler Corporation  
Research Office  
Dept. 9000  
P. O. Box 1118  
Detroit, Michigan 48231 1
33. Elliott Company  
Jeannette, Pennsylvania 15644  
Attention: J. Rodger Shields  
Director-Engineering 1
34. R. H. Carmody  
Dresser Industries Inc.  
Clark Gas Turbine Division  
16530 Peninsula Boulevard  
P. O. Box 9989  
Houston, Texas 77015 1
35. California Institute of Technology  
Pasadena, California 91109  
Attention: Professor Duncan Rannie 1
36. Massachusetts Institute of Technology  
Cambridge, Massachusetts 02139  
Attention: Dr. J. L. Kerrebrock 1